INFORMATION TO USERS

This manuscript has been reproduced from the microfilm master. UMI films the text directly from the original or copy submitted. Thus, some thesis and dissertation copies are in typewriter face, while others may be from any type of computer printer.

The quality of this reproduction is dependent upon the quality of the copy submitted. Broken or indistinct print, colored or poor quality illustrations and photographs, print bleedthrough, substandard margins, and improper alignment can adversely affect reproduction.

In the unlikely event that the author did not send UMI a complete manuscript and there are missing pages, these will be noted. Also, if unauthorized copyright material had to be removed, a note will indicate the deletion.

Oversize materials (e.g., maps, drawings, charts) are reproduced by sectioning the original, beginning at the upper left-hand corner and continuing from left to right in equal sections with small overlaps. Each original is also photographed in one exposure and is included in reduced form at the back of the book.

Photographs included in the original manuscript have been reproduced xerographically in this copy. Higher quality 6" x 9" black and white photographic prints are available for any photographs or illustrations appearing in this copy for an additional charge. Contact UMI directly to order.

UMI®

Bell & Howell Information and Learning
300 North Zeeb Road, Ann Arbor, MI 48106-1346 USA
800-521-0600

RIDE AND ROLL PERFORMANCE ANALYSIS OF A VEHICLE WITH SPRING LOADED INTERCONNECTED HYDRO-PNEUMATIC SUSPENSION

SANJEEV CHAUDHARY

A Thesis

in

The Department

of

Mechanical Engineering

Presented in Partial Fulfillment of the Requirements

for the Degree of Master of Applied Science at

Concordia University

Montreal, Quebec, Canada

April 1998

ABSTRACT

RIDE AND ROLL PERFORMANCE ANALYSIS OF A VEHICLE WITH SPRING LOADED INTERCONNECTED HYDRO-PNEUMATIC SUSPENSION

Sanjeev Chaudhary

The design of vehicle suspensions is essentially a compromise between the functional use of the system, the desired ride comfort, vehicle handling performance, and the economic factors to produce such suspension. Generally, softer suspensions are desired for smoother ride which can effectively isolate the vehicle body from the effects of road disturbances. On the other hand, handling performance due to braking, cornering and accelerating are generally more severe with softer suspensions. Anti-roll bar, in conjunction with softer suspensions, are frequently implemented to attain a compromise between ride and handling performance of a vehicle. Alternatively, an improved compromise between ride and handling can be realized by developing a passive interconnection between hydro-pneumatic suspension struts in roll plane. The interconnected suspension can provide a soft suspension rate for improved ride quality, and enhance stiffness and damping against roll motions for adequate handling performance and roll control. Although hydro-pneumatic suspensions interconnected in roll plane can be used to achieve such goal, such systems designed to support load may lead to an unrealistic and bulky configuration. Introducing mechanical springs in parallel with hydro-pneumatic struts can help to design realistic interconnected hydro-pneumatic system for vehicle suspensions. In this dissertation, spring loaded hydro-pneumatic

suspension, interconnected in roll plane, is analytically investigated for its ride and handling performance.

A highway bus equipped with passive type spring loaded interconnected hydro-pneumatic suspension unit is modeled in roll plane as a four-degree-of-freedom dynamical system subject to excitations arising from road irregularities and roll moment caused by directional maneuvers. The static and dynamic properties of the interconnected suspension are derived and discussed in terms of its suspension rate, roll stiffness, and damping forces. The model is analyzed to examine the effects of percentage load assigned to the springs and hydro-pneumatic struts in view of component size and effective interconnection. The ride and handling performance of selected interconnected suspension are investigated and compared to those of the unconnected and conventional systems for deterministic excitations. The vibration isolation performance characteristics of the interconnected suspension employing a concept of variable sequential damping are further investigated for deterministic excitations. From computer simulation results, it is concluded that implementation of mechanical springs with hydro-pneumatic struts lead to realistic design parameters for the suspension components. However, the percentage load carried by the spring is an important factor. Large spring rate leads to reduce interconnection effect whereas, smaller rate leads to large strut size and pressure. Hence a compromise is needed in spring selection. In general, the results show that the proposed interconnected hydro-pneumatic suspension can provide comparatively improved performance in both bounce and roll modes.

ACKNOWLEDGMENTS

I would like to express my sincere appreciation to my supervisors, Dr. A. K. W. Ahmed and, Dr. R. B. Bhat for their constant guidance and dedication throughout the realization of this investigation.

Thanks are due to the colleagues, faculty members and students of Concave Research Center, and the Department of Mechanical Engineering for their contribution during the course of this work.

Financial support provided by my supervisors in the form of research assistantships, is gratefully acknowledged.

Finally, I would particularly like to express my special thanks to Dr. Subhash Rakheja, Prof. Zhanqi Wang for their technical support, advice and helpful suggestion and members of my family, for their encouragement and support.

TABLE OF CONTENTS

CHAPTER 3

PROPERTIES OF THE SPRING LOADED INTERCONNECTED HYDRO-PNEUMATIC SUSPENSION SYSTEM

CHAPTER 5

DETERMINISTIC ANALYSIS OF THE INTERCONNECTED SUSPENSION WITH TUNABLE SEQUENTIAL DAMPING

CHAPTER 6

CONCLUSIONS AND RECOMMENDATIONS FOR FUTURE WORK

LIST OF FIGURES

LIST OF TABLES

NOMENCLATURE

SYMBOL	DESCRIPTION
a	general orifice area
a_1	fixed orifice area of variable interlinked hydro-pneumatic damper model
a_ℓ, a_r	orifice area of the left and right struts of suspensions, respectively
a_{vl}, a_{vr}	left and right valve opening area of variable interlinked hydro-pneumatic damper
a_y	lateral acceleration acting on the sprung mass
A_1	general piston rod side area
A_2	general piston head side area
$A_{1\ell}$, A_{1r}	piston rod side area of left and right strut
$A_{2\ell}$, A_{2r}	piston head side area of left and right strut
A_m	amplification factor
A_r	piston rod area
c_{trl}, c_{trr}	damping coefficients of the left and right tires, respectively
c_d	discharge coefficient
c_1	damping coefficient corresponding to the fixed orifice area a_1
c_2	damping coefficient corresponding to variable orifice area a_{vl}
d	diameter of anti-roll bar
D	diameter of interconnected pipe
F	total restoring force of gas spring
F_d	forces developed at each end of anti-roll bar during out-of-phase road input
F_{fl}, F_{fr}	dynamic suspension forces developed by left and right independent hydro-pneumatic struts

$F'_{f\ell}, F'_{fr}$	dynamic suspension forces developed by left and right interconnected hydro-pneumatic struts
$F_{\ell c}, F_{rc}$	damping force developed by one strut of independent hydro-pneumatic unit
F'_{ℓ}, F'_{r}	generalized suspension forces of interconnected suspension
F_{ℓ}, F_{r}	restoring forces, developed at the left and right strut of suspension
$F'_{\ell s}, F'_{rs}$	restoring forces due to left and right gas spring
$F'_{\ell c}, F'_{rc}$	damping force due to left and right hydraulic strut
F_{TL}, F_{TR}	total force developed by left and right side of suspension unit
F_{dB}, F_{dR}	damping force in bounce and roll, respectively
g	acceleration due to gravity
G	shear modules of the anti-roll bar
h_2	vertical distance from the center of gravity of sprung mass to its roll center
I_s	mass moment of inertia of the sprung mass
I_u	mass moment of inertia of unsprung mass
K	stiffness of the load carrying spring
K_d	spring constant of anti-roll bar
K_{eq}	equivalent stiffness of strut
k'	static stiffness of the spring loaded interconnected suspension
k_u	non-linear stiffness of independent hydro-pneumatic struts at design ride height
k_{vl}, k_{vr}	static stiffness of left and right strut of interconnected hydro-pneumatic unit
k^*_{eq}	equivalent spring stiffness due to independent hydro-pneumatic struts at static ride height

$K_{tr\ell}$, K_{trr}	stiffness coefficients of the left and right tires, respectively
$k^*_{v\ell}$, k^*_{vr}	static stiffness of the interconnected suspension system at static ride height
k^*_ℓ, k^*_r	static stiffness of the left and right side of the spring loaded independent suspension
K_θ	roll stiffness of the interconnected system
k^*_θ	roll stiffness of interconnected unit corresponding to the design ride height
$k_{\theta sp}$	roll stiffness due to mechanical spring
$k^0_{\theta u}$	roll stiffness developed by independent hydro-pneumatic struts at design ride height
$k'_{\theta T}$	roll stiffness of spring loaded independent hydro-pneumatic suspension with anti-roll bar
$k_{\theta T}$	roll stiffness of spring loaded independent hydro-pneumatic suspension with anti-roll bar and due to mechanical spring
ℓ	half the suspension strut track
L	length of interconnected pipe
l_b	distance between two ends of the trailing edges
L_c	gas column in accumulator
L_l, L_r	lateral distances from the left and right suspension struts to the center of gravity of the sprung mass
L_{wl}, L_{wr}	lateral distances from the left and right tires to the center of gravity of the sprung mass
M	rolling moment
m_s	sprung mass of the vehicle
m_u	unsprung mass of the vehicle
n	polytropic gas constant
N_U	number of struts

$p_{23\ell}$, p_{23r}	pressure differential across the left and right damping restrictions
$p_{1\ell}$, $p_{2\ell}$, $p_{3\ell}$	instantaneous pressures in chambers I, II, III of left strut, respectively
p_{1r}, p_{2r}, p_{3r}	instantaneous pressures in chambers I, II, III of right strut, respectively
$p_{1\ell 0}$, p_{1r0}	static gas pressure of left and right chamber of 1st strut interconnected suspension at design ride height
$p_{2\ell 0}$, p_{2r0}	static gas pressure of left and right chamber of IInd strut interconnected suspension at design ride height
$p_{3\ell 0}$, p_{3r0}	static gas pressure of left and right chamber of IIIrd interconnected suspension at design ride height
$p_{3\ell c}$, p_{3rc}	charge pressure in III, left and right accumulator of suspension systems
$p_{2\ell 1r}$	pressure differential between chamber II of the left strut (II_ℓ) and chamber I of the right strut (I_r)
$p_{2r1\ell}$	pressure differential between chamber II of the right strut (II_r) and chamber I of the right strut (I_ℓ)
p_{23i}	pressure difference across the orifice restriction of strut i
$p_{23v\ell}$, p_{23vr}	pressure differential across the left and right valve opening
$(p_{23i})_o$	preset pressure differential of strut i; i= (ℓ, r)
p_a	atmospheric pressure
p_c	initial charge pressure
p_o	static fluid pressure at design ride position
$Q_{1\ell}$, Q_{1r}	volume flow rate in chamber I of left and right struts,
$Q_{2\ell}$,Q_{2r}	volume flow rate in chamber II of left and right struts
$Q_{23\ell}$,Q_{23r}	volume flow rate from chamber II to III of left and right struts
$Q_{2\ell 1r}$	volume flow rate from chamber II_ℓ to chamber I_r of left and right struts

$Q_{2r1\ell}$	volume flow rate from chamber II_r to chamber I_ℓ of left and right struts
r	length of trailing lever
R	Reynolds number
sgn(○)	sign function
v_{3lc}, v_{3rc}	initial charge pressure in III, left and right chamber of suspension unit
$\Delta V_{3\ell}$, ΔV_{3r}	small change in volume in accumulator due to road disturbance
$v_{3\ell o}$, v_{3ro}	static gas volume of left and right struts in the interconnected suspension at design ride height
W	static load due to sprung mass on suspension unit
w_ℓ, w_r	static load on left and right suspension units
x_s, x_u	vertical displacement of sprung mass and unsprung mass
x_{il}, x_{ir}	vertical road excitations (m) at the left and right tires, respectively
y	vertical displacement between left and right end of anti-roll bar
Z_ℓ, Z_r	relative displacements across the left and right suspension struts, respectively
$\dot{Z}_\ell$, $\dot{Z}_r$	relative velocities across the left and right suspension struts, respectively
ψ	piston area ratio
δ_1, δ_2	static deflection in rear left and right tires
δ_f	static deflection in load supporting spring
$\delta_{1\ell}$, δ_{1r}	static deflection across the left and right struts
δ_i	static deflection in hydraulic strut
δ^*	effective static deflection of an independent strut under equal load

δ^{**}	effective static deflection of an interconnected strut under equal load
θ_s, θ_u	generalized coordinates represent the roll angles of the sprung mass and unsprung masses, respectively
α	damping force coefficient
β	damping parameter
ζ	system spring stiffness ratio
λ	pressure differential ratio across the left and right orifice restrictions
γ	tuning factor of pressure limiting interconnected hydraulic damper
ϱ	mass density of fluid
μ	dynamic viscosity of fluid
ω	angular frequency (rad/s)
ω_n	angular undamped natural frequency of the isolator (rad/s)

CHAPTER 1

INTRODUCTION AND LITERATURE REVIEW

1.1 GENERAL

Suspensions are used in vehicles to support the load, protect the passengers from shock and vibrations arising from tire and road interaction, and to provide the directional stability and yaw control of the vehicle. However, all these objectives require conflicting parameters and are difficult to achieve. The suspension systems are thus designed to achieve a compromise among these conflicting requirements. The prime objective of using suspensions is to improve the ride quality, directional stability and handling of the vehicle. Vehicle suspension requires soft spring for comfortable ride, while hard springs are needed to attain good handling and directional control. Anti-roll bars are frequently used with non-linear springs to achieve enhanced directional stability without affecting pure bounce motions. Anti-roll bar, however, has significant effect on the ride quality under one wheel bump. Alternatively, diagonally interconnected hydro-pneumatic suspension in roll plane has the potential to enhance roll stiffness as well as damping while maintaining soft characteristics for ride.

A previous investigation [1] of hydro-pneumatic interconnected suspension has demonstrated its enhanced roll stiffness and damping properties. The study further demonstrated the inherent difficulties associated with initialization of pure hydro-

pneumatic struts for suspension, as it violates the work space criteria. It was found that the dimensions for strut diameter and accumulator as well as the pressure buildup in such system is highly excessive and impractical from both design and maintenance point of view [2].

In order to realize the potential benefits of interconnected hydro-pneumatic suspensions it is necessary to introduce a parallel mechanical springs for support of the load. However, it is expected that a compromise will be needed in selecting spring stiffness or the percentage load carried by the spring in order to ensure effectiveness of the hydro-pneumatic interconnection.

In this dissertation, a detailed roll plane model of vehicle with beam axle incorporating hydro-pneumatic interconnected suspension with parallel springs is developed. The model is extensively analyzed to examine the influence of percentage load carried by the spring on the maximum pressure, strut parameters as well as the suspension properties. For a selected configuration and vehicle parameters, the model is simulated to evaluate dynamic performance characteristics under bounce and roll inputs. Results are compared for various suspension configurations and with those of unconnected systems. Along with fixed orifice damping the performance is analyzed for variable sequential damping.

1.2 REVIEW OF RELEVANT LITERATURE

Various types of passive, semi-active and active vehicle suspensions have been proposed and analyzed using a variety of analytical and experimental techniques. Ride, handling and directional control of various vehicle suspensions have been widely investigated in attempts to improve the performance characteristics of the suspension. A review of relevant literature related to interconnected suspensions, variable damping as well as performance criteria are briefly discussed in the following subsections.

1.2.1 Interconnected Suspension System

In attempts to improve vehicle ride and handling performance and its conflicting requirements, various interconnected suspensions have been investigated over the years. The roll and pitch properties of a suspension can be varied considerably by employing the interconnection in-between the different wheel suspensions of a vehicle. The interconnection among the different wheel suspensions can be developed by using a mechanical, fluid or pneumatic coupling.

Mechanical coupling involves a mechanical interlink between the front and rear wheel suspensions to improve the ride quality by reducing the amplitude in pitch plane [3, 4, 5]. Three different mechanical interconnections between front and rear wheels are presented in Figure 1.1. In Figure 1.1(a) mechanical coupling is developed by using soft springs A and hard spring B between vehicle body D and lever C. Under pure vertical motions, the body and lever remain parallel to the road, thus suspension rate depends on

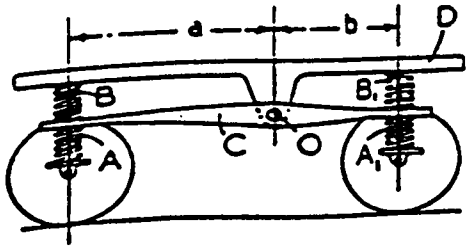

(a)

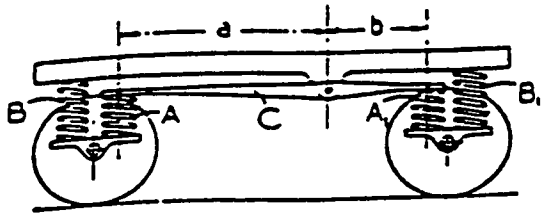

(b)

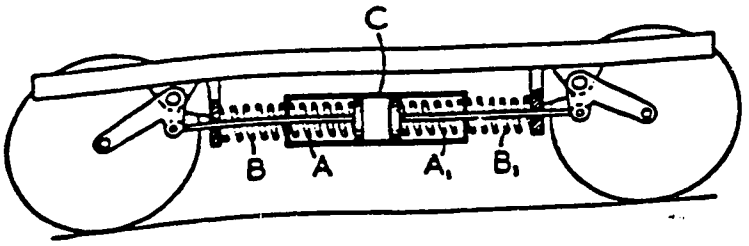

(c)

Figure 1.1 Mechanical interconnected front and rear wheel suspensions [4]

the stiffness of the spring. While in pitch motion vehicle body oscillates about point O, response of the body from the pitch motion depends on the stiffness of the spring B. Thus to obtain the desirable pitch and bounce frequency, appropriate spring rate of A and B are selected. Earlier suspension designs involved a soft spring B and a hard spring A to achieve lower pitch frequency than bounce frequency. Problem associated with this type of suspension is that it provides poor anti-pitch performance and yaw control during dynamic load shift.

In 1978, Moulton developed a rubber based interconnected hydroelastic suspension and then replaced rubber springs by gas springs in order to improve the standard of ride comfort [6, 7, 8]. As shown in Figure 1.2, a lever acts on the hydragas suspension through a ball joint on the lower suspension arm at a typical ratio of 4.5:1. This suspension unit has two hermetically sealed spherical chambers. The upper chamber is divided into two parts by using an elastic diaphragm. Top of the chamber is charged with compressed nitrogen gas in order to reduce the aeration problem, since gases obey the principle of Boyle's law ($P_1V_1 = P_2V_2$), which acts as a gas spring, and lower chamber is filled with hydraulic fluid. Nitrogen gas and working fluid are separated by butyl liner. The lower container comprising an elastic diaphragm is also filled with hydraulic fluid. The underside of the diaphragm is acted upon by a tapered displacer. The weight of the sprung mass is supported by the pressurized fluid acting on flexible diaphragm displacers. The damping is achieved due to fluid flow between the upper and lower

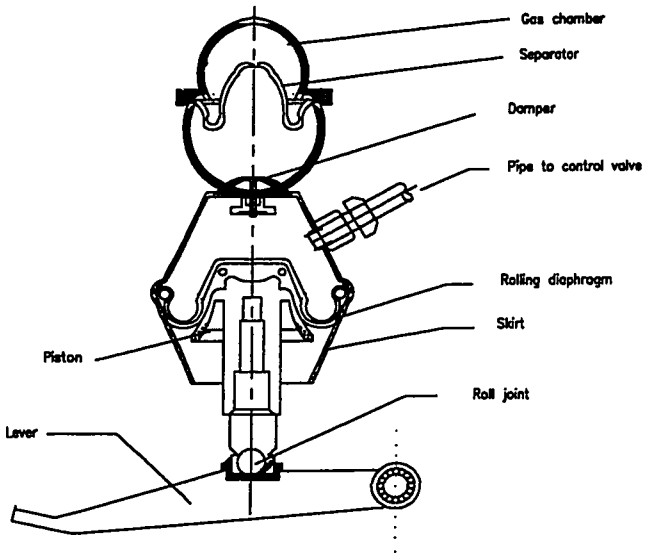

Figure 1.2 Moulton hydragas suspension unit [9]

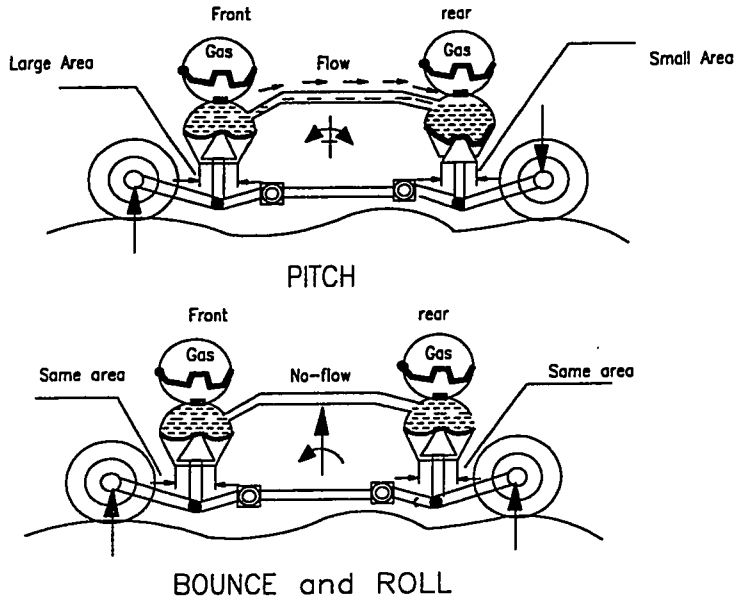

Figure 1.3 Fluid flow in interconnected suspension of a pitch plane vehicle model [9]

chambers via a leaf damper valve [9]. Figure 1.3 describes the interconnection between the front and rear suspensions. In the bounce and roll modes both displacers on one side move together. No fluid flows occur between the suspensions, and as a result gas in an upper chamber is compressed increasing the suspension rate; while in pitch mode, the fluid flows between the suspension units, resulting in low pitch rate. Although the interconnected Moulton suspension resulted in improved ride in pitch mode, it was more sensitive to dynamic load shift during acceleration and breaking action.

Another type of passive and active hydraulic interconnections have been analytically modeled by Felez and Vera [10]. In this model hydraulic coupling is achieved by interconnecting the rear wheel suspensions diagonally as shown in Figure 1.4. The mathematical models were analyzed to evaluate the vehicle response under vertical and roll displacement. The study demonstrated improved anti-roll characteristics of the interconnected suspension.

Interconnected suspension can be incorporated with variable damping and self-leveling capacity in order to achieve improved performance of a vehicle. Tanahashi et al. [11] proposed and investigated an interconnected and feedback modulated hydro-pneumatic suspension. The experimental and analytical approaches indicate that enhanced vehicle control and ride comfort characteristics can be easily achieved.

Various active vibration isolation systems comprising controlled hydraulic actuators

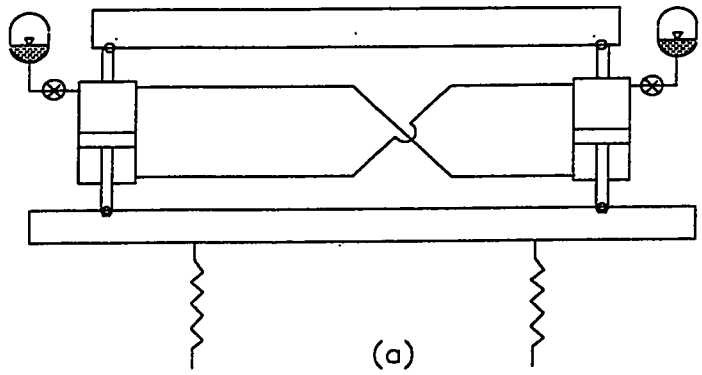

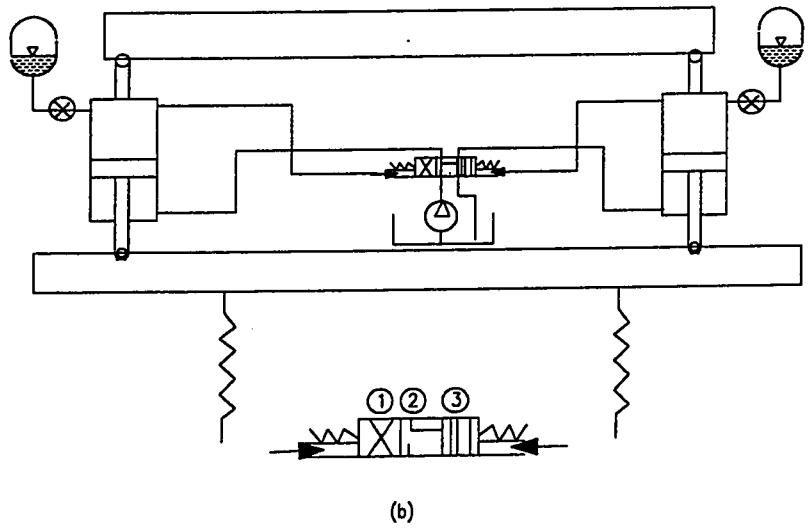

Figure 1.4 Schematic of interconnected hydro-pneumatic suspension configurations (a) passive (b) active suspensions [10]

and mechanical servo-valves, have been proposed and investigated by Sutton [12], Coterrell [13] and Dominy and Bulman [14]. The analysis of active hydraulic actuators, controlled by a servo-valve employing a mechanical linkage feedback mechanism demonstrated that the sprung mass response to bump excitations can be minimized while maintaining a constant ride attitude [15]. However, high power consumption of an active suspension has limited its general use in vehicle application.

Recently, practical hydro-pneumatic slow active systems have been used [16], which are designed to improve the ride comfort and maneuverability. Results show that this suspension unit permits a good design compromise between the conflicting requirements of ride comfort and, suspension working space, and also influences the bounce, pitch and roll stiffnesses. These systems have a low bandwidth capability, using a low external power consumption and representing a compromise between passive and fully active systems.

After recognizing the superior anti-roll capability of diagonally interconnected hydro-pneumatic suspension in roll plane, the vehicle suspension interconnected in pitch plane have been attempted to achieve the improved anti-pitch performance [17, 18, 19]. Figure 1.5 shows the schematic of a semi-active hydro-pneumatic suspension interconnected in the pitch as well as roll plane, studied by Crolla and Horton [20]. In pitch plane, upper chambers of front axle suspension struts are connected to the lower chambers of the rear suspension struts, and the upper chambers of the rear suspension struts are connected laterally. Inertial control valves, as shown in Figure 1.6, were

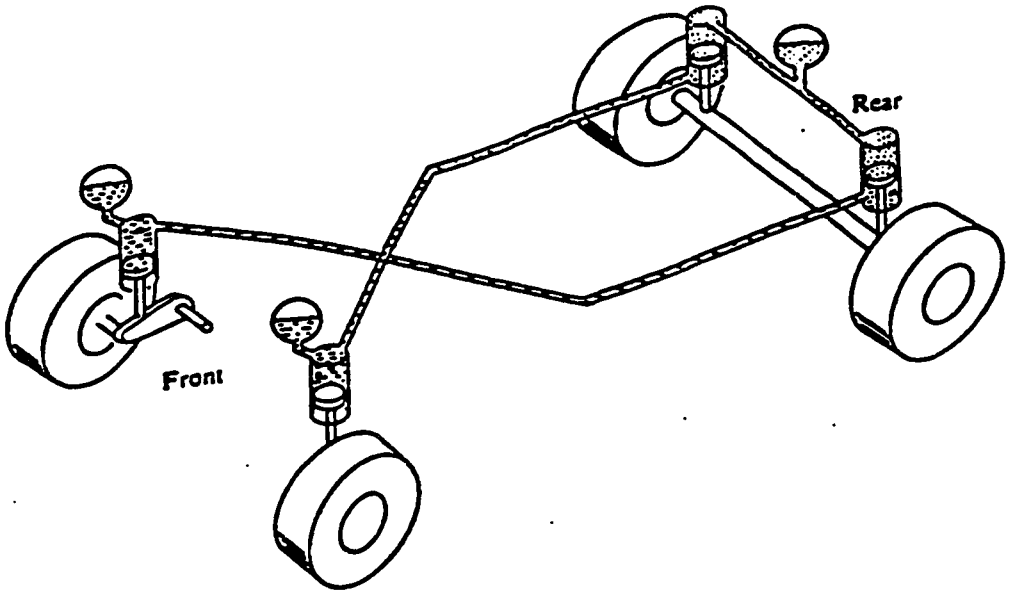

Figure 1.5 Schematic of the AP suspension interconnected in the pitch and roll planes [20]

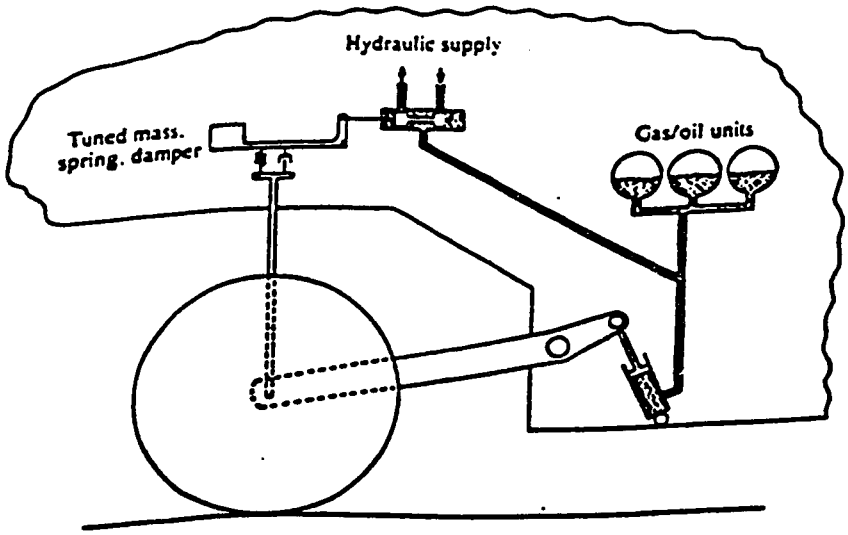

Figure 1.6 Schematic diagram of a single wheel station of AP suspension [20]

implemented to achieve soft response to road irregularities, and hard response to vehicle maneuvers to attain attitude control and self- leveling. The results of the analytical and experimental studies show enhanced ride comfort and attitude control of the vehicle.

1.2.2 Variable Suspension Damping

In view of the inherent performance limitations of fixed orifice suspension, many multi-stage and variable damping mechanisms have been proposed. The analytical models of various multi-stage shock absorbers have been presented in literature and are widely used in practice.

Sireteanu [21] developed a sequential damper to control the magnitude of damping within a cycle. The experimental results represent improved ride comfort and attitude control of the vehicle. Van Vliet [22] developed analytical model of hydraulic shock absorber with a fixed relief valve. The main function of the valve was to open during compression stroke in order to limit the magnitude of damping force. The damping characteristics of variable dampers have been analyzed by Asami et al [23] and Hundal [24]. Rakheja, Sankar, and Su [25, 26, 27] proposed and analyzed a tunable passive sequential hydraulic damper shown in Figure 1.7 to achieve variable damping within vehicle suspension. The sequential damping was realized by implementing compression and rebound pressure relief valves to the fixed orifice hydraulic damper. The analytical model incorporating the non- linearity's due to valve dynamics, fluid compressibilities and turbulent fluid flows through orifices was analyzed for deterministic excitations. The results reveal that the tunable sequential damper offered

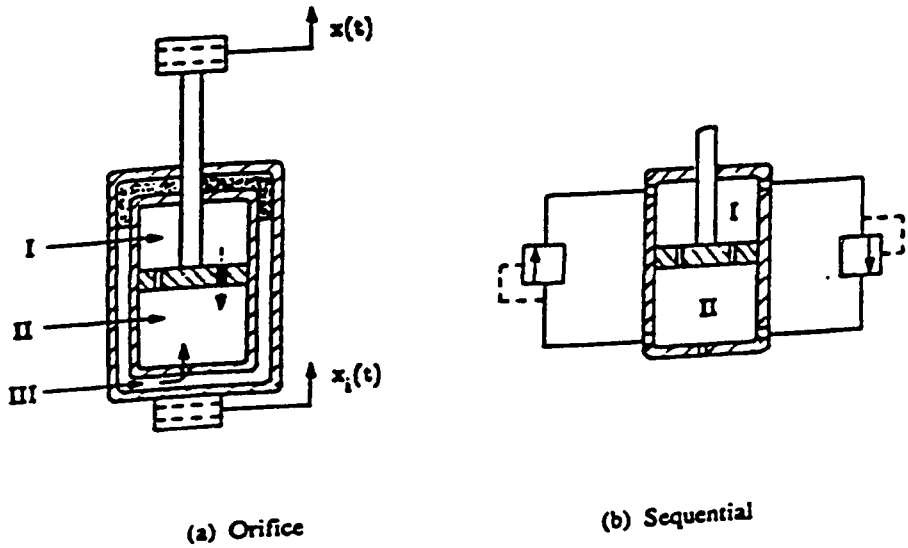

Figure 1.7 Schematic of the conventional and sequential hydraulic dampers [26]

considerable potential to improve the vehicle ride comfort.

A three -stage adjustable shock absorber was developed by Nissan Co. Ltd., which has a passive spring combined with a variable-rate damper as shown in Figure 1.8. The damper can be controlled externally by driver to select the best damping property for various driving conditions [28, 29, 30]. Toyota motor corporation developed an improved suspension with three different control modes, which can be selected by the drivers; normal mode, sport mode and auto mode [31, 32]. In normal mode, the damping force of shock absorber was kept relatively small, while in the sport mode damping force was relatively high. In auto mode the damping force of shock absorbers was automatically varied in between the normal mode and sport modes based upon the feedback received from the tire-terrain interface. Poyser has described an adaptive suspension control system that uses simple valve and micro processor control. In this system a computer controlled the spring rate according to load conditions to provide constant ride frequency. The fast response of damping valves reveals good ride vibration isolation and handling characteristics [33, 34]. Ford motor Co. [35] developed a program based suspension called programmed ride control (PRC) suspension. Rock switch is used to achieve the firm and automatic mode . In automatic mode, the computer adjusts the shock absorber damping force to provide a soft ride during normal driving conditions. However, damping changes to firm during hard cornering, breaking or acceleration to achieve improved handling of vehicle.

Active vehicle suspension units in which parameters change automatically with

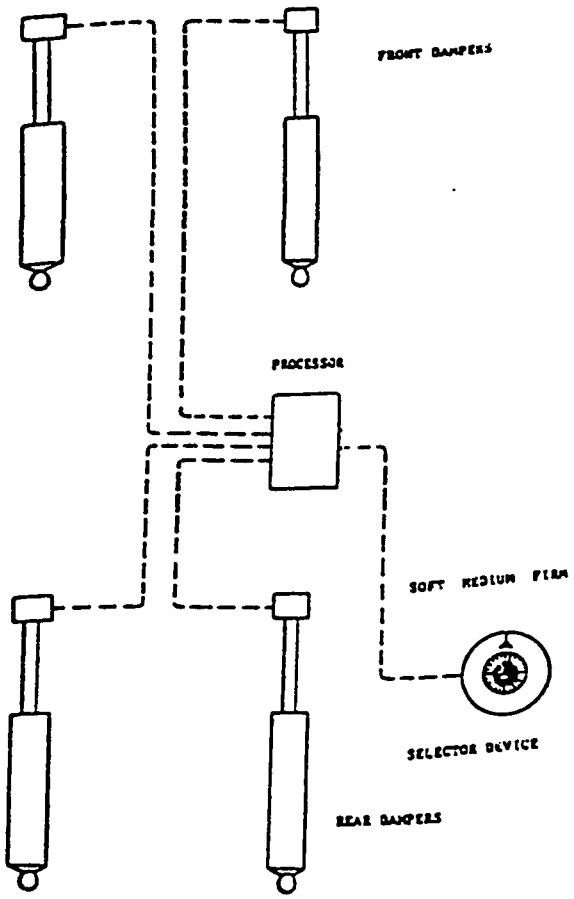

Figure 1.8 Adjustable System [28]

variations in road profile, provide superior shock and vibration isolation performance, have also been extensively investigated. Two forms of active suspensions are commonly recognized [36]: high bandwidth active suspension and low bandwidth active suspension. In high bandwidth active suspension the actuator sits parallel with the road spring, between the body and unsprung mass. In low bandwidth active suspension the actuator sits in series with the road spring and controls the body motion, while unsprung mass is controlled by the passive damper. Oley [37] developed a low bandwidth pneumatic spring and damper suspension unit to improve the ride comfort of the luxury cars. In this suspension, the spring, damper and active actuator form a single unit. Idea behind selecting low bandwidth system was that it required high quality, low cost automotive components; while a high bandwidth system requires very precise technology to control the motion of sprung and unsprung masses. Although, active suspensions bring improvements in ride comfort and vehicle handling, the requirement of external energy source and large number of control systems and sensors limit the application of active suspensions in ordinary vehicles.

Recently active roll control system for the interconnected hydragas suspension has been analytically studied by Rosam and Darling [38, 39, 40]. Actively interconnected hydragas suspension has fluid displacers to control the body roll during lane change maneuvers or any sharp cornering. The main feature of this suspension system is that a modest control system bandwidth is required for effective roll control during fast transient maneuvers. Therefore cost of the actuation system is considerably lower than that of a fully active system. In addition, due to presence of the fluid interconnection

between the front and rear suspension units of the hydragas car, only one actuator (or shuttle) is required to control body roll motion; generally four actuators are necessary for a fully active system. It also compares favorably with active roll bar systems which require two actuators to ensure satisfactory front /rear lateral load transfer distribution during maneuvers. Semi-active suspensions offer a compromise between the performance benefits of an active and passive suspension. A number of semi-active damping mechanisms have been proposed and investigated [41, 42, 43, 44, 45].

1.2.3 Performance Criteria

In vehicle system dynamics various performance criteria have been proposed in order to assess the ride comfort and handling performance of different vehicle suspensions. Root mean square value of vertical acceleration of vehicle body at passenger and driver location is recommended by ISO to evaluate the ride performance of ground vehicles [46, 47, 15]. Alternatively, acceleration PSD of body response and vibration transmissibility are also used to assess the relative ride performance of different suspensions [48]. There are many other methods to evaluate handling performance of a vehicle. Although oversteer and understeer characteristics are commonly used to assess the steady state handling behavior of vehicles, the response parameters, such as tire slip angles, wheel load fluctuations, yaw rate, and vehicle path have been employed to carry out relative performance evaluations of different suspensions [49, 50]. While ride quality can be evaluated directly from the vertical or bounce response characteristics of the vehicle, the handling performance is significantly more complex. Roll response of the vehicle,

however, has direct influence on the handling performance and is often used as a measure of handling.

1.3 SCOPE OF PRESENT INVESTIGATION

A detailed review of literature on interconnected and hydro-pneumatic suspensions clearly demonstrate the potential of such system for design compromise between ride and handling performance. Interconnection in the roll plane has the most potential as it enhances both stiffness and damping in the roll mode with minimum influence on bounce. Such systems are obviously desirable for heavy passenger vehicles such as buses where ride is very important while roll control is essential due to high c.g. of sprung mass. Hydro-pneumatic interconnected suspension in roll plane, therefore, has the potential to improve ride and handling performance of buses.

The literature review further reveals that pure hydro-pneumatic suspension for heavy vehicle is not practical as it requires large number of struts or struts and accumulators of very large diameter. The dynamic pressure buildup in such system is also highly excessive which will impose serious design problems.

The potential benefit of such system for bus application can however, be realized by introducing a mechanical spring in parallel with the struts to carry partial load of the vehicle. Since the rate of the mechanical spring will influence the effectiveness of the interconnection, it must be selected carefully through a parameteric study.

For any given mode, since the response must be isolated in a wide range of input and frequency, active and semi-active system have been widely investigated as discussed in the previous sections. Although their potential is promising, their application in general purpose vehicles are not yet possible due to demand on power, cost, complexity and maintenance. Passive system such as variable sequential damper has the demonstrated potential for significant performance improvement over the fixed damper. Such damping can be easily incorporated in a spring loaded interconnected hydro-pneumatic suspension system proposed in this investigation.

1.3.1 Objective of Present Investigation

The prime objective of this research work is to develop a realistic mathematical model of a vehicle suspension in roll plane incorporating a set of hydro-pneumatic struts and passive springs where the struts are hydraulically interconnected in the roll plane. Fixed and variable orifice restriction in a passive manner is further introduced in proposed vehicle suspension model in order to achieve enhanced ride comfort and body roll control. The specific objectives of this thesis are:

(1) To develop roll plane models of vehicles incorporating mechanical springs, set of hydro-pneumatic struts, hydraulic interconnection and variable orifice damper.

(2) To analyze the inherent static and dynamic properties of the interconnected suspension system in terms of suspension rates, roll stiffness, and damping force

characteristics for variation in system parameters and stiffness of mechanical spring.

(3) To evaluate the vibration isolation performance and roll response of the vehicle employing interconnected suspension for deterministic excitations arising from road irregularities, and directional maneuvers.

(4) To evaluate and compare suspension performance with and without tunable sequential damping for deterministic road excitations.

1.3.2 Organization of the Thesis

In chapter 2, spring loaded independent hydro-pneumatic suspension system and interlinked suspension unit is analytically modeled in the roll plane. The roll plane model of the vehicle is represented by a four-degree-of-freedom dynamical system under excitations arising from tire-terrain interface and roll moment caused by directional maneuvers. The equations of motion for the vehicle models are derived in terms of generalized suspension forces using Lagrange's equations. The generalized suspension forces are derived assuming incompressible fluid in hydraulic struts, turbulent flows through the orifice restrictions, polytropic process of gas in accumulators, and laminar flows within the interconnecting pipes.

The static and dynamic properties of spring loaded independent and interlinked hydro-pneumatic suspensions are derived and presented in chapter 3. The suspension properties are expressed in terms of their suspension rate, roll stiffness and damping

forces. Analytical expressions are derived to characterize the force -relative displacement and force-relative velocity characteristics of the suspension unit. The influence of mechanical spring on the overall dynamic property is evaluated and examined to select a baseline configuration.

In chapter 4, ride performance characteristics of baseline hydro-pneumatic suspension is investigated for deterministic road excitations using fourth order Runge-Kutta approach. The nature of excitations arising from tire-terrain interaction and steering inputs are described. The roll performance characteristics of the suspension system is evaluated in terms of transient and steady state roll response of the sprung and unsprung masses subjected to constant radius turning and lane change maneuvers. Vibration transmissibility characteristics of different suspension configurations are investigated and computed.

In chapter 5, a passive limiting control approach is proposed to achieve the variable sequential damping in a interlink hydro-pneumatic vehicle suspension system. The pressure limiting valve may be opened during the compression or extension strokes under preset pressure in order to allow fluid flow through the valve opening restriction and consequently reduce the damping force. The vibration isolation performance of the vehicle suspension employing variable damping is further investigated for deterministic road excitations.

High lights of the study, important conclusions and a set of recommendation for further study are summarized in chapter 6.

CHAPTER 2

ANALYTICAL MODEL OF ROLL PLANE VEHICLE SUSPENSION

2.1 INTRODUCTION

Design of a passive vehicle suspension involves a compromise among the performance characteristics related to ride comfort, suspension working space, static and dynamic attitude control, handling and directional control. The primary design requirement is to develop a suspension unit which provides adequate ride comfort and directional control. Soft springs are inherently more capable to isolate the vehicle body from the effects of road irregularities, while hard suspensions are desired for control. These conflicting requirements often result in a compromise between handling performance and ride comfort. In case of heavy freight vehicles, due to their poor directional stability limits, the suspension systems are designed in such a manner as to provide improved handling, directional control and stability at the expense of ride comfort [51]. In highway buses, an equal emphasis is placed on the ride comfort of passengers, as well as handling, directional control and stability of the vehicle [52]. In order to improve the directional control during cornering, anti-roll bars are preferred in mechanical coupled and hydraulic coupled suspensions. Alternatively, hydraulic coupling can be developed between laterally interconnected hydro-pneumatic struts in roll plane in order to achieve the enhanced roll stiffness. As discussed in section 1.3, there are practical limitations in using

pure hydro-pneumatic struts in application of heavy vehicle such as buses, and parallel springs are proposed in this investigation.

In this chapter, spring loaded independent hydro-pneumatic struts with and without anti-roll bar, as well as interlinked hydro-pneumatic struts with parallel springs are presented. Mathematical models for these suspension configurations are developed to investigate their overall characteristics and influence on vehicle performance.

2.2 INDEPENDENT HYDRO-PNEUMATIC STRUTS WITH PARALLEL SPRINGS

Several investigations have been carried out on vehicle models ranging from a simple two DOF quarter vehicle to three-dimensional dynamical models with several DOF in order to assess the ride, handling and directional control characteristics of vehicle systems. A simple 2-DOF vehicle model provides the ride performance only in the vertical direction. A four-DOF roll plane model as shown in Figure 2.1 can be used to evaluate vehicle performance in vertical and roll modes. In the following subsection, 4-DOF roll plane model of a highway bus, equipped with independent hydro-pneumatic struts and mechanical springs is developed to study its vertical as well as roll characteristics.

2.2.1 Equation of Motion of Spring Supported Independent Hydro-pneumatic Suspension Unit

Vehicle model in roll plane as shown in Figure 2.1, has load supporting parallel springs along with hydro-pneumatic struts and beam axle. As illustrated, it is a four-degree-of-

freedom roll plane model having vertical and roll motions of the sprung mass and unsprung mass. The vertical motion of the sprung mass and unsprung mass, respectively, are denoted by x_s and x_u, while the roll motion of sprung mass and unsprung mass, respectively, are denoted by θ_s and θ_u. The sprung and unsprung masses of the vehicle are lumped separately and denoted by m_s and m_u, respectively. The tires are modeled as a combination of parallel springs $K_{t\ell}, K_{tr}$ and dampers $C_{t\ell}, C_{tr}$ and it is assumed that tires have point contact with the road. The vertical road inputs at the tire-terrain interfaces under left and right tire, respectively, are denoted by $X_{i\ell}$, X_{ir}.

As shown in Figure 2.1, primary vehicle suspension comprises of parallel load supporting springs with independent hydro-pneumatic suspension struts. The forces generated by the left and right unit of the suspension system are represented by strut forces $F_{f\ell}, F_{fr}$, and spring forces. It is assumed that height of roll center of vehicle with respect to the c.g. of sprung mass and unsprung mass remain unchanged. The differential equations of motion for the 4-DOF system are derived and presented below:

Equation of motion in bounce mode for sprung mass:

For dynamic equilibrium of forces in vertical direction,

$$m_s\ddot{x}_s = F_{fl} + F_{fr} - K[x_s - \theta_s L_\ell - x_u + \theta_u L_\ell - \delta_f] - K[x_s + \theta_s L_r - x_u - \theta_u L_r - \delta_f] - m_s g \qquad (2.1)$$

where L_ℓ and L_r are lateral distance of left and right struts from the c.g., and δ_f is the static deflection.

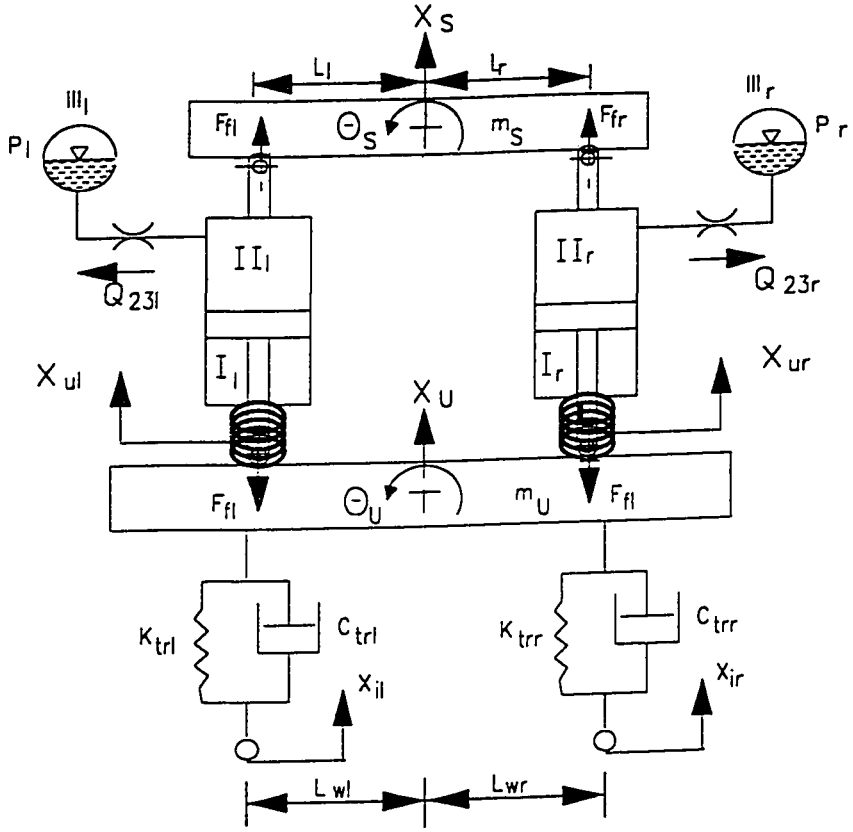

Figure 2.1 Roll plane model of spring loaded independent hydro-pneumatic suspension for a beam axle.

Equation of motion of sprung mass in roll mode:

Considering dynamic equilibrium of moments about the centroid of the vehicle,

$$I_S\ddot{\theta}_S = -F_{\ell t}L_\ell + F_{rr}L_r + K[x_s - \theta_s L_\ell - x_u + \theta_u L_\ell - \delta_f]L_\ell - K[x_s + \theta_s L_r - x_u - \theta_u L_r - \delta_f]L_r - T_\theta \qquad (2.2)$$

where I_s is the mass moment of inertia of the sprung mass. The term 'T_θ' in this equation represents an external moment resulting from lateral acceleration during lane change maneuver or steady steering. Generally the lateral acceleration causes a roll motion of sprung mass around its roll center as shown in Figure 2.2. Taking moment about roll center of sprung mass, the roll moment $T_\theta^{'}(t)$, due to the lateral acceleration a_y, can be expressed as:

$$T_\theta^{'}(t) = m_s a_y h_2$$

Due to lateral shift of the sprung mass c.g. under roll 'ϕ_s' there is additional overturning moment $T_\theta^{''}(t)$, which for small angle can be expressed as:

$$T_\theta^{''}(t) = m_s g \phi_s h_2$$

where h_2 is the distance of c.g. from the roll centre of sprung mass. The total overturning moment experienced by the sprung mass under a lateral acceleration is therefore:

$$T_\theta(t) = T_\theta^{'}(t) + T_\theta^{''}(t) \qquad (2.2.1)$$

Equation (2.2.1) reveals that vehicles that experience a large roll motion due to smaller roll stiffness will be subjected to larger moment under same lateral acceleration.

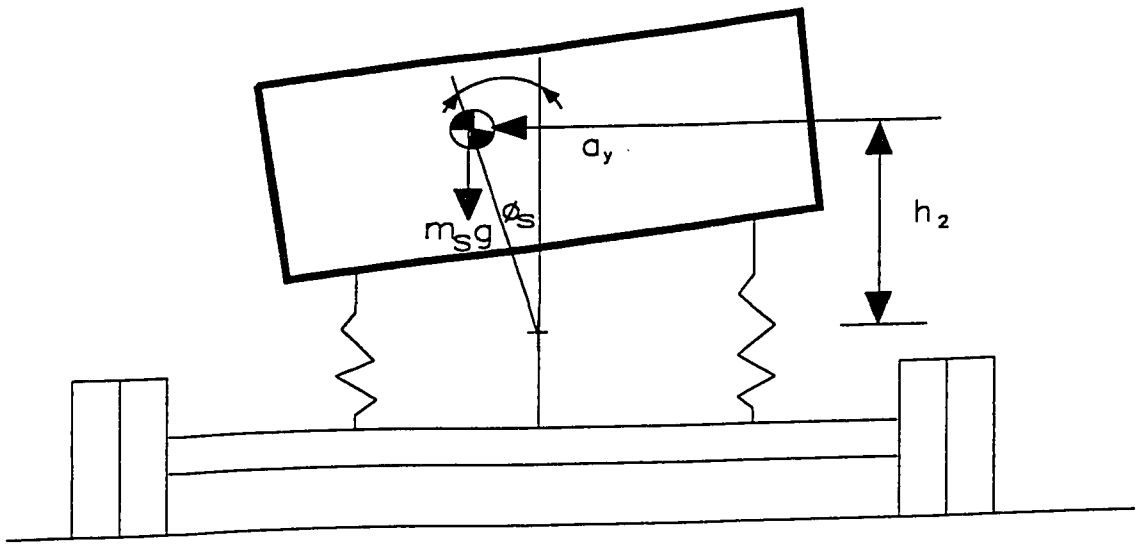

Figure 2.2 Lateral acceleration excitation to roll plane vehicle model during turning maneuvers

Equation of motion of unsprung mass in bounce mode:

Sum of vertical forces acting on the unsprung mass lead to:

$$
\begin{aligned}
&m_u\ddot{x}_u = -F_{f\ell} - F_{fr} - K[x_u - \theta_u L_f - x_s + \theta_s L_\ell + \delta_f] \\
&-K[x_u + \theta_u L_r - x_s - \theta_s L_r + \delta_f] - K_{tr\ell}(x_u - x_{i\ell} - \theta_u L_{w\ell} - \delta_1) - C_{tr\ell}(\dot{x}_u - \dot{x}_{i\ell} - \dot{\theta}_u L_{w\ell}) \\
&-K_{trr}(x_u - x_{ir} + \theta_u L_{wr} - \delta_2) - C_{trr}(\dot{x}_u - \dot{x}_{ir} + \dot{\theta}_u L_{wr}) - m_u g
\end{aligned}
\tag{2.3}
$$

where $L_{w\ell}$ and L_{wr} are half track width for left and right tire, respectively. δ_1, δ_2 represent the static deflection of the left and right tire, respectively.

Equation of motion of unsprung mass in roll mode:

Sum of moments about the c.g. of unsprung mass lead to:

$$
\begin{aligned}
&I_u\ddot{\theta}_u = F_{f\ell}L_f - F_{fr}L_r - K[x_u - \theta_u L_f - x_s + \theta_s L_f + \delta_f]L_\ell + K[x_u + \theta_u L_r - x_s - \theta_s L_r + \delta_f]L_r \\
&-K_{tr\ell}(x_u - x_{il} - \theta_u L_{wf} - \delta_1)L_{wf} + K_{trr}(x_u - x_{ir} + \theta_u L_{wr} - \delta_2)L_{wr} \\
&-C_{tr\ell}(\dot{x}_u - \dot{x}_{il} - \dot{\theta}_u L_{wf})L_{w\ell} + C_{trr}(\dot{x}_u - \dot{x}_{ir} + \dot{\theta}_u L_{wr})L_{wr}
\end{aligned}
\tag{2.4}
$$

where I_u is the mass moment of inertia of the unsprung mass. K_{tr} and C_{tr} in the above equations represent the tire stiffness and damping, respectively.

2.2.2 Unconnected Suspension Forces

Various forces developed by unconnected spring loaded suspension include: Damping forces due to orifice restriction between top chamber and accumulator; and restoring forces due to gas spring of the accumulator and mechanical spring. The masses of the systems oscillate about the static equilibrium position dictated by the static deflection. In the following sub-sections, equations of static equilibrium, effective suspension stiffness, fluid flow in the struts and expression for strut forces are developed.

Static Equilibrium Equations

Static loads acting upon the left and right suspension struts and on the parallel springs, are balanced by the internal pressures in the left and right chambers of struts and linear springs of the independent suspension unit. Identical static pressures are assumed in all the three chambers as shown in Figure 2.1, of the struts ($p_{3\ell 0} = p_{2\ell 0} = p_{1r0}$; $p_{3r0} = p_{2ro} = p_{1\ell 0}$) and polytropic process is used to relate the charge pressures in left and right suspension struts to the static loads W_ℓ and W_r.

Static load due to sprung mass on left and right strut:

Static load on the left and right strut can be expressed as:

$$W_\ell = P_{2\ell o}A_{2\ell} - P_a A_{2\ell} \tag{2.5}$$

$$W_r = P_{2ro}A_{2r} - P_a A_{2r} \tag{2.6}$$

where $P_{2\ell o}$ and P_{2ro} are the static pressure in chamber II of the left and right struts. $A_{2\ell}$ and A_{2r} are the piston head side areas of left and right struts, respectively and P_a is the atmospheric pressure. The static pressure and volume in chamber III of left and right strut can further be related to charge pressure and volume as:

$$P_{3\ell o}V_{3\ell o}^n = P_{3\ell c}V_{3\ell c}^n \tag{2.7}$$

$$P_{3ro}V_{3ro}^n = P_{3rc}V_{3rc}^n \tag{2.8}$$

where $P_{3\ell o} = P_{2\ell o}$ and $P_{3ro} = P_{2ro}$

The change in chamber III volume due to static load can now be expressed as:

$$\Delta V_{3f} = V_{3fc} - V_{3fo} \tag{2.9}$$

$$\Delta V_{3r} = V_{3rc} - V_{3ro} \tag{2.10}$$

The static deflection of the suspension struts, $\delta_{1\ell}$, δ_{1r} are derived as functions of the volume changes of the gas chamber under static equilibrium condition and are given by:

$$\Delta V_{3f} = A_{2\ell}\delta_{1\ell} \tag{2.11}$$

$$\Delta V_{3_r} = A_{2r}\delta_{1r} \tag{2.12}$$

For symmetric vehicle with identical struts, the static pressure in all chambers will be equal to P_0, equations (2.5 and 2.6) can therefore, be simplified to:

$$W_f = W_r = (P_o - P_a)A_2 \tag{2.13}$$

where A_2 is the piston side area for each strut. Further, the static and charge volume can be related to static deflection from equations (2.9 and 2.12) which for symmetric case yield:

$$V_0 = V_c - A_2\delta_f \tag{2.14}$$

where $\delta_f = \delta_{1f} = \delta_{1r}$

The derivations so far assume that the total load of the vehicle is carried by the struts which has been found to generate excessive dynamic pressure and requires general struts [1].

A parallel spring with the strut is therefore, introduced in this study. The load in this case is shared by the strut and spring. The static deflection of sprung mass δ_f will, therefore, be dictated not only by the strut but primarily by spring stiffness as it will support bulk of the load. The static deflection and corresponding spring and total effective stiffness will depend on the percentage load carried by each component. These parameters are next evaluated and presented in the following section.

Determination of Spring and Effective Suspension Stiffness

In order not to defeat the purpose of hydro-pneumatic suspension, the stiffness of the spring must be selected such that a percentage of load is carried by the strut. On the other hand, the percentage load carried by the strut must not lead to excessive size, dynamic pressure, or working space. Furthermore, the effective stiffness of the suspension should be such that for representative sprung mass, the natural frequency is in the range of 1.2 to 1.6 Hz. in order to satisfy human body comfort criteria.

For parallel combination of strut and mechanical spring with stiffness k, the static load on left and right suspension unit can be expressed by modifying equation (2.13) as:

$$W_\ell = W_r = (P_o - P_a)A_2 + K\delta_f \tag{2.15}$$

where δ_f is the static deflection of the suspension and P_o is the corresponding static pressure in the strut which has a piston area A_2. The static strut force:

$$F = (P_o - P_a)A_2 \tag{2.16}$$

can now be expressed in terms of charge pressure P_c, and volume V_c by substituting equation (2.7), which for symmetric case is:

$$F = \left(\frac{P_c V_c^n}{V_o^n}\right) A_2 - P_a A_2 \tag{2.17}$$

where V_0 is the volume at static ride height position of accumulator which can be expressed in terms of δ_f using equation (2.14):

$$F = \left(\frac{P_c V_c^n}{(V_c - A_2\delta_f)^n}\right) A_2 - P_a A_2 \tag{2.18}$$

The equivalent stiffness 'K_{eq}' of the hydro-pneumatic spring can now be estimated by using Taylor's expansion and determining variation of force with static deflection which yield:

$$\frac{\partial F}{\partial \delta_f} = \frac{n P_c A_2^2}{V_c} \tag{2.19}$$

Substituting for V_c equation (2.14), the equivalent stiffness of the strut can be expressed as:

$$K_{eq} = \frac{n p_c A_2^2}{V_o + A_2\delta_f} = \frac{\alpha m_s g}{2\delta_f} \tag{2.20}$$

where α is the percentage of sprung mass weight ($m_s g$) carried by the hydro-pneumatic strut.

The stiffness $\dot{K}$ for each of the mechanical spring can simply be expressed as:

$$K = \frac{(1-\alpha)m_s g}{2\delta_f} \tag{2.21}$$

where $(1-\alpha)$ is the percentage of sprung mass weight ($m_s g$) carried by the two springs.

Human body comfort criteria based on ISO standard require that bounce natural frequency of the sprung mass should be in the range of 1.2 to 1.6 Hz. A procedure is, therefore, adapted in selecting the spring stiffness K and strut parameters such that P_o, V_o, V_c, and A_2, are as described in the following.

First, the natural frequency 'f' of the sprung mass is selected in the desired range. Noting that the natural frequency of a vibrating system is related to static deflection as:

$$2\pi f = \sqrt{\frac{g}{\delta_f}} \tag{2.22}$$

the static deflection δ_f can be predetermined. For a given vehicle weight, and percentage assigned to the spring, the spring rate K can be determined from equation (2.21). Static deflection δ_f established by equation (2.22) is also used to determine K_{eq} of strut using equation (2.20). Equation (2.20) is further used in conjunction with equations, (2.7, 2.8, and 2.14) in an iterative manner to establish the strut parameters A_2, P_o, V_o, and V_c such that practical size, volume and work space requirement are satisfied.

The expressions for strut dynamic forces in equation of motion (2.1 and 2.4) are next established based on fluid flow equations as presented in the following subsection.

Fluid Flow Equations for Independent Hydro-pneumatic Strut

In independent suspension struts, the rate of change of fluid volume in chamber II can be expressed in terms of the deflection across the strut. Assuming incompressible fluid, the flow rates can be expressed as:

$$Q_{2\ell} = A_{2\ell}\dot{Z}_\ell; \quad Q_{2r} = A_{2r}\dot{Z}_r \tag{2.23}$$

where $Q_{2\ell}, Q_{2r}$ are the rate of change of fluid volume in chamber II of the left and right suspension strut, $\dot{Z}_\ell, \dot{Z}_r$ are the relative velocities across the respective struts, which in terms of system response can be expressed as:

$$\dot{Z}_\ell = \dot{x}_s - \dot{\theta}_s L_\ell - \dot{x}_u + \dot{\theta}_u L_\ell \tag{2.24}$$

$$\dot{Z}_r = \dot{x}_s + \dot{\theta}_s L_r - \dot{x}_u - \dot{\theta}_u L_r \tag{2.25}$$

Due to piston displacement in forward and backward strokes in suspension struts, fluid will flow through the left and right orifice restrictions into the left and right accumulators. Assuming turbulent fluid flow through the small orifice restriction, the flow rate from chamber II to chamber III can be expressed as:

$$Q_{23\ell} = C_d a_\ell \sqrt{\frac{2|P_{23\ell}|}{\varrho}}\,\mathrm{sgn}(P_{23\ell}); \quad \mathrm{sgn}(P_{23\ell}) = 1;\ \text{when } p_{23\ell} \geq 0$$

$$\mathrm{sgn}(P_{23\ell}) = -1;\ \text{when } p_{23\ell} < 0 \tag{2.26}$$

$$Q_{23r} = C_d a_r \sqrt{\frac{2|P_{23r}|}{\varrho}}\,\mathrm{sgn}(P_{23r}); \quad \mathrm{sgn}(P_{23r}) = 1;\ \text{when } p_{23r} \geq 0$$

$$\mathrm{sgn}(P_{23r}) = -1;\ \text{when } p_{23r} < 0 \tag{2.27}$$

where C_d is the discharge coefficient; a_ℓ, a_r are the left and right orifice areas; ϱ is the mass density of the fluid. $p_{23\ell}$, p_{23r} are the pressure differences across the left and right orifice restrictions. Sgn terms describe the direction of fluid flow. Using conservation of mass, volume flow rate can be expressed as:

$$Q_{2\ell} = -Q_{23\ell} \quad \text{and} \quad Q_{2r} = -Q_{23r} \tag{2.28}$$

Equations (2.26 and 2.27) can be rearranged to express pressure differential across the left and right orifice restrictions as:

$$P_{23\ell} = \frac{\varrho}{2}\left(\frac{Q_{23\ell}}{C_d a_\ell}\right)^2 \operatorname{sgn}(Q_{23\ell}) \tag{2.29}$$

$$P_{23r} = \frac{\varrho}{2}\left(\frac{Q_{23r}}{C_d a_r}\right)^2 \operatorname{sgn}(Q_{23r}) \tag{2.30}$$

After substituting for $Q_{23\ell}$ and Q_{23r} from equations (2.28 and 2.23) the pressure differentials across the left and right orifices are given by:

$$P_{23\ell} = \frac{\varrho}{2}\left(\frac{A_{2\ell}\dot{Z}_\ell}{C_d a_\ell}\right)^2 \operatorname{sgn}(A_{2\ell}\dot{Z}_\ell) \tag{2.31}$$

$$P_{23r} = \frac{\varrho}{2}\left(\frac{A_{2r}\dot{Z}_r}{C_d a_r}\right)^2 \operatorname{sgn}(A_{2r}\dot{Z}_r) \tag{2.32}$$

Instantaneous gas pressures in the accumulators are established by assuming polytropic process. For the left and right accumulators, the pressures in chamber III_ℓ and III_r are expressed as follows:

$$p_{3\ell} = p_{3\ell 0}\left(\frac{V_{3\ell o}}{V_{3\ell o} - V_{23\ell}}\right)^n \tag{2.33}$$

$$p_{3r} = p_{3r0}\left(\frac{V_{3ro}}{V_{3ro} - V_{23r}}\right)^n \tag{2.34}$$

where, $V_{3\ell O}, V_{3r0}$ are static volume in chambers III_ℓ, and III_r, respectively. $V_{23\ell}$, V_{23r} represent change of gas volume within the left and right accumulator of suspension, due to flow between chambers II and III. These changes in volume can be directly related to relative motion across the strut and piston head area A_2 as:

$$V_{23\ell} = \int Q_{23\ell} dt = A_{2\ell} Z_\ell \quad ; \; V_{23r} = \int Q_{23r} dt = A_{2r} Z_r \tag{2.35}$$

where relative motion across the struts are:

$$Z_\ell = x_s - \theta_s L_\ell - x_u + \theta_u L_\ell$$

$$Z_r = x_s + \theta_s L_r - x_u - \theta_u L_r$$

Dynamic Forces of Independent Hydro-pneumatic Damper

Pressures acting upon the pistons are considered with respect to the static equilibrium positions. The total dynamic suspension forces, F_ℓ and F_r developed at the left and right suspension units can be expressed as:

$$F_{f\ell} = (P_{2\ell} - P_{2\ell o})A_{2\ell} \tag{2.36}$$

$$F_{fr} = (P_{2r} - P_{2ro})A_{2r} \tag{2.37}$$

where $p_{2\ell} = p_{23\ell} + p_{3\ell}$ and $p_{2r} = p_{23r} + p_{3r}$, are the instantaneous pressures in accumulators. After substituting the values of $p_{23\ell}, p_{23r}$ and $p_{3\ell}, p_{3r}$ from equations (2.31) to equation

(2.35) the dynamic suspension forces generated by left and right struts can be expressed as:

$$F_{f\ell} = \frac{\varrho A_{2\ell}^3}{2C_d^2 a_\ell^2}\dot{Z}_\ell^2 \operatorname{sgn}(\dot{Z}_\ell) + p_{o\ell}A_{2\ell}\left[\left(\frac{v_{o\ell}}{v_{o\ell} - A_{2\ell}Z_\ell}\right) - 1\right] \tag{2.38}$$

$$F_{fr} = \frac{\varrho A_{2r}^3}{2C_d^2 a_r^2}\dot{Z}_r^2 \operatorname{sgn}(\dot{Z}_r) + p_{or}A_{2r}\left[\left(\frac{v_{or}}{v_{or} - A_{2r}Z_r}\right) - 1\right] \tag{2.39}$$

First term of these equations describe the non-linear damping force component related to square of the relative velocities across the suspension unit developed due to turbulent flow through the orifice restrictions. The second term describes the nonlinear restoring force due to the gas in the accumulators.

2.3 ROLL PLANE MODEL OF SPRING LOADED INTERCONNECTED HYDRO-PNEUMATIC SUSPENSION

A four-DOF roll plane model as shown in Figure 2.3 having vertical and roll motions of sprung and unsprung masses equipped with interconnected hydro-pneumatic dampers with mechanical springs is developed in order to study the effect of interconnection on vertical as well as roll characteristics.

Various components of the model are essentially same as these presented in section 2.2 for unconnected system. In this case of interconnected system, the top chamber of left strut (II_ℓ) is connected to bottom chamber of right strut (I_r) and vice versa as shown in Figure 2.3. The interconnections are made of hydraulic piping that allows

fluid flow from one chamber to the other. Due to cross interconnection, its primary influence is under roll motion when relative displacement is different from left and right struts. All assumptions made for unconnected suspension in section 2.2 are also valid for this model.

2.3.1 Equations of Motion

The equations of motion for the 4-DOF model are derived following identical approach as that of unconnected system and are essentially same as those presented in equations (2.1 to 2.4). In this case of interconnected system, however, the expression for left and right suspension forces (F_{fl}, F_{fr}) will be different than those for unconnected. These expressions are next formulated in the following subsection.

2.3.2 Interconnected Suspension Forces

Various forces developed by spring loaded hydro-pneumatic interconnection suspension units include: damping forces due to orifice restriction between top chambers and accumulators; forces due to fluid flow between left and right struts; and restoring forces due to gas in accumulators and linear mechanical springs. The suspension forces oscillate about its equilibrium dictated by the static equilibrium parameters. In the following subsections, equation of static equilibrium, fluid flow and suspension force are developed.

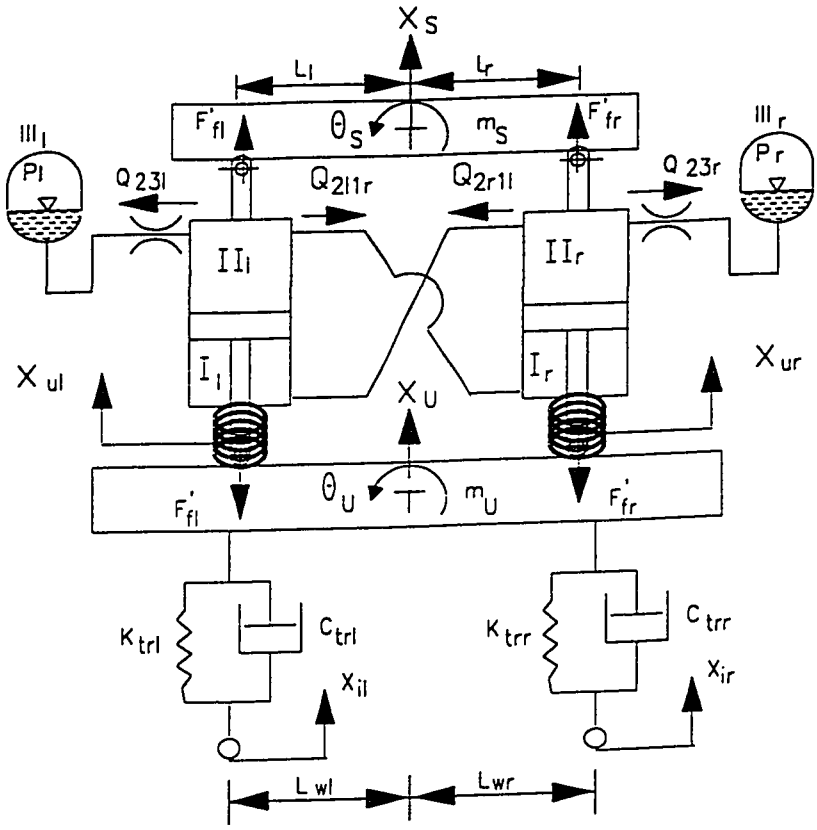

Figure 2.3 Roll plane model of spring loaded interconnected hydro-pneumatic suspension unit.

Static Equilibrium Equations

Static loads acting upon the left and right suspension struts are balanced by the internal pressures in the interconnected left and right chambers. Identical static pressure are assumed in the interconnected struts ($p_{3\ell o} = p_{2\ell o} = p_{1ro}; p_{3ro} = p_{2ro} = p_{1\ell o}$) and polytropic processs is used to relate the charge pressures in left and right suspension struts and static loads w_ℓ, w_r.

Static load due to sprung mass on left and right strut:

For the interconnected case, static load on the left and right strut can be related to the pressure as:

$$W_\ell = P_{2\ell o}A_{2\ell} - P_{1\ell o}A_{1\ell} - P_a(A_{2\ell} - A_{1\ell}) \tag{2.40}$$

$$W_r = P_{2ro}A_{2r} - P_{1ro}A_{1r} - P_a(A_{2r} - A_{1r}) \tag{2.41}$$

where $P_{2\ell 0}$ and P_{2r0} are the static pressure in chamber II of the left and right strut. $A_{2\ell}, A_{2r}$ are the piston side area of respective strut, where as $A_{1\ell}, A_{1r}$ are the corresponding rod side area. The static pressure and volume in left and right accumulator (chamber III) can be further expressed as:

$$P_{3\ell o}V_{3\ell o}^n = P_{3\ell c}V_{3\ell c}^n \tag{2.42}$$

$$P_{3ro}V_{3ro}^n = P_{3rc}V_{3rc}^n \tag{2.43}$$

where $P_{3\ell o} = P_{2\ell o}$ and $P_{3ro} = P_{2ro}$

Since the change in volume of accumulator (chamber III) can be expressed as:

$$\Delta V_{3\ell} = V_{3\ell c} - V_{3\ell o} \tag{2.44}$$

$$\Delta V_{3r} = V_{3rc} - V_{3ro} \tag{2.45}$$

The static deflection of the suspension struts, $\delta_{1\ell}, \delta_{1r}$, can be derived as functions of the volume changes and are given by:

$$\Delta V_{3\ell} = (A_{2\ell}\delta_{1\ell} - A_{1r}\delta_{1r}) \tag{2.46}$$

$$\Delta V_{3_r} = (A_{2r}\delta_{1r} - A_{1\ell}\delta_{1\ell}) \tag{2.47}$$

For symmetric vehicle with identical left and right suspension, the static pressure in all chambers will be equal to P_o. Equations (2.40 and 2.41) can therefore, be simplified to:

$$W_\ell = W_r = (P_o - P_a)(A_2 - A_1) \tag{2.48}$$

where A_2 and A_1 are piston and rod side area, respectively. Further, for the symmetric case, the static and charge volume in term of static deflection can be obtained using equations (2.44 to 2.47):

$$V_o = V_c - (A_2 - A_1)\delta_f \tag{2.49}$$

where $\delta_f = \delta_{1\ell} = \delta_{1r}$

The equations presented above are based on static equilibrium for load supported by the struts. With the introduction of parallel springs, the static equilibrium equation (2.48) becomes:

$$W_\ell = W_r = (P_o - P_a)(A_2 - A_1) + K\delta_f \tag{2.50}$$

A comparison of equations (2.15)and (2.50) reveals that the load carrying capacity of interlinked system is lower than that of spring loaded independent hydro-pneumatic

system for identical parameters. In the case of interconnected system, the load is proportional to piston rod area (A_2-A_1) and not the piston area. It is therefore necessary to adjust the initial charge pressure or strut configuration of the interlinked suspension unit in order to carry the same load.

Similar to unconnected system, based on selected natural frequency and percentage load assigned to spring and strut, the spring and strut stiffness can be determined. In this case of interconnected system, the spring stiffness is same as that of unconnected given by equation (2.21).

$$K = \frac{(1-\alpha)m_s g}{2\delta_f} \tag{2.51}$$

where $(1-\alpha)$ is the percentage load carried by the two springs. Similar to equation (2.20), the equivalent strut stiffness can be found as:

$$K_{eq} = \frac{np_c(A_2 - A_1)^2}{V_o + (A_2 - A_1)\delta_f} = \frac{\alpha m_s g}{2\delta_f} \tag{2.52}$$

where (A_2-A_1) represents the rod area and α is the percentage load carried by the strut.

The procedure for determine the static parameters for the suspension system are identical to that presented earlier for unconnected system.

Fluid Flow Equations For Interconnected Strut

In interconnected hydro-pneumatic system as shown in Figure 2.3, fluid flows through connecting pipes, and orifice restrictions due to the piston movements in their

respective struts and due to fluid compressibility. Su investigated the effect of variations in the fluid bulk modulus on the ride performance characteristics of an interconnected hydraulic suspension [26]. The study demonstrated that the effects of fluid compressibility are negligible and can be omitted for simplicity. The relationships among the various volume flow rates are established from fluid continuity equations, based on the conservation of mass. Assuming that the flow through orifice restriction between chamber II and III is turbulent, the volume flow rates through the orifices in left and right suspension units are related to pressure differentials across the orifices, in the following manner:

$$Q_{23\ell} = C_d a_\ell \sqrt{\frac{2|P_{23\ell}|}{\varrho}}\, \mathrm{sgn}(P_{23\ell}) \quad ; \quad \mathrm{sgn}(P_{23\ell})=+1;\ \text{when } P_{23\ell} \geq 0$$

$$\mathrm{sgn}(P_{23r})= -1;\ \text{when } P_{23\ell} < 0 \qquad (2.53)$$

$$Q_{23r} = C_d a_r \sqrt{\frac{2|P_{23r}|}{\varrho}}\, \mathrm{sgn}(P_{23r}); \quad \mathrm{sgn}(p_{23r})=+1;\ \text{when } P_{23r} \geq 0$$

$$\mathrm{sgn}(p_{23r})= -1;\ \text{when } P_{23r} < 0 \qquad (2.54)$$

Where

$Q_{23\ell}, Q_{23r}$ = volume flow rate through the orifices between chambers II_ℓ and III_ℓ and between II_r and III_r, respectively (m^3/s)

a_ℓ, a_r = orifice areas of left and right suspension units, respectively (m^2)

$P_{23\ell}, P_{23r}$ = instantaneous pressure differential across the left and right orifices, respectively (Pa)

Assuming laminar fluid flow through the interconnecting pipes, negligible entry and exit losses, and identical length and diameter for the interconnected pipes, the

laminar fluid assumption is verified by computing the Reynolds number, R, by using the following equation [2]:

$$R = \frac{4\varrho Q}{\pi \mu D} \tag{2.55}$$

Since pipe diameters of interconnected pipe are larger than that of orifices, it is found that Reynolds number is much less than 2000. Therefore the assumption of laminar flow in interconnected pipe is justified. The volume flow rates through the pipes linearly relate to the pressure differentials in the following manner:

$$Q_{2\ell 1r} = \frac{\pi D^4}{128 \mu L} p_{2\ell 1r} \tag{2.56}$$

$$Q_{2r1\ell} = \frac{\pi D^4}{128 \mu L} p_{2r1\ell} \tag{2.57}$$

$Q_{2\ell 1r}$ = volume flow rate from chamber II_ℓ to I_r (m^3/s)

$Q_{2r1\ell}$ = volume flow rate from chamber II_r to I_ℓ (m^3/s)

D = diameter of interconnected pipe

L = length of interconnected pipe

μ = absolute viscosity of fluid ($N.s/m^2$)

$p_{2\ell 1r}$ = Pressure differential ($p_{2\ell} - p_{1r}$), (pa)

$p_{2r1\ell}$ = Pressure differential ($p_{2r} - p_{1\ell}$), (pa)

The rate of change of fluid volume in chambers I and II of left and right struts are related to the relative velocity across the respective strut, hence:

$$\begin{aligned} Q_{1\ell} &= A_{1\ell}\dot{Z}_\ell, \qquad Q_{2\ell} = A_{2\ell}\dot{Z}_\ell \\ Q_{1r} &= A_{1r}\dot{Z}_r, \qquad Q_{2r} = A_{2r}\dot{Z}_r \end{aligned} \tag{2.58}$$

$Q_{1\ell}$, Q_{1r} = rate of change of fluid volume due to piston displacement in chamber I_ℓ, I_r

$Q_{2\ell}$, Q_{2r} = rate of change of fluid volume due to piston displacement in chamber II_ℓ, II_r

$\dot{Z}_\ell, \dot{Z}_r$ = relative velocity across the left and right side struts described by equations (2.24 and 2.25), respectively.

Assuming incompressible fluid, the fluid continuity yields the following flow equations for chambers I_ℓ and I_r:

$$Q_{1\ell} + Q_{2r1\ell} = 0; \quad Q_{1r} + Q_{2\ell 1r} = 0 \tag{2.59}$$

$$Q_{2r1\ell} = -A_{1\ell}\dot{Z}_\ell \quad \text{and} \quad Q_{2\ell 1r} = -A_{1r}\dot{Z}_r \tag{2.60}$$

Similarly, the fluid flow associated with chambers II_ℓ and II_r of struts are expressed by the following continuity equations:

$$Q_{23\ell} + Q_{2\ell} + Q_{2\ell 1r} = 0 \tag{2.61}$$

$$Q_{23r} + Q_{2r} + Q_{2r1\ell} = 0 \tag{2.62}$$

After substituting the values of $Q_{2\ell}$, Q_{2r}, $Q_{2\ell 1r}$ and $Q_{2r1\ell}$ from equations (2.58) and (2.60), the fluid flow across the damping restrictions can be expressed by:

$$Q_{23\ell} = A_{1r}\dot{Z}_r - A_{2\ell}\dot{Z}_\ell; \quad \text{and} \quad Q_{23r} = A_{1\ell}\dot{Z}_\ell - A_{2r}\dot{Z}_r \tag{2.63}$$

Equation (2.63) shows that the flow rate through the orifice in the left suspension is related to not only the relative velocity across the left strut but also the relative velocity across the right strut, and similarly flow rate through the right orifice also depends upon the relative velocity across the left and right struts of the suspension.

Pressure Equations:

Pressure differentials, $p_{23\ell}$, p_{23r} can be expressed by rearranging equation (2.53 and 2.54) to yield:

$$P_{23\ell} = \frac{\varrho}{2}\left(\frac{Q_{23\ell}}{C_d a_\ell}\right)^2 \operatorname{sgn}(Q_{23\ell}) \tag{2.64}$$

$$P_{23r} = \frac{\varrho}{2}\left(\frac{Q_{23r}}{C_d a_r}\right)^2 \operatorname{sgn}(Q_{23r}) \tag{2.65}$$

After substituting the values of $Q_{23\ell}$ and Q_{23r} from equation (2.63), the pressure differentials across the left and right orifices are given by:

$$P_{23\ell} = \frac{\varrho}{2}\left(\frac{A_{1r}\dot{Z}_r - A_{2\ell}\dot{Z}_\ell}{C_d a_\ell}\right)^2 \operatorname{sgn}(A_{1r}\dot{Z}_r - A_{2\ell}\dot{Z}_\ell) \tag{2.66}$$

$$P_{23r} = \frac{\varrho}{2}\left(\frac{A_{1\ell}\dot{Z}_\ell - A_{2r}\dot{Z}_r}{C_d a_r}\right)^2 \operatorname{sgn}(A_{1\ell}\dot{Z}_\ell - A_{2r}\dot{Z}_r) \tag{2.67}$$

Instantaneous gas pressures in the accumulators are established by assuming polytropic process. For the left and right accumulators, the pressures in chamber III_ℓ and III_r are expressed as follows:

$$P_{3\ell} = P_{3\ell 0}\left(\frac{V_{3\ell o}}{V_{3\ell o} - V_{23\ell}}\right)^n \tag{2.68}$$

$$P_{3r} = P_{3r0}\left(\frac{V_{3ro}}{V_{3ro} - V_{23r}}\right)^n \tag{2.69}$$

where, $V_{3\ell O}, V_{3rO}$ are static volume in chambers III_ℓ, and III_r, respectively. $v_{23\ell}$, v_{23r} are change of gas volume within the left and right accumulator of suspension, due to flow between chambers II_ℓ, II_r and III_ℓ, III_r, respectively.

$$\text{Since } \frac{dv_{23\ell}}{dt} = Q_{23\ell}; \qquad \frac{dv_{23r}}{dt} = Q_{23r}$$

the change in volume can be directly related to relative motion across the strut:

$$v_{23\ell} = \int Q_{23\ell} = A_{1r}Z_r - A_{2\ell}Z_\ell \quad ; \; v_{23r} = \int Q_{23r} = A_{1\ell}Z_\ell - A_{2r}Z_r \tag{2.70}$$

where Z_l and Z_r are the relative motion defined earlier after equation (2.35).

Upon combining equations (2.56) to equation (2.60), the pressure differentials due to laminar flows through the interconnected pipes, $p_{2\ell 1r}$ and $p_{2r1\ell}$, can be related to the relative velocity of the struts:

$$P_{2\ell 1r} = \frac{-A_{1r}\dot{Z}_r}{Y} \; ; \tag{2.71}$$

$$P_{2r1\ell} = \frac{-A_{1\ell}\dot{Z}_\ell}{Y} \tag{2.72}$$

where $$Y = \frac{\pi D^4}{128\mu L}$$

The fluid pressures in chambers I and II of each strut can further be related as follows:

$$p_{1\ell} = p_{2r} - p_{2r1\ell}; \qquad p_{1r} = p_{2\ell} - p_{2\ell 1r} \tag{2.73}$$

$$p_{2\ell} = p_{23\ell} + p_{3\ell}; \qquad p_{2r} = p_{23r} + p_{3r} \tag{2.74}$$

Substitution of equation (2.68) to (2.72), in the above lead to the final expressions for fluid pressure in different chambers of the interconnected struts:

$$p_{1\ell} = p_{3ro}\left(\frac{v_{3r0}}{v_{3ro} - A_{1\ell}Z_\ell + A_{2r}Z_r}\right)^n + \frac{\varrho}{2}\left(\frac{A_{1\ell}\dot{Z}_\ell - A_{2r}\dot{Z}_r}{C_d a_r}\right)^2 \mathrm{sgn}(A_{1\ell}\dot{Z}_\ell - A_{2r}\dot{Z}_r) + A_{1\ell}\dot{Z}_\ell / Y \qquad (2.75)$$

$$p_{1r} = p_{3\ell o}\left(\frac{v_{3\ell 0}}{v_{3\ell o} - A_{1r}Z_r + A_{2\ell}Z_\ell}\right)^n + \frac{\varrho}{2}\left(\frac{A_{1r}\dot{Z}_r - A_{2\ell}\dot{Z}_\ell}{C_d a_\ell}\right)^2 \mathrm{sgn}(A_{1r}\dot{Z}_r - A_{2\ell}\dot{Z}_\ell) + A_{1r}\dot{Z}_r / Y \qquad (2.76)$$

$$p_{2\ell} = p_{3\ell o}\left(\frac{v_{3\ell 0}}{v_{3\ell o} - A_{1r}Z_r + A_{2\ell}Z_\ell}\right)^n + \frac{\varrho}{2}\left(\frac{A_{1r}\dot{Z}_r - A_{2\ell}\dot{Z}_\ell}{C_d a_\ell}\right)^2 \mathrm{sgn}(A_{1r}\dot{Z}_r - A_{2\ell}\dot{Z}_\ell) \qquad (2.77)$$

$$p_{2r} = p_{3ro}\left(\frac{v_{3r0}}{v_{3ro} - A_{1\ell}Z_\ell + A_{2r}Z_r}\right)^n + \frac{\varrho}{2}\left(\frac{A_{1\ell}\dot{Z}_\ell - A_{2r}\dot{Z}_r}{C_d a_r}\right)^2 \mathrm{sgn}(A_{1\ell}\dot{Z}_\ell - A_{2r}\dot{Z}_r) \qquad (2.78)$$

Dynamic Forces of Interconnected Suspension

Pressures acting upon the pistons are with respect to the static equilibrium position. Similar to equations (2.36) and (2.37), the total dynamic suspension forces, $F_{fl}^{'}$ and $F_{fr}^{'}$ developed at the left and right suspension units of interconnected system can be expressed as:

$$F_{fl}^{'} = (P_{2\ell} - P_{2\ell o})A_{2\ell} - (P_{1\ell} - P_{1\ell o})A_{1\ell} \qquad (2.79)$$

$$F_{fr}^{'} = (P_{2r} - P_{2ro})A_{2r} - (P_{1r} - P_{1ro})A_{1r} \qquad (2.80)$$

The total dynamic forces can further be expressed in terms of pressure differentials, by substituting equations (2.74):

$$F_{fl}^{'} = (P_{3\ell} + P_{23\ell} - P_{3\ell o})A_{2\ell} - (P_{3r} - P_{3ro} + P_{23r})A_{1\ell} + P_{2r1\ell}A_{1\ell} \qquad (2.81)$$

$$F_{fr}^{'} = (P_{3r} + P_{23r} - P_{3ro})A_{2r} - (P_{3\ell} + P_{23\ell} - P_{3\ell o})A_{1r} + P_{2\ell 1r}A_{1r} \qquad (2.82)$$

Equations (2.81) and (2.82) show that the connecting pipes between two cylinders produce fluid feedback effects within the interconnected suspension. The total dynamic force generated by one suspension unit consists of the following three components:

(I) The first term, $(p_{3\ell}+ p_{23\ell} -p_{3\omega})A_{2\ell}$ and $(p_{3r}+ p_{23r} -p_{3r0})A_{2r}$ in equation (2.81) and (2.82), represent the damping and restoring forces developed due to flow within the suspension unit.

(II) The second term, $(p_{3r}-p_{3r0}+p_{23r})A_{1\ell}$ and $(p_{3\ell}+ p_{23\ell}-p_{3\omega})A_{1r}$, in the same equations represent the negative feedback damping and restoring forces due to flows within the other suspension unit.

(III) $p_{2r1\ell}A_{1\ell}$ and $p_{2\ell 1r}A_{1r}$, represent the damping forces due to flow through the pipes interconnecting the left and right struts.

The generalized suspension forces $F'_{f\ell}$ and F'_{fr}, developed by the interconnected suspension, depend on the number of suspension unit on the axle:

$$F'_{f\ell} = N_U F'_{\ell} \qquad \text{and} \qquad F'_{fr} = N_U F'_{r} \tag{2.83}$$

The generalized suspension forces can further be expressed as combinations of damping ($F'_{\ell c}$ and F'_{rc}) and restoring forces ($F'_{\ell s}$ and F'_{rs}):

$$F'_{\ell} = F'_{\ell C} + F'_{\ell S} \qquad \text{and} \qquad F'_{r} = F'_{rC} + F'_{rS} \tag{2.84}$$

Under equal static load conditions, identical charge pressures and identical geometry of the left and right struts ($p_{1\ell 0}=p_{2\ell 0}=p_{1r0}=p_{2r0}=p_{a0}$, $v_{3\ell 0}=v_{3r0}=v_0$, $A_{2\ell}=A_{2r}=A_2$, $A_{1\ell}=A_{1r}=A_1$ and $a_\ell=a_r=a$), the restoring forces and damping forces are:

Restoring Forces:

$$F'_{\ell s} = p_0 A_2 N_U\left[\left(\frac{v_0}{v_0 - A_1 Z_r + A_2 Z_\ell}\right)^n - 1\right] - p_0 A_1 N_u\left[\left(\frac{v_0}{v_0 - A_1 Z_\ell + A_2 Z_r}\right)^n - 1\right] \tag{2.85}$$

$$F'_{rs} = p_0 A_2 N_U\left[\left(\frac{v_0}{v_0 - A_1 Z_\ell + A_2 Z_r}\right)^n - 1\right] - p_0 A_1 N_u\left[\left(\frac{v_0}{v_0 - A_1 Z_r + A_2 Z_\ell}\right)^n - 1\right] \tag{2.86}$$

Damping Forces:

$$F'_{\ell C} = \frac{\varrho A_1^3 N_U}{2C_d^2 a^2}\left[\psi(\dot{Z}_r - \psi\dot{Z}_\ell)^2 \operatorname{sgn}(\dot{Z}_r - \psi\dot{Z}_\ell) - (\dot{Z}_\ell - \psi\dot{Z}_r)^2 \operatorname{sgn}(\dot{Z}_\ell - \psi\dot{Z}_r)\right] - \frac{128\mu L A_1^2 N_U}{\pi D^4}\dot{Z}\ell \tag{2.87}$$

$$F'_{rC} = \frac{\varrho A_1^3 N_U}{2C_d^2 a^2}\left[\psi(\dot{Z}_\ell - \psi\dot{Z}_r)^2 \operatorname{sgn}(\dot{Z}_r - \psi\dot{Z}_r) - (\dot{Z}_r - \psi\dot{Z}_\ell)^2 \operatorname{sgn}(\dot{Z}_r - \psi\dot{Z}_r)\right] - \frac{128\mu L A_1^2 N_U}{\pi D^4}\dot{Z}_r \tag{2.88}$$

where $\psi = \frac{A_2}{A_1}$, and N_u is the number of strut on each side.

These equations show that the generalized suspension forces of interconnected system have both elastic and damping components. The damping and restoring forces are influenced not only by the relative velocity and displacement of the same side struts but also effected by the other side of the struts.

Finally the total force developed by the left and right struts and springs are established by adding the above restoring and damping forces along with the restoring force due to parallel springs:

$$F_{TL}=\frac{\varrho A_1^3 N_U}{2C_d^2 a^2}\left[\psi(\dot{Z}_r-\psi\dot{Z}_\ell)^2\,\mathrm{sgn}(\dot{Z}_r-\psi\dot{Z}_\ell)-(\dot{Z}_\ell-\psi\dot{Z}_r)^2\,\mathrm{sgn}(\dot{Z}_\ell-\psi\dot{Z}_r)\right]-\frac{128\mu L A_1^2 N_U}{\pi D^4}\dot{Z}_r+$$

$$P_0 A_2 N_U\left[\left(\frac{V_0}{V_0-A_1Z_r+A_2Z_\ell}\right)^n-1\right]-P_0 A_1 N_u\left[\left(\frac{V_0}{V_0-A_1Z_\ell+A_2Z_r}\right)^n-1\right]+K\delta_f \tag{2.89}$$

$$F_{TR}=\frac{\varrho A_1^3 N_U}{2C_d^2 a^2}\left[\psi(\dot{Z}_\ell-\psi\dot{Z}_r)^2\,\mathrm{sgn}(\dot{Z}_r-\psi\dot{Z}_r)-(\dot{Z}_r-\psi\dot{Z}_\ell)^2\,\mathrm{sgn}(\dot{Z}_r-\psi\dot{Z}_r)\right]-\frac{128\mu L A_1^2 N_U}{\pi D^4}\dot{Z}_r+$$

$$P_0 A_2 N_U\left[\left(\frac{V_0}{V_0-A_1Z_\ell+A_2Z_r}\right)^n-1\right]-P_0 A_1 N_u\left[\left(\frac{V_0}{V_0-A_1Z_r+A_2Z_\ell}\right)^n-1\right]+K\delta_f \tag{2.90}$$

where F_{TL}, F_{TR} are total force developed by left and right side of suspension unit.

2.4 ROLL PLANE MODEL OF SPRING LOADED INDEPENDENT HYDRO-PNEUMATIC SUSPENSION UNIT WITH ANTI-ROLL BAR

In general, a soft spring is used for vehicle suspension such that it yields a natural frequency of around one hertz. This is a primary requirement for satisfying ride comfort criteria. However, generally of on road heavy duty and light duty vehicles suspension require an extra anti-roll stiffness for improved handling. An anti-roll bar is frequently used in vehicle suspension in order to introduce additional anti-roll stiffness without affecting pure bounce response. As shown in Figure 2.4, anti-roll bar is fitted across the chassis and its trailing edges are linked with the wheels on the opposite sides which can move up and down with wheel motion. Bushing are provided at the center part of the anti-roll bar to give the free rotation of the bar and to limit the roll angle. Twisting moment is developed by the anti-roll bar against roll motion during lane changing or sharp turning. The additional stiffness is also effective when left and right wheels are

subjected to out-of-phase road input. However, the influence of anti-roll bar is negligible under in-phase tire-terrain disturbances, leading to pure bounce response.

2.4.1 Modeling of Anti-roll Bars

Anti-roll bars are essentially torsional springs. As shown in Figure 2.5, equal and opposite forces F_d are developed at each end of the anti-roll bar under out-of-phase road input. Thus spring force acting at each wheel can be expressed as :

$$F_d = K_d y \tag{2.91}$$

where K_d is the spring constant, and, y is the vertical displacement between left and right end of the bar. Based on material property and bar dimension, the vertical spring rate, K_d, can be established as:

$$K_d = \frac{\pi G d^4}{32 \ell_b r^2} \tag{2.92}$$

where G is the shear modulus of the anti-roll bar, d is the diameter of the bar, l_b is the distance between two ends of the trailing edges and r is the length of trailing lever. The torsional couple produced by the bar can be expressed in terms of vertical displacement and stiffness as:

$$T_{an} = K_d y \ell_b \tag{2.93}$$

which in term of auxiliary roll stiffness K_θ and relative roll angle 'θ' is expressed as:

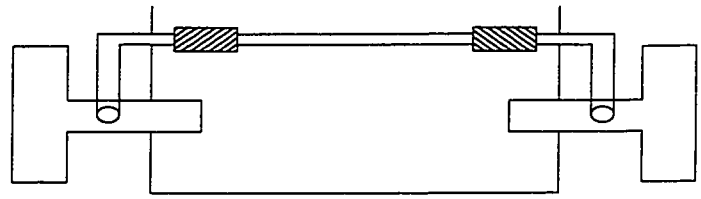

Figure 2.4 Typical connection of anti-roll bar across the chasis.

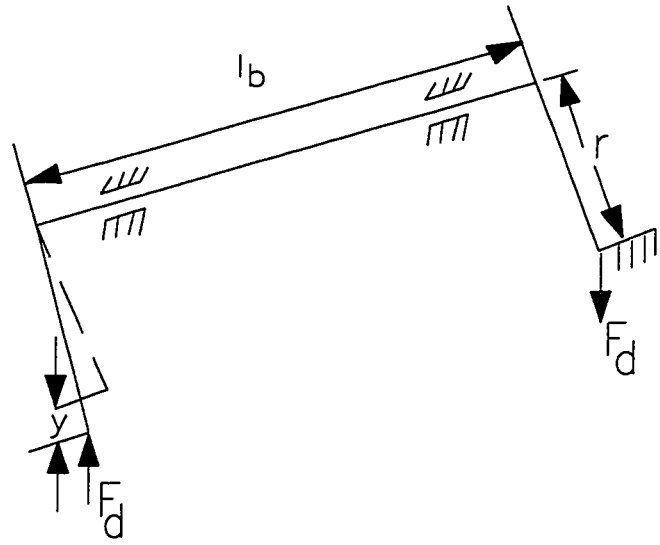

Figure 2.5 Schematic for modeling of anti-roll bar.

$$T_{an} = K_\theta \theta \tag{2.94}$$

$$K_\theta = \frac{\pi G d^4 \ell_b}{32 r^2} = K_d \ell_b^2 \tag{2.95}$$

2.4.2 Equations of Motion of Spring Loaded Independent Hydro-pneumatic Struts With Auxiliary Roll Stiffener

Roll plane model of spring loaded independent hydro-pneumatic struts with anti-roll bar is presented in Figure 2.6. This model is identical to independent hydro-pneumatic suspension unit as presented in Figure 2.1. Anti-roll bar is added in this model in order to achieve enhanced roll stiffness. The equations of motion of proposed roll plane model is obtained by adding roll moment due to K_θ to roll equations obtained earlier as equations (2.2) and (2.4). The final expression for the 4-DOF model are presented as follows.

Equation of motion in bounce mode for sprung mass:

$$m_s \ddot{x}_s = F_{f\ell} + F_{fr} - K[x_s - \theta_s L_\ell - x_u + \theta_u L_\ell - \delta_f] - K[x_s + \theta_s L_r - x_u - \theta_u L_r - \delta_f] - m_s g \tag{2.96}$$

Equation of motion of sprung mass in roll mode:

$$I_s \ddot{\theta}_s = -F_{f\ell} L_\ell + F_{fr} L_r + K[x_s - \theta_s L_\ell - x_u + \theta_u L_\ell - \delta_f] L_\ell - K[x_s + \theta_s L_r - x_u - \theta_u L_r - \delta_f] L_r - K_\theta (\theta_s - \theta_u) - T_\theta \tag{2.97}$$

Equation of motion of unsprung mass in bounce mode:

$$\begin{aligned} m_u \ddot{x}_u = & -F_{f\ell} - F_{fr} - K[x_u - \theta_u L_\ell - x_s + \theta_s L_\ell + \delta_f] \\ & - K[x_u + \theta_u L_r - x_s - \theta_s L_r + \delta_f] - K_{tr\ell}(x_u - x_{i\ell} - \theta_u L_{w\ell} - \delta_1) - C_{tr\ell}(\dot{x}_u - \dot{x}_{i\ell} - \dot{\theta}_u L_{w\ell}) \\ & - K_{trr}(x_u - x_{ir} + \theta_u L_{wr} - \delta_2) - C_{trr}(\dot{x}_u - \dot{x}_{ir} + \dot{\theta}_u L_{wr}) - m_u g \end{aligned} \tag{2.98}$$

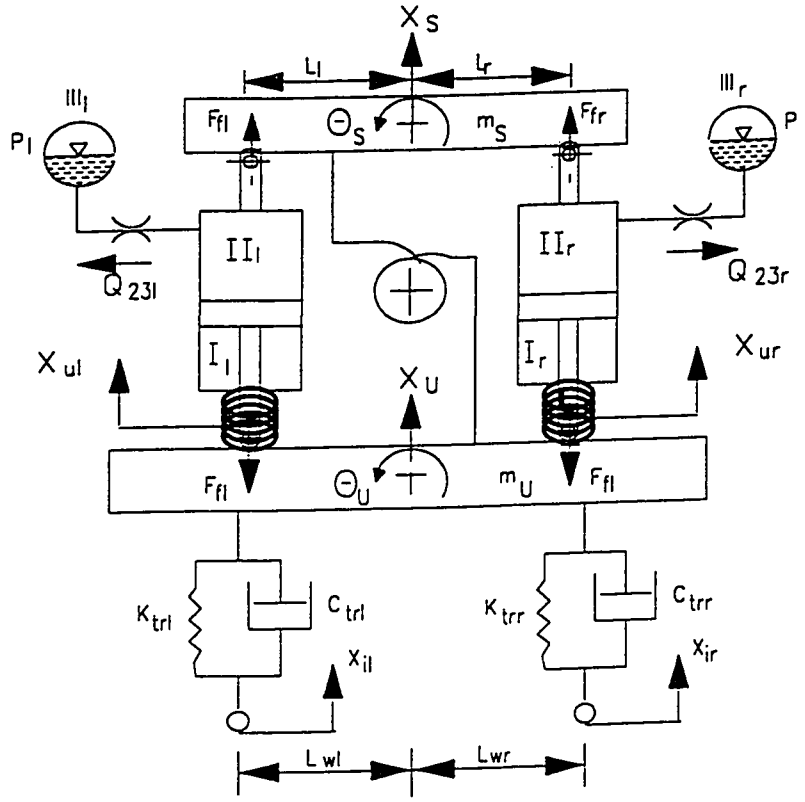

Figure 2.6 Roll plane model of spring loaded independent hydro-pneumatic suspension with anti-roll bar.

Equation of motion of rear unsprung mass roll mode:

$$I_u\ddot{\theta}_u = F_{f\ell}L_\ell - F_{fr}L_r - K[x_u - \theta_u L_\ell - x_s + \theta_s L_\ell + \delta_f]L_\ell + K[x_u + \theta_u L_r - x_s - \theta_s L_r + \delta_f]L_r$$
$$-K_{tr\ell}(x_u - x_{il} - \theta_u L_{w\ell} - \delta_1)L_{w\ell} + K_{trr}(x_u - x_{ir} + \theta_u L_{wr} - \delta_2)L_{wr}$$
$$-C_{tr\ell}(\dot{x}_u - \dot{x}_{il} - \dot{\theta}_u L_{w\ell})L_{w\ell} + C_{trr}(\dot{x}_u - \dot{x}_{ir} + \dot{\theta}_u L_{wr})L_{wr} - K_\theta(\theta_u - \theta_s) \quad (2.99)$$

Damping force and restoring forces due to left and right hydro-pneumatic struts have the same expression as given in equation (2.38) and (2.39) respectively.

2.5 SUMMARY

This chapter is devoted to the development of detailed models for hydro-pneumatic suspension system in parallel with mechanical springs. Three models are developed namely, unconnected system; interconnected system in roll plane; and unconnected with anti-roll bar. Detailed procedure is outlined for establishing static equilibrium, static deflection and corresponding spring and strut stiffness. Complete equation for the 4-DOF models are presented along with expressions for suspension restoring and damping forces. In chapter 3, these models are used for detailed analysis of static and dynamic properties of the suspension systems.

CHAPTER 3

PROPERTIES OF THE SPRING SUPPORTED INTERCONNECTED HYDRO-PNEUMATIC SUSPENSION SYSTEM

3.1 INTRODUCTION

Performance of various suspensions are evaluated by comparing their capabilities to control the vehicle in the direction of motion, potential to improve the ride quality and ability to carry the load under static and dynamic conditions. To achieve high ride quality soft springs are frequently used and hard springs are desired to enhance control of the vehicle. Auxiliary stiffeners acting as torsional springs are commonly used with soft springs to control roll motions of the body during turning and at the same time to maintain the ride performance of the vehicle. Alternatively, an improved compromise between ride and vehicle handling may be obtained by introducing an interconnected hydro-pneumatic suspension system [53].

Various hydro-pneumatic suspension models interconnected in roll plane have been developed and studied to evaluate the vehicle response to roll and vertical inputs. The study demonstrated improved anti-roll characteristics of the interconnected suspensions [54]. Su [55] analyzed a tunable interconnected hydro-pneumatic suspension including the fluid compressibility and valve dynamics. The study demonstrates that ride quality and vehicle handling performance can be improved by interconnecting which enhances the suspension damping in roll plane.

The above studies have clearly demonstrated the anti-roll performance benefit of the suspension interconnected in the roll plane. In this study, practical designs are explored by incorporating mechanical springs in parallel with hydro-pneumatic struts. In the previous chapter several suspension configurations, namely, unconnected, interconnected and unconnected with anti-roll bar were introduced and 4-DOF roll plane vehicle models were developed. In this chapter, fundamental properties of suspension systems are investigated and discussed in terms of their load carrying capacities, suspension rate, damping rate, and roll stiffness. Spring loaded independent hydro-pneumatic suspension vehicle model with anti-roll bar has been developed in roll plane in order to compare the roll stiffness properties of the vehicle with spring loaded interconnected hydro-pneumatic suspension unit. Analytical expressions are derived to describe the static and dynamic properties of the suspension units. Parametric study has been carried out to investigate the influence of mechanical spring on the size and parameters of hydro-pneumatic struts, and to establish the influence of various parameters on suspension properties. Computer simulation technique is adopted to evaluate the various suspension properties and their design parameters.

3.2 LOAD CARRYING CAPACITY OF HYDRO-PNEUMATIC STRUTS WITH SPRING

Load carrying capacity of the suspension system is defined as load carried by the suspension at predetermined design ride height, which is related to its suspension characteristics. The design of passive suspension requires an effective compromise

between the various constraints of the vehicle such as, vehicle working space, ride comfort, vehicle attitude control. One of the most important constraints in any suspension design is the maximum allowable relative displacement between sprung mass and unsprung mass under different road inputs, as it is limited by available working space.

In the present study, parallel springs are introduced with hydro-pneumatic strut which together constitute the suspension system. The static deflection of suspension, load carried by spring and strut as well as the natural frequency of the system directly depend on the stiffness of the mechanical spring and strut effective stiffness. The following sub-sections outlines the selection criteria for load distribution on the two components of the suspension.

3.2.1 Selection Criteria for Load Distribution

The primary objectives of suspension unit is to support the vehicle load and minimize transmissibility within a given work space. The initial study of various models developed in chapter 2, involves selection of appropriate stiffness of the mechanical spring introduced with hydro-pneumatic strut. Previous investigation of interconnected hydro-pneumatic strut [1] clearly demonstrate that struts of very large diameter are needed and that they develop excessively large dynamic pressure.

Parallel springs are introduced in the present study in order to carry the bulk of the load and to achieve practical design parameters for the strut. However, in order to achieve effective interlink between the suspensions through hydraulic connection the strut gas

spring must be assigned a percentage of the load. As discussed in chapter 2, one most important parameter that dictates the static pressure, static volume and charge pressure is the static deflection due to vehicle load. The static deflection is again a direct function of the stiffness of mechanical spring. Furthermore, the static deflection δ_f can not be selected arbitrarily as it has direct influence on the natural frequency which must be maintained between 1.2 to 1.6 Hz in order to satisfy comfort criteria. The procedure adapted in selecting static deflection and corresponding spring stiffness, and in evaluating resulting strut parameters is presented in the flow-chart in Figure 3.1.

The critical strut design parameters P_o, V_o, A_r for different load assigned to spring and strut are obtained for interconnected and unconnected hydro-pneumatic suspension as presented in the following sub-sections.

3.2.2 Load Carrying Capacity of Interconnected Hydro-Pneumatic Struts With Parallel Spring

Following the criteria and procedure outlined in section 3.2.1, the design parameters for the interconnected suspension are obtained for a total load of 69.21 KN representing the sprung mass of Prevost car bus model H3-40. Results are obtained for 5% to 100% of the load assigned to the strut while the remaining load is assigned to the spring. Figure 3.2 presents the results in terms of static pressure developed in the strut, relative static volume in the accumulator and design rod area of hydro-pneumatic strut as a function of load supported by the strut. The load carrying capacity of the interconnected suspension can be obtained as:

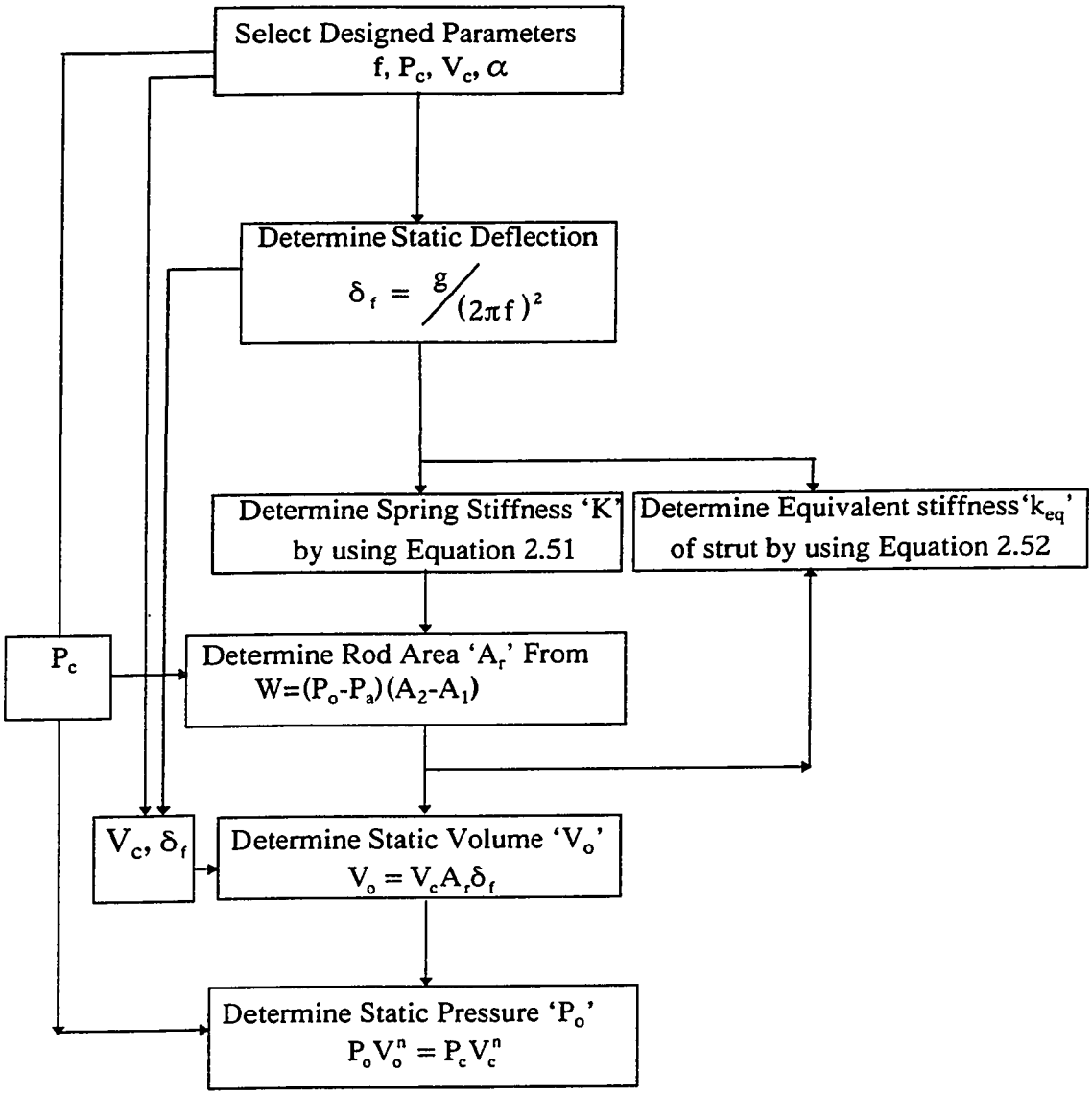

Figure 3.1 Flow-chart for determining the various design parameters of interconnected hydro-pneumatic suspension unit

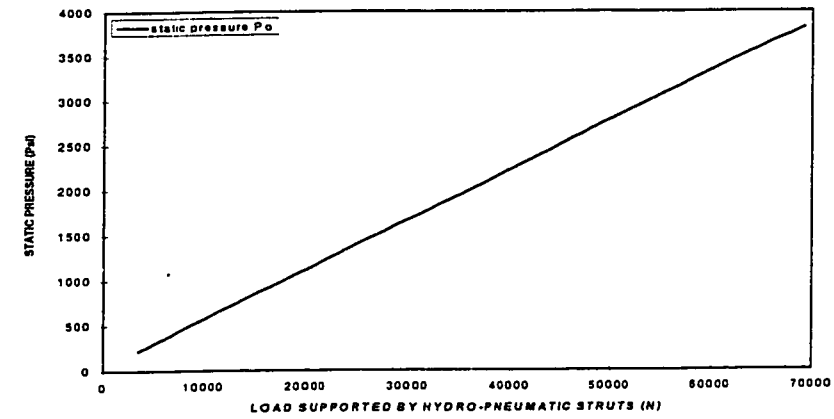

(a)

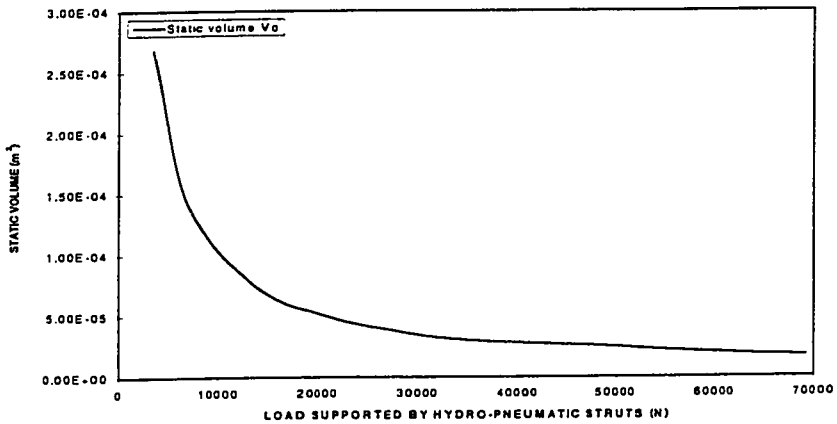

(b)

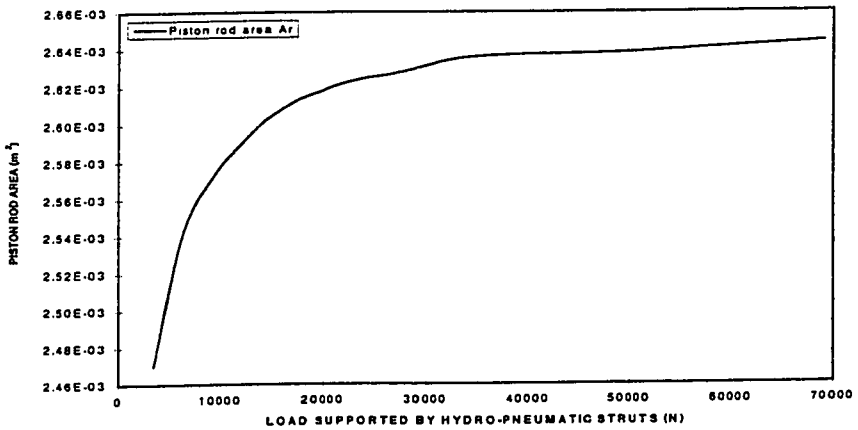

(c)

Figure 3.2 Effect of varying static load on (a) Static pressure (b) Static volume and (c) Rod area

$$W = (P_0 - P_a)A_r + K\delta_f \tag{3.1}$$

where W is the total vehicle weight, δ_f is the static deflection of mechanical spring (K) and strut, P_o is the static strut pressure and $A_r = A_2 - A_1$ is the rod area.

The design parameters as a function of load presented in Figure 3.2 are summarized in Table 3.1. As the results show, the static pressure developed in the strut increases linearly with strut load up to a value of 3814 Psi for 100% load. The resulting accumulator volume decreases rapidly with increasing strut load. The results further show that increase in strut load requires larger rod area dictated by equation 3.1. The trends and magnitudes obtained in these results (Figure 3.2 and Table 3.1) clearly favor assignment of minimum load to the strut, since large pressure P_o will lead to sealing difficulties due to excessive pressures and excessive strength. Furthermore, very low static volume will introduce constraint in relative motion across the strut. Large rod area in the strut is also not desirable as it increases the effective stiffness of the strut (Equation 2.20) that adversely effects ride quality.

In view of the above constraints, 5% of the load assigned to the strut is selected as baseline configuration.

3.2.3 Load Carrying Capacity of Independent Hydro-Pneumatic Struts With Parallel Spring

Unlike interconnected system, the independent hydro-pneumatic strut has significantly large load carrying capacity as given by equation (2.15):

Table 3.1

Comparison of various static load distribution on hydro-pneumatic struts and linear springs

Load (N) on struts [%] and load (N) on mechanical springs [%] of suspension unit under static ride height	Static pressure P_o (Psi)	Static volume V_o (m^3)	Piston rod area A_r (m^2)
3460.5 (5%) and 65749.0 (95%)	218.0	$2.68x10^{-4}$	$2.47x10^{-3}$
6920.0 (10%) and 62288.5 (90%)	408.0	$1.43x10^{-4}$	$2.55x10^{-3}$
13841.9 (20%) and 55367.6 (80%)	787.0	$7.41x10^{-5}$	$2.60x10^{-3}$
20763.0 (30%) and 48446.6 (70%)	1166.0	$5.00x10^{-5}$	$2.62x10^{-3}$
27683.8 (40%) and 41525.7 (60%)	1546.0	$3.77x10^{-5}$	$2.63x10^{-3}$
34604.7 (50%) and 34604.7 (50%)	1925.0	$3.03x10^{-5}$	$2.636x10^{-3}$
48446.65 (60%) and 27683.8 (40%)	2704.0	$2.53x10^{-5}$	$2.638x10^{-3}$
55367.6 (70%) and 20762.8 (30%)	3084.0	$2.17x10^{-5}$	$2.64x10^{-3}$
62288.55 (80%) and 13841.9 (20%)	3463.0	$1.90x10^{-5}$	$2.642x10^{-3}$
69209.5 (100%) and no load on springs	3814.0	$1.72x10^{-5}$	$2.644x10^{-3}$

$$W = (P_o - P_a)A_2 + K\delta_F \tag{3.2}$$

where A_2 is the piston side area.

For symmetric load distribution in the roll plane, anti-roll bars have no effect on the suspension rate. The load carrying capacity of unconnected suspension with anti-roll bar is thus same as that of unconnected suspension as given by equation (3.2).

The model for the unconnected suspension is developed for comparison only and its properties along with those of interconnected system are presented in the following sections.

3.3 SUSPENSION RATE OF SPRING LOADED HYDRO-PNEUMATIC STRUTS

Suspension rate according to SAE is defined as [56] resultant spring rate of mechanical springs and hydra-gas struts of all the suspension units used in the roll plane model. The suspension rate is therefore related to the stiffness property of hydro-pneumatic struts and linear springs used in the present investigation.

3.3.1 Suspension Rate of Independent Hydro-Pneumatic Struts With Parallel Springs

The schematic of a single hydro-pneumatic strut with parallel spring is shown in Figure 3.3. The static gas volume V_{30} in the accumulator (chamber III) is a function of charge

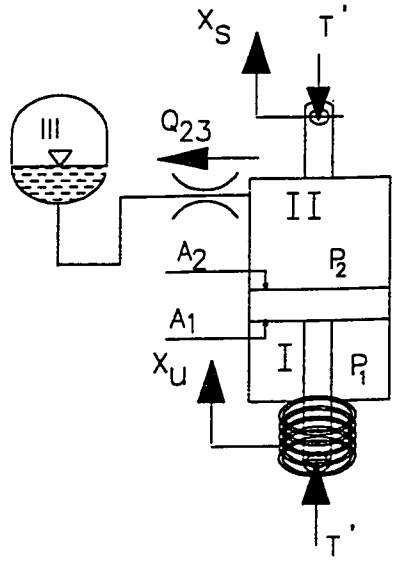

Figure 3.3 Spring loaded independent hydro-pneumatic strut

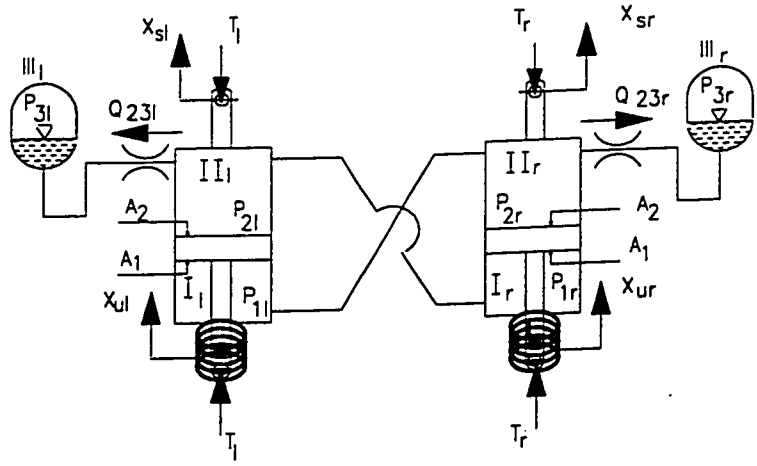

Figure 3.4 Spring loaded interconnected struts

volume and static deflection across the strut as was defined in equation (2.14). In the presence of relative motion across the strut fluid flows between chambers II and III. This volume V_{23} can be expressed as:

$$V_{23} = -A_2 Z \tag{3.3}$$

where relative displacement Z is defined as $(x_s - x_u)$, and A_2 is piston area. The instantaneous gas volume in the accumulator V_3 can therefore, be defined as:

$$V_3 = V_{3o} - V_{23} = V_{3o} + A_2 Z \tag{3.4}$$

The corresponding instantaneous pressure in the accumulator can be obtained using the relationship for polytropic gas pressure to yield:

$$P_3 = \frac{P_0 V_0^n}{V_3^n} = P_0 V_0^n \frac{1}{(V_0 + A_2 Z)^n} \tag{3.5}$$

Under static equilibrium condition, the pressure in accumulator P_3 is same as the pressure in chamber II denoted by P_2. The corresponding static force T' across the strut can therefore, be expressed as:

$$T' = (P_3 - P_o)A_2 = \left[P_0 V_0^n \frac{1}{(V_0 + A_2 Z)^n} - P_a \right] A_2 \tag{3.6}$$

The static stiffness of each hydro-pneumatic strut can be derived by differentiating the static force equation (3.6) with respect to relative displacement across the strut:

$$k_u = \frac{-dT'}{dz}$$

This leads to an expression for static stiffness of the strut due to accumulator as:

$$k_u = nP_0V_0^n\left[\frac{A_2^2}{(V_0 + A_2Z)^{n+1}}\right] \tag{3.7}$$

The static stiffness of each unconnected strut corresponding to design ride height can be obtained by letting Z=0 in equation (3.7) to yield:

$$k_u = \frac{nP_oA_2^2}{V_o} \tag{3.8}$$

Equation (3.8) reveals that the static stiffness of gas accumulator of strut is proportional to absolute static pressure, and inversely proportional to the static gas volume V_0 in the accumulator.

Based on the static stiffness (equation 3.8), the static deflection of each strut can be obtained as:

$$\delta^* = \frac{0.5\alpha W}{k_u} = \frac{0.5\alpha WV_0}{nP_0A_2^2} \tag{3.9}$$

where W is the total load produced by the vehicle. As discussed earlier, the load carried by each strut is dependent on α which designates the percentage of the total load carried

by the struts. The remaining vehicle load $(1-\alpha)$, carried by the mechanical springs, can be used to obtain the static stiffness of the mechanical springs as:

$$K = \frac{0.5(1-\alpha)W}{\delta} \tag{3.10}$$

where δ is the static deflection of the spring and is equal to the static deflection of the strut δ^*.

The total static stiffness of the unconnected hydro-pneumatic strut with parallel spring is:

$$k^* = K + k_u \tag{3.11}$$

where K and k_u are expressed by equations (3.10) and (3.8) respectively. Only symmetric vehicle configuration is considered in this study, and hence left and right strut has identical static stiffness, $k_l^* = k_r^*$.

3.3.2 Suspension Rate of Interconnected Hydro-pneumatic Struts With Parallel Springs

In this case of interconnected hydro-pneumatic strut, as shown in Figure 3.4, the left and right strut in the roll plane must be considered together as motion induces flow between the left and right struts. For symmetric case under static equilibrium, the static gas volume is identical for left and right struts and rod area (A_2-A_1) as was defined in equation (2.49).

In the presence of relative motion across the struts on both side, fluid flow takes place between the chambers as well as between struts. The gas volume in the left and right strut in this case can be expressed in the following manner:

$$V_{3\ell} = V_{3o} + A_2 Z_\ell - A_1 Z_r$$
$$V_{3r} = V_{3o} + A_2 Z_r - A_1 Z_\ell \tag{3.12}$$

where V_{30} is the static accumulator volume, A_1 and A_2 are the piston area for chamber I and II, respectively, and Z_ℓ, Z_r are the relative motion across the left and right strut defined as $Z_\ell = x_{s\ell} - x_{u\ell}$, $Z_r = x_{sr} - x_{ur}$.

Similar to unconnected case, the corresponding gas pressure in the accumulator can be obtained using the relationship for polytropic gas process to yield:

$$P_{3\ell} = P_0 V_0^n \frac{1}{(V_0 + A_2 Z_\ell - A_1 Z_r)^n}$$
$$P_{3r} = P_0 V_0^n \frac{1}{(V_0 + A_2 Z_r - A_1 Z_\ell)^n} \tag{3.13}$$

Under static equilibrium, the fluid pressure in all the interconnected chambers approach an identical value, such that (P_{1r}=$P_{2\ell}$=$P_{3\ell}$) and ($P_{1\ell}$=P_{2r}=P_{3r}). Therefore, static forces developed by the left (T_ℓ) and right (T_r) struts can be expressed as function of accumulator pressure and piston area as:

$$T_\ell = P_{3\ell} A_2 - P_{3r} A_1 - P_a (A_2 - A_1)$$
$$T_r = P_{3r} A_2 - P_{3\ell} A_1 - P_a (A_2 - A_1) \tag{3.14}$$

Upon substituting for absolute accumulator pressure $P_{3\ell}, P_{3r}$ from equation (3.13) in to (3.14), the strut forces are:

$$T_r = P_0 V_0^n \left[\frac{A_2}{(V_o - A_1 Z_\ell + A_2 Z_r)^n} - \frac{A_1}{(V_o - A_1 Z_r + A_2 Z_\ell)^n} \right] - P_a (A_2 - A_1) \tag{3.15}$$

$$T_\ell = P_0 V_0^n \left[\frac{A_2}{(V_o - A_1 Z_r + A_2 Z_\ell)^n} - \frac{A_1}{(V_o - A_1 Z_\ell + A_2 Z_r)^n} \right] - P_a (A_2 - A_1) \tag{3.16}$$

The static stiffness of the left and right hydro-pneumatic strut can now be obtained by differentiating the static forces with respect to respective relative displacement:

$$k_{v\ell} = \frac{-dT_\ell}{dz_\ell}; \qquad \text{and} \qquad k_{vr} = \frac{-dT_r}{dz_r}$$

where $k_{v\ell}$, k_{vr} are static stiffness of the left and right struts, respectively and are given by

$$k_{vr} = nP_0 V_0^n \left[\frac{A_2^2 - A_1 A_2 \frac{dz_\ell}{dz_r}}{(V_o - A_1 Z_\ell + A_2 Z_r)^{n+1}} + \frac{A_1^2 - A_1 A_2 \frac{dz_\ell}{dz_r}}{(V_o - A_1 Z_r + A_2 Z_\ell)^{n+1}} \right] \tag{3.17}$$

$$k_{v\ell} = nP_0 V_0^n \left[\frac{A_2^2 - A_1 A_2 \frac{dz_r}{dz_\ell}}{(V_o - A_1 Z_r + A_2 Z_\ell)^{n+1}} + \frac{A_1^2 - A_1 A_2 \frac{dz_r}{dz_\ell}}{(V_o - A_1 Z_\ell + A_2 Z_r)^{n+1}} \right] \tag{3.18}$$

For symmetric roll plane model under bounce mode, the relative displacements across the left and right struts will be same ($Z_\ell = Z_r = Z$), and $dz_\ell/dz_r = dz_r/dz_\ell = 1$. Substitution of these

in to equation (3.17) and (3.18) lead to simplified expressions for left and right strut stiffness as:

$$k_v = k_{v\ell} = k_{vr} = \frac{nP_0V_0^nA_r^2}{(V_0 + A_rZ)^{n+1}} \tag{3.19}$$

where A_r is effective piston rod area of interconnected strut and is equal to $(A_2\text{-}A_1)$. Comparison of equation (3.19) with equation (3.7) demonstrates that the expression for stiffness of interconnected suspension in bounce mode is similar to that of independent unit. Only major difference is that the effective area of an interconnected unit is the piston rod area, while in independent unit piston head area acts as effective area.

The strut accumulator stiffness given by equation (3.19) can be solved for static stiffness at design ride height by using relative deflection z=0; to yield:

$$k_{v=0} = \frac{nP_oA_r^2}{V_o} \tag{3.20}$$

Equation (3.20) reveals that the static stiffness k_v is proportional to absolute static pressure, and inversely proportional to the static gas volume V_o in accumulator.

The effective static deflection of an interconnected strut under symmetrical loading can be obtained from the effective ride height stiffness, which yields similar expression as that of equation (3.9).

$$\delta^{**} = \frac{0.5\alpha W}{k_{eq}} = \frac{0.5\alpha WV_0}{nP_0A_r^2} \tag{3.21}$$

where $0.5\alpha W$ represents the load carried by each strut corresponding to design ride height.

Based on the static deflection, the stiffness of mechanical spring under static load condition can be expressed as:

$$K = \frac{0.5(1-\alpha)W}{\delta_f} \tag{3.22}$$

where $0.5(1-\alpha)W$ is the load carried by each spring, δ_f is the static deflection of the spring and is same as strut static deflection δ^{**}.

The total static stiffness of hydro-pneumatic strut with parallel spring in bounce mode can be given by:

$$k' = K + k_v \tag{3.23}$$

3.4 DAMPING PROPERTIES OF SPRING LOADED HYDRO-PNEUMATIC SUSPENSION UNIT

Vehicle ride and roll characteristics are strongly related to the damping properties of the suspension. The damping in hydro-pneumatic strut is primarily provided by fluid flow through the orifice between chambers II and III. Interconnected hydro-pneumatic suspension in roll plane provides additional damping due to fluid flow through the interconnected pipes. In the following sub-sections expressions are presented for simulation of damping forces developed by an unconnected and interconnected hydro-pneumatic struts.

3.4.1 Damping Properties of Spring Loaded Independent Hydro-pneumatic Struts

Fluid flow equations for constant area orifice in an unconnected hydro-pneumatic suspension was derived in section 2.2. Assuming turbulent orifice flow, the dynamic suspension strut forces were obtained as presented by equations (2.38) and (2.39). The terms in these equations that represent damping force for left and right struts are as follows:

Damping Forces:

$$F_{\ell c} = \frac{\varrho A_2^3}{2C_d^2 a^2} \dot{Z}_\ell^2 \, \mathrm{sgn}(\dot{Z}_\ell) \tag{3.24}$$

$$F_{rc} = \frac{\varrho A_2^3}{2C_d^2 a^2} \dot{Z}_r^2 \mathrm{sgn}(\dot{Z}_r) \tag{3.25}$$

These equations show that damping forces developed by the left and right struts have non-linear components due to fluid flow through the orifice restrictions. In pure bounce mode, since $\dot{Z}_\ell = \dot{Z}_r = \dot{Z}$, the damping force developed by each independent hydro-pneumatic strut can be expressed as:

$$F_{\ell c} = \frac{\varrho A_2^3}{2C_d^2 a^2} \dot{Z}^2 \mathrm{sgn}(\dot{Z}) \tag{3.26}$$

In roll mode, relative velocities across the struts, $\dot{Z}_\ell$ and $\dot{Z}_r$ can be related to the relative roll velocity between the sprung and unsprung masses. In this case the damping forces developed by the left and right struts are equal in magnitude but opposite in directions. In unconnected system there is no coupling effect due to absence of interconnection, and

hence the damping forces developed by a single strut in roll mode have the same expression as that in the bounce mode.

3.4.2 Damping Properties of Spring Loaded Interconnected Hydro-pneumatic Struts

Roll plane model of an interconnected hydro-pneumatic suspension system was developed in section 2.3. The dynamic forces across the suspension strut based on fluid flow and pressure equations were obtained in equation (2.85) to (2.88). The expression for damping forces developed across the left and right struts obtained as equations (2.87) and (2.88) are as follows:

Damping Forces:

$$F_{\ell C}^{'} = \frac{\varrho A_1^3}{2C_d^2 a^2}\left[\psi(\dot{Z}_r - \psi\dot{Z}_\ell)^2 \operatorname{sgn}(\dot{Z}_r - \psi\dot{Z}_\ell) - (\dot{Z}_\ell - \psi\dot{Z}_r)^2 \operatorname{sgn}(\dot{Z}_\ell - \psi\dot{Z}_r)\right] + \frac{128\mu L A_1^2 N}{\pi D^4}\dot{Z}_\ell \qquad (3.27)$$

$$F_{rC}^{'} = \frac{\varrho A_1^3}{2C_d^2 a^2}\left[\psi(\dot{Z}_\ell - \psi\dot{Z}_r)^2 \operatorname{sgn}(\dot{Z}_r - \psi\dot{Z}_r) - (\dot{Z}_r - \psi\dot{Z}_\ell)^2 \operatorname{sgn}(\dot{Z}_r - \psi\dot{Z}_r)\right] + \frac{128\mu L A_1^2 N}{\pi D^4}\dot{Z}_r \qquad (3.28)$$

These equations reveal that damping forces developed by the interconnected struts have both linear and non-linear components due to fluid flow through the interconnected pipes and orifice restrictions, respectively. In pure bounce mode, since $\dot{Z}_\ell = \dot{Z}_r = \dot{Z}$ and $\psi = \frac{A_2}{A_1} > 1$, the velocity square term in damping force equation can be further simplified as:

$$(\dot{Z}_\ell - \psi Z_r)^2 = (\dot{Z}_r - \psi\dot{Z}_\ell)^2 = (1-\psi)^2\dot{Z}^2$$

$$\mathrm{sgn}(\dot{Z}_\ell - \psi\dot{Z}_r) = \mathrm{sgn}(\dot{Z}_r - \psi\dot{Z}_\ell) = -\mathrm{sgn}(\dot{Z})$$

The damping force developed in bounce mode by each of the interconnected struts thus can be expressed as:

$$F_{dB} = \frac{\varrho A_i^3}{2C_d^2 a^2}(\psi - 1)^3 \dot{Z}^2 \,\mathrm{sgn}(\dot{Z}) + \frac{128\mu L A_i^2}{\pi D^4}\dot{Z} \tag{3.29}$$

In roll mode, relative velocities across the struts, $\dot{Z}_\ell$ and $\dot{Z}_r$ are related to the roll velocity of sprung mass with respect to unsprung mass and possess opposite directions. The damping forces developed by the left and right struts are therefore equal in magnitude but opposite in directions. Thus the damping force developed by one strut in the roll mode can be expressed as:

$$F_{dR} = \frac{\varrho A_i^3}{2C_d^2 a^2}(\psi + 1)^3 \dot{Z}^2 \,\mathrm{sgn}(\dot{Z}) + \frac{128\mu L A_i^2}{\pi D^4}\dot{Z} \tag{3.30}$$

The damping force equation in roll mode shows that this force is higher than the force developed in bounce mode, due to coupling effects of the left and right struts of the interconnected suspension system.

3.5 ROLL STIFFNESS OF VEHICLE SUSPENSION

Vehicle suspension roll is defined as the rotation of sprung mass about its roll center. Suspension roll stiffness can be derived from the restoring moment developed by the suspension subject to a static roll angle. During roll motion of sprung mass unequal forces are developed by the left and right side of suspension struts. Three types of vehicle

suspension models, namely: spring loaded interconnected hydro-pneumatic struts; and spring loaded independent hydro-pneumatic struts with and without anti-roll bar; are considered in roll plane in order to evaluate their roll stiffness characteristics under static and dynamic conditions.

3.5.1 Roll Stiffness of The Interconnected Struts With Parallel Springs

The sprung mass of a suspended vehicle, experiences a roll motion about its roll center when subjected to a roll moment. The roll motion of the sprung mass also excites a vertical motion due to the nonlinear property of the gas springs. Figure 3.5 demonstrates that under a roll moment, the c.g. of sprung mass experiences a motion in the upward direction. This is due to the fact that the hardening characteristics of the left accumulator under compression is significantly greater under such motion. When vehicle body is under roll motion, the corresponding pressures in the left and right struts $P_{3\ell}$ and P_{3r} can be expressed as a function of static pressure and volume and relative displacements across the struts:

$$P_{3\ell} = P_0 V_0^n \frac{1}{(V_0 + A_2 Z_\ell - A_1 Z_r)^n} \tag{3.31}$$

$$P_{3r} = P_0 V_0^n \frac{1}{(V_0 + A_2 Z_r - A_1 Z_\ell)^n} \tag{3.32}$$

where $Z_\ell = x - \ell\theta$ and $Z_r = x + \ell\theta$. 'x' is the relative vertical displacement of the sprung mass with respect to the unsprung mass, and θ is the roll angle of the sprung mass around its roll center. Under static conditions, the pressures of fluid in interconnected

chambers will be equal ($P_{1\ell} = P_{2r} = P_{3r}$) and ($P_{1r} = P_{2\ell} = P_{3\ell}$). For symmetric case the restoring moment can therefore, be derived as:

$$M = (P_{3\ell} - P_{3r})(A_2 + A_1)\ell \tag{3.33}$$

Substituting $P_{3\ell}$ and P_{3r} in Equation (3.33) yields:

$$M = P_o V_o^n (A_1 + A_2)\ell \left[\frac{1}{\{V_o + A_2(x - \ell\theta) - A_1(x + \ell\theta)\}^n} - \frac{1}{\{V_o + A_2(x + \ell\theta) - A_1(x - \ell\theta)\}^n} \right] \tag{3.34}$$

Roll stiffness, which is defined as the rate of change of roll moment with respect to roll angle, is derived as:

$$k_\theta = nP_o V_o^n (A_1 + A_2)\ell \left[\frac{(A_1 + A_2)\ell - (A_2 - A_1)\frac{dx}{d\theta}}{\{V_o + A_2(x - \ell\theta) - A_1(x + \ell\theta)\}^{n+1}} + \frac{(A_1 + A_2)\ell + (A_2 - A_1)\frac{dx}{d\theta}}{\{V_o + A_2(x + \ell\theta) - A_1(x - \ell\theta)\}^{n+1}} \right] \tag{3.35}$$

The rate of change of x with respect to roll angle θ, $(dx/d\theta)$ can be evaluated from the corresponding static equilibrium equation:

$$(P_{3\ell} + P_{3r} - 2P_0)(A_2 - A_1) = 0 \tag{3.36}$$

Substituting the values of $P_{3\ell}$ and P_{3r} in the above equation, the static equilibrium equation can be expressed as a function of x and θ to yield:

$$f(x,\theta) = \left[\frac{1}{\{(V_o + A_2(x - \ell\theta) - A_1(x + \ell\theta)\}^n} \right] + \left[\frac{1}{\{(V_o + A_2(x + \ell\theta) - A_1(x - \ell\theta)\}^n} \right] - \frac{2}{V_0^n} = 0 \tag{3.37}$$

Hence, $dx/d\theta$ can be obtained by taking partial derivatives of the above equation as follows:

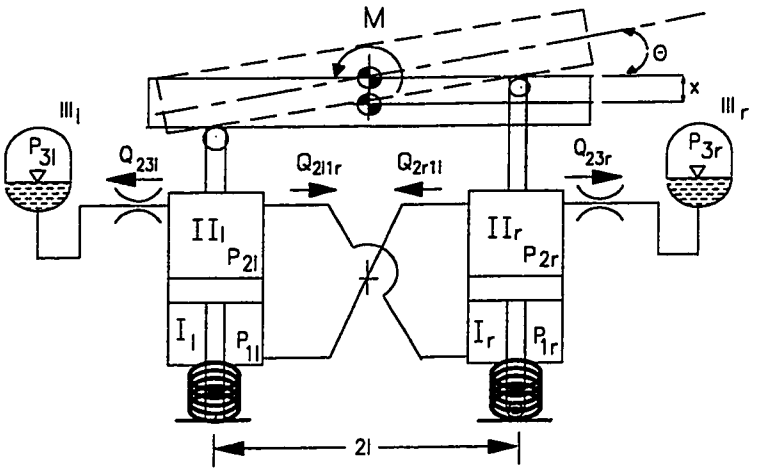

Figure 3.5 Roll motion of spring loaded interconnected hydro-pneumatic struts

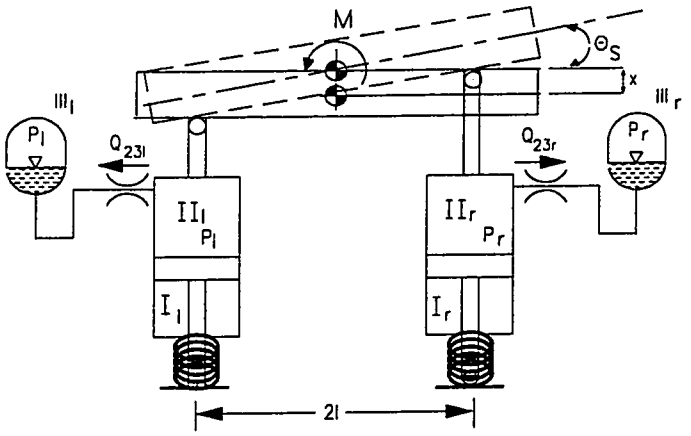

Figure 3.6 Roll motion of spring loaded independent hydro-pneumatic struts

$$\frac{dx}{d\theta}=\frac{\frac{df}{d\theta}}{\frac{df}{dx}}=\frac{(A_2+A_1)\ell}{(A_2-A_1)}\left[\frac{\{V_o+A_2(x+\ell\theta)-A_1(x-\ell\theta)\}^{n+1}-\{V_o+A_2(x-\ell\theta)-A_1(x+\ell\theta)\}^{n+1}}{\{V_o+A_2(x+\ell\theta)-A_1(x-\ell\theta)\}^{n+1}+\{V_o+A_2(x-\ell\theta)-A_1(x+\ell\theta)\}^{n+1}}\right] \tag{3.38}$$

For a given vehicle body roll angle, equations (3.37) and (3.38) can be solved to determine x and $^{dx}/_{d\theta}$, respectively. Substitution of these in equation (3.35) will yield the effective roll stiffness of interconnected suspension, (k_θ). If there is no roll angle, values of x and $^{dx}/_{d\theta}$ will be zero.

The roll stiffness corresponding to the design ride height can be obtained in a simplified form as:

$$k_\theta^*=\frac{2np_o(A_2+A_1)^2\ell^2}{V_o} \tag{3.39}$$

Using equation (3.20) and by multiplying and dividing equation (3.39) by A_r^2, defined as $(A_2\text{-}A_1)^2$, the static roll stiffness can be expressed in terms of suspension rate k_v as:

$$k_\theta^* = 2k_v\ell^2\left(\frac{\psi+1}{\psi-1}\right) \tag{3.40}$$

where $\psi=\frac{A_2}{A_1}$ is piston area ratio of the interconnected struts, which is always greater than one. Above equations show that the effective roll stiffness of interconnected suspension can be evaluated by selecting smaller value of piston area ratio. The term under bracket in equation (3.40) can therefore, be defined as a roll stiffness amplification factor:

$$A_m=\left(\frac{\psi+1}{\psi-1}\right) \tag{3.41}$$

The effective roll stiffness of interconnected suspension derived above is for hydro-pneumatic strut alone. Additional roll stiffness exists in the present model due to parallel mechanical springs introduced with the struts. The suspension moment for the linear mechanical springs can be expressed as:

$$M_{SP} = 2K(x_s - \theta\ell)\ell \tag{3.42}$$

where K is the mechanical spring stiffness, x_s is the vertical motion of sprung mass. The effective roll stiffness due to mechanical springs can be obtained by differentiating moment with respect to roll angle to yield:

$$k_{\theta sp} = 2K\ell^2 \tag{3.43}$$

3.5.2 Roll Stiffness of Spring Loaded Independent Struts With And Without Anti-roll Bar

A model of unconnected or independent hydro-pneumatic suspension was developed in chapter 2 for comparative study with that of interconnected system. In the case of unconnected suspension, the roll stiffness amplification factor shown in the previous section will be absent. In conventional vehicle suspension with softer vertical springs, anti-roll bars are frequently used to enhance roll stiffness. In the case of unconnected system considered in this investigation, effective roll stiffness is formulated for both cases with and without anti-roll bars. In anti-roll bar case, total roll stiffness of the vehicle can be described as sum of the roll stiffness arising from the spring loaded independent hydro-pneumatic struts and auxiliary roll stiffness.

Similar to interconnected system, the sprung mass of independent hydro-pneumatic suspension, experiences a translatory motion 'x' due to presence of non-linear property of gas spring, as shown in Figure 3.6. Unequal pressures are developed by the left and right struts during static roll deflection of the vehicle body; which can be expressed as:

$$P_{3\ell} = P_0 V_0^n \frac{1}{(V_0 + A_2 Z_\ell)^n} \tag{3.44}$$

$$P_{3r} = P_0 V_0^n \frac{1}{(V_0 + A_2 Z_r)^n} \tag{3.45}$$

where $P_{3\ell}$ and P_{3r} are the instantaneous pressure of the gas in left and right struts, while $Z_\ell = x - \ell\theta_s$ and $Z_r = x + \ell\theta_s$. 'x' is the relative vertical displacement of the sprung mass with respect to the unsprung mass, 'ℓ' is half the suspension track and θ_s is the roll angle of the sprung mass around its roll center. The restoring moment of the suspension unit can be expressed as:

$$M = (P_{3\ell} - P_{3r}) A_2 \ell \tag{3.46}$$

where A_2 is the effective piston side area for each strut. Substituting for $P_{3\ell}$ and P_{3r} in the above equation leads to the following expression for moment:

$$M = P_o V_o^n A_2 \ell \left[\frac{1}{\{V_o + A_2(x - \ell\theta)\}^n} - \frac{1}{\{V_o + A_2(x + \ell\theta)\}^n} \right] \tag{3.47}$$

Roll stiffness can now be defined as the rate of change of roll moment with respect to roll angle, which yields:

$$k_{\theta u} = nP_o V_o^n A_2^2 \ell \left[\frac{1 - \frac{dx}{d\theta_s}\Big/\ell}{\{V_o + A_2(x - \ell\theta_s)\}^{n+1}} + \frac{1 + \frac{dx}{d\theta_s}\Big/\ell}{\{V_o + A_2(x + \ell\theta_s)\}^{n+1}} \right] \tag{3.48}$$

where, similar to interconnected system, $dx/d\theta_s$ results due to non-linear property of gas springs. $dx/d\theta_s$ can be obtained from the static equilibrium equation as:

$$(P_{3\ell} + P_{3r} - 2P_0)A_2 = 0 \tag{3.49}$$

Substituting the values of $P_{3\ell}$ and P_{3r} in the above equation leads to the following static equilibrium equation:

$$P(x,\theta_s) = \left[\frac{1}{\{V_o + A_2(x - \ell\theta_s)\}^n}\right] + \left[\frac{1}{\{V_o + A_2(x + \ell\theta_s)\}^n}\right] - \frac{2}{V_0^n} = 0 \tag{3.50}$$

and $\dfrac{dx}{d\theta_s}$ can be obtained by taking partial derivative of the above equation as follows:

$$\frac{dx}{d\theta_s} = -\frac{\frac{\partial p}{\partial \theta_s}}{\frac{\partial p}{\partial x}} = \ell \left[\frac{\{V_o + A_2(x + \ell\theta_s\}^{n+1} - \{V_o + A_2(x - \ell\theta_s)^{n+1}}{\{V_o + A_2(x + \ell\theta_s)\}^{n+1} + \{V_o + A_2(x - \ell\theta_s)\}^{n+1}} \right] \tag{3.51}$$

For a given vehicle body roll angle, equations (3.50) and (3.51) can be solved to determine x and $\dfrac{dx}{d\theta_s}$, respectively. Substitution of these results in equation (3.48) will yield the effective roll stiffness of the unconnected hydro-pneumatic strut $k_{\theta u}$. If there is

no roll angle, values of x and $\frac{dx}{d\theta_s}$ will be zero. The roll stiffness corresponding to the design ride height can be obtained in a simplified form as:

$$k^{o}_{\theta u} = \frac{2nP_o A_2^{\,2} \ell^2}{V_o} \tag{3.52}$$

The roll stiffness of unconnected hydro-pneumatic unit corresponding to the design ride height is then expressed in terms of suspension rate k_u by using equations (3.8), as

$$k^{o}_{\theta u} = 2k_u \ell^2 \tag{3.53}$$

where $k^{0}_{\theta u}$ is the roll stiffness of independent hydro-pneumatic struts at design ride height.

A comparison of equation (3.39) and (3.52) clearly reveals that the roll stiffness of the interconnected suspension corresponding to the design ride height is larger than that of the unconnected suspension.

For the case of unconnected system, the effective roll stiffness can be evaluated by introducing anti-roll bars. The auxiliary roll stiffness k_θ of the anti-roll bar defined earlier in equation (2.95) can be added to the effective strut roll stiffness $k^{o}_{\theta u}$ to yield total roll stiffness:

$$k'_{\theta T} = k^{0}_{\theta u} + k_\theta \tag{3.54}$$

The above roll stiffness is due to unconnected hydro-pneumatic strut with antiroll bars. The additional parallel springs used in this investigation will introduce additional roll stiffness. Similar to interconnected case, the roll stiffness due to the mechanical spring can be added to equation (3.54) to give:

$$k_{\theta T} = k'_{\theta T} + k_{\theta sP} = k^{o}_{\theta u} + k_{\theta sp} + k_{\theta} \tag{3.55}$$

where $k_{\theta sp}$ is the effective roll stiffness due to mechanical springs given in equation (3.43). An amplification factor for independent system with antiroll bar can be defined as:

$$A_n = 1 + \left(k_{\theta} / k_u\right) \ell^2 \tag{3.56}$$

where k_u is the effective vertical stiffness at design ride height.

3.6 SELECTION OF SUSPENSION CONFIGURATION AND SIMULATION PARAMETERS

Based on the two basic models namely: interconnected system and unconnected with and without antiroll stiffness, several suspension configurations are established. These configurations are based on a set of physical parameters such as, working pressure, charge and static volume, orifice area, length and diameter of interconnection pipe. Various considerations and procedure used in arriving at a set of configurations are discussed in this section. Each of the configurations are based on vehicle parameters that represent Prevost car H 3-40 highway bus. These parameters are presented in Table 3.2.

Parameters for various configurations are selected based on identical load-carrying capacity, static deflection and static stiffness at design ride height. This ensures that the sprung mass natural frequency in each case is same and within the preferred range for ride quality. As discussed earlier, equation (2.22) dictates that for a natural frequency of 1.4 Hz, the corresponding static deflection is 0.126 m, which is used

TABLE 3.2

Technical data of pre vost car H3-40 bus model

Symbols	Description of parameters	Values
m_s	Sprung mass	14110 Kg
m_u	Unsprung mass	3616 Kg
I_s	Mass moment of inertia of sprung mass	19300 kgm^2
I_u	Mass moment of inertia of unsprung mass	3819.0 Kgm^2
K_{tl}, K_{tr}	Stiffness coefficient of left and right tire	3574800 N/m
C_{tl}, C_{tr}	Damping coefficient of left and right tire	9500 Ns/m
L_{wl}, L_{wr}	Lateral distances between c.g. of unsprung mass and left and right tires	1.03 m
L_l, L_r	Lateral distances between c.g. of sprung mass and left and right hydraulic struts	0.7 m
h_1	Vertical distance between c.g. of unsprung mass and vehicle roll center	0.0 m
h_2	Vertical distance between c.g. of sprung mass and vehicle roll center	0.62 m
ϱ	Mass density of fluid	797 Kg/m^2
μ	Dynamic viscosity of fluid	0.6 Ns/m^2
C_d	Discharge coefficient	0.7
P_a	Atmospheric pressure	101300 N/m^2
n	Polytropic gas constant	1.0
N	Number of struts on each side of suspension unit	1

throughout the study. Effect of load distribution between the mechanical springs and hydro-pneumatic strut is also investigated to arrive at a baseline load distribution that ensures acceptable property and practical design parameters.

3.6.1 Selection of Hydro-pneumatic Components

Simulations are carried out using interconnected and unconnected suspension systems to evaluate influence of hydro-pneumatic parameters and load distribution on static pressure, static volume and effective damping.

Working Pressure of Hydro-Pneumatic Struts

In spring loaded hydro-pneumatic suspension unit, hydraulic struts are used to provide the damping, while springs for load support is provided by accumulators and mechanical springs. Maximum working pressure of the struts are obtained using the static equilibrium expression for hydraulic struts presented by equation (2.48) for interconnected suspension, and by equation (2.13) for independent suspension system. The load in these equations represent the part of load supported by hydro-pneumatic struts. Maximum working pressure of hydraulic unit both for interconnected and unconnected cases is constrained within the range of 250 to 400 Psi in order to design realistic struts and to ensure sufficient damping.

Piston Head Area of Hydraulic strut

Various factors that affect piston head area include, charge volume, static volume, acceptable static and charge pressure. The piston head area in this study is estimated by assuming the practical design parameters (d, ℓ) of accumulator:

$$V_c = \frac{\pi d^4}{4} \ell' \tag{3.57}$$

where d is diameter of accumulator, which is selected in the range of (2.54 ~ 3.85 cm) and ℓ' is length of gas column in accumulator, which is taken in the range of (10.0 ~ 15.0 cm). By using static equilibrium and gas law equations, static pressure can be expressed as:

$$P_o = \frac{P_g V_c}{V_o} \tag{3.58}$$

where P_g is gauge pressure. The static volume V_o is a function of charge volume and static deflection as presented in equation (3.57). For the given static deflection of 0.126 m, and taking accumulator charge volume as (2.38×10^{-4} m^3) piston head area can be estimated and found to be in the range of 14.0 cm^2 (2.17 in^2) to 14.5 cm^2 (2.25 in^2). Considering limitation of work space in between sprung mass and unsprung mass, piston head area A_2= 14.4 cm^2 (2.16 in^2) is selected. The net area of the piston on the rod side can be obtained for a selected rod area as $A_1=A_2-A_r$.

Orifice Area, Diameter of Interconnected Pipe and Pipe Length

Orifice area, between chambers II and III directly affects the damping provided by the strut, and pipes used in hydro-pneumatic suspension unit to provide interconnection will also introduce damping based on their length and diameter. All these parameters are selected in such a way as to achieve sufficient damping force to control the vertical amplitude of vibration and to control the body roll. For variation of these parameters in the range as presented in Table 3.3, simulations were carried out to evaluate effective damping force as a function of relative velocity in the bounce and roll modes.

Table 3.3

Ten different values of design parameters of interconnected hydro-pneumatic strut

	Interconnected unit			Independent unit
S. No.	Orifice area a (m^2)	Diameter of pipe D (m^2)	Pipe length L (m)	Orifice area a (m^2)
1.	0.0015×10^{-3}	0.0028	0.71	0.0015×10^{-3}
2.	0.0016×10^{-3} *	0.0029 *	0.852	0.0016×10^{-3} *
3.	0.0017×10^{-3}	0.0030	0.994	0.0017×10^{-3}
4.	0.0018×10^{-3}	0.0031	1.136	0.0018×10^{-3}
5.	0.0019×10^{-3}	0.0032	1.278	0.0019×10^{-3}
6.	0.0020×10^{-3}	0.0034	1.4246922 *	0.0020×10^{-3}
7.	0.0024×10^{-3}	0.0036	1.562	0.0024×10^{-3}
8.	0.0036×10^{-3}	0.0039	1.704	0.0036×10^{-3}
9.	0.0042×10^{-3}	0.0042	1.846	0.0042×10^{-3}
10.	0.0044×10^{-3}	0.0043	1.988	0.0044×10^{-3}

* Nominal value

Figures 3.7 and 3.8 show the damping force developed by the interconnected strut in bounce and roll modes, respectively. The expressions for these forces for a single strut are given in equations (3.29) and (3.30), respectively, as a function of relative velocity ($\dot{Z}$). These results are obtained for a range of orifice areas while other parameters in Table 3.3 are kept equal to the nominal value. As shown, the trends for damping force are very similar in bounce and roll modes where damping force decreases with increase in orifice area. The results further show that the overall damping force is higher in the roll mode since additional damping is present in roll due to interlink pipes. This effect is absent in the case of unconnected system as shown for identical parameters in Figures 3.9 and 3.10. However, when the unconnected damping force is compared to that of interconnected, it is evident that unconnected system for identical parameters produces slightly larger damping as it is dependent on piston head area rather than rod area.

Damping force results are also plotted in bounce and roll mode for variation of interconnection pipe diameter and pipe length. One parameter is varied at a time while the others are kept equal to their nominal value. Figures 3.11 and 3.12 show the results for variation of pipe diameter, while Figures 3.13 and 3.14 present the effect of pipe length. These parameters clearly demonstrate negligible influence of these parameters in the range considered.

For further studies with the suspension models, a low value for orifice area (0.0016 x 10^{-3} m^2) and pipe diameter (0.0029 m) along with a intermediate value for pipe length (1.424 m) is taken as nominal parameter to ensure sufficient damping.

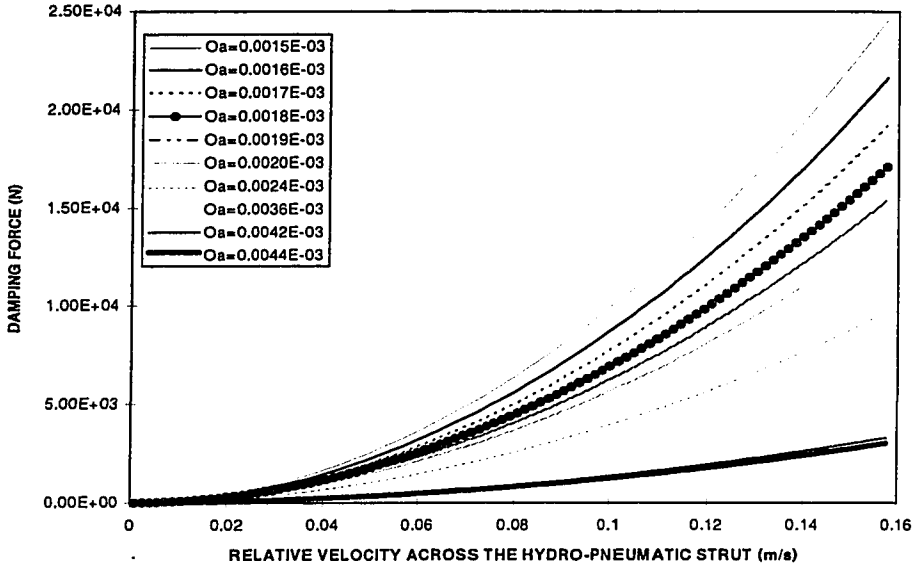

Figure 3.7 Damping force developed by one strut under bounce mode

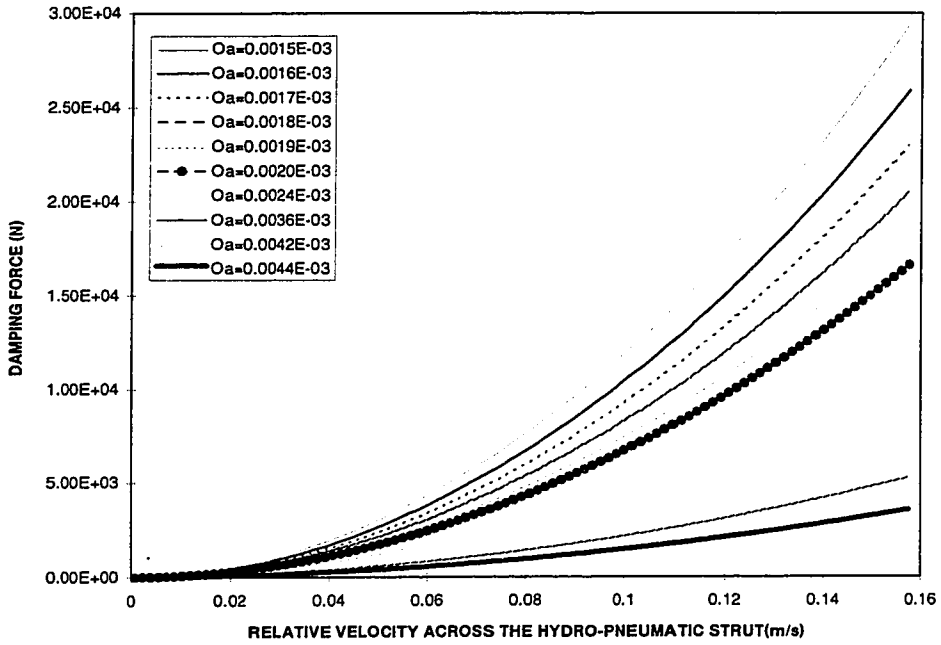

Figure 3.8 Damping force developed by one strut under roll mode

DAMPING FORCE UNDER VARYING ORIFICE AREA OF INDEPENDENT UNIT

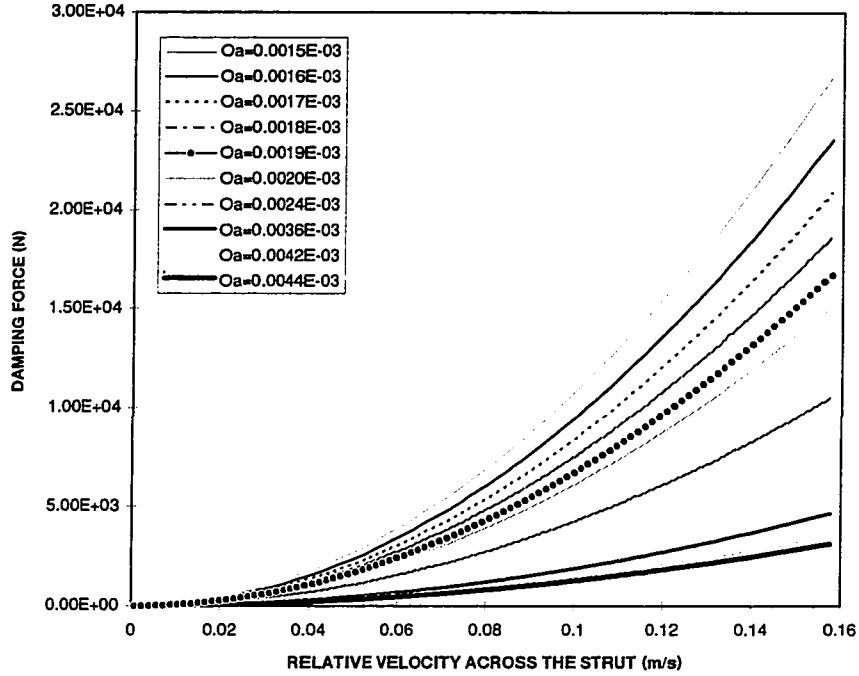

Figure 3.9 Damping force developed by one strut under bounce mode

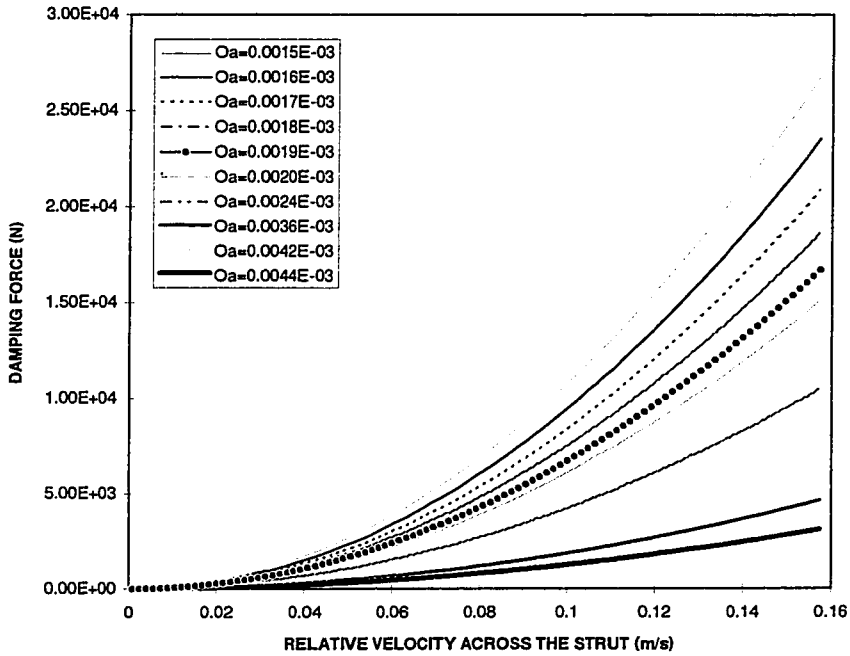

Figure 3.10 Damping force developed by one strut under roll mode

DAMPING FORCE UNDER VARYING INTERCONNECTED PIPE DIAMETER

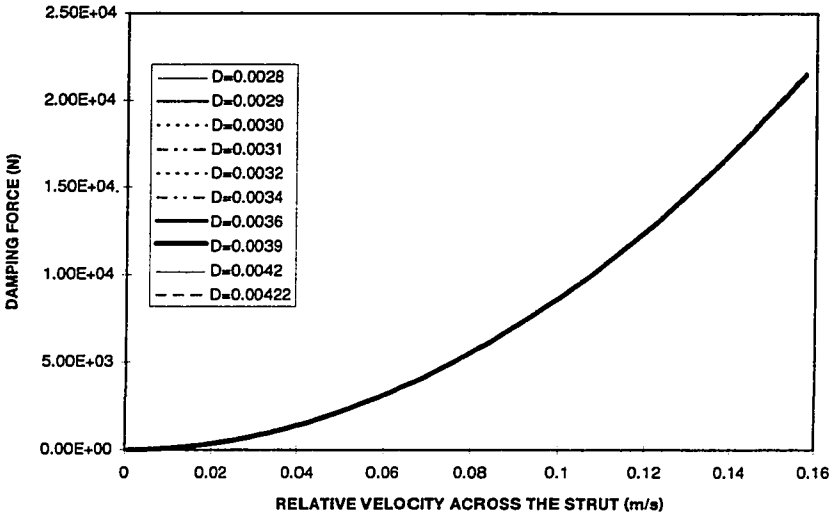

Figure 3.11 Damping force developed by one strut under bounce mode

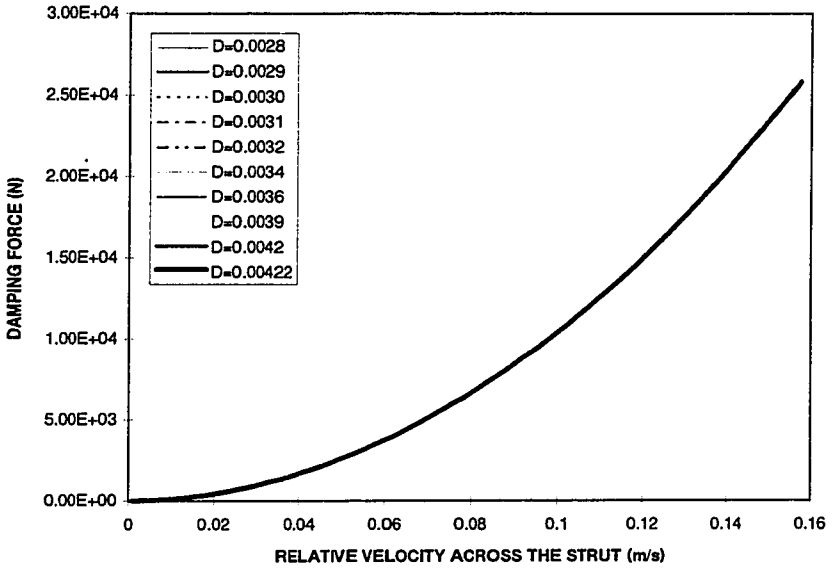

Figure 3.12 Damping force developed by one strut under roll mode

DAMPING FORCE UNDER VARYING INTERCONNECTED PIPE LENGTH

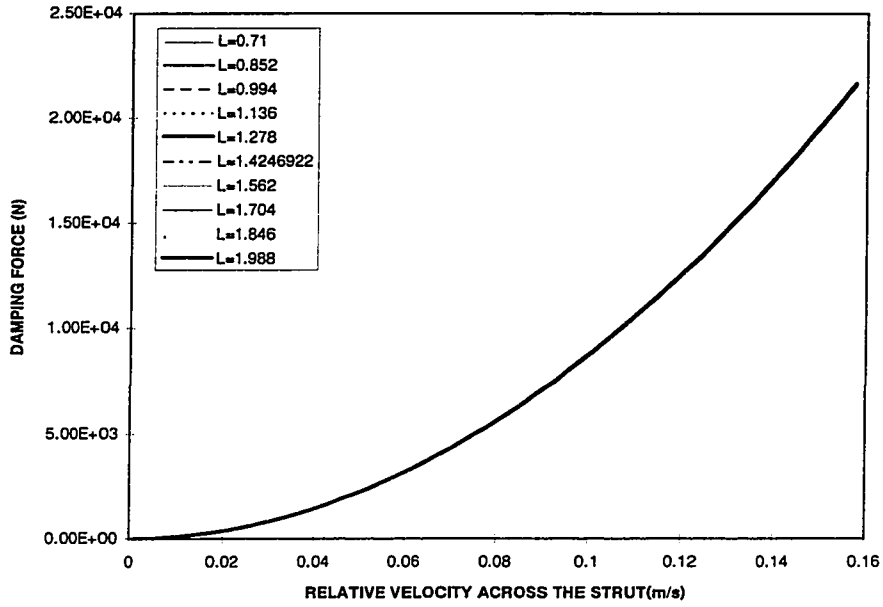

Figure 3.13 Damping force developed by one strut under bounce mode

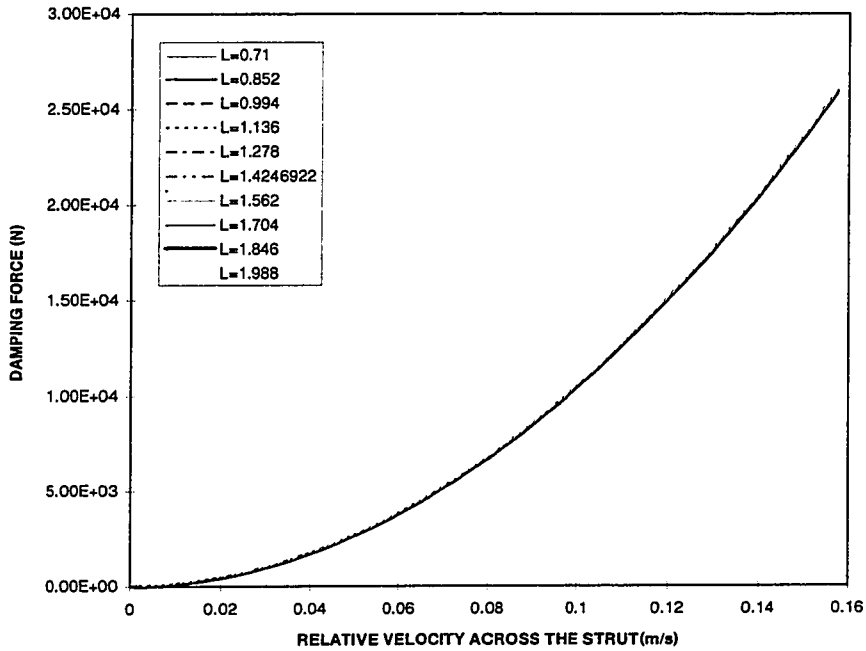

Figure 3.14 Damping force developed by one strut under roll mode

3.6.2 Base Line Load Distribution

The present investigation introduces parallel spring with the hydro-pneumatic struts. The load carried by the spring and the strut can be varied by design as was discussed earlier in section 3.2.2. In view of the static pressure and volume, 5% load assignment to the strut was selected as preferred combination. In this section, the effect of variation from 5% to 20% is examined on the suspension rate and damping force developed. The suspension properties are calculated based on a fixed static deflection following the procedure outlined by the flow-chart in section 3.2.2.

Figures 3.15 and 3.16 show the strut damping force at 5% and 20% load to the strut under bounce mode for interconnected and unconnected systems, respectively. These results clearly reveal the significant influence of strut load, where the damping force developed for larger load is greater as it develops larger pressure. These results presented in roll mode are shown in Figures 3.17 and 3.18. Same trend is observed here which further shows that damping is larger in roll mode for interconnected system, and is unaffected for the unconnected system.

Figure 3.19 shows the effective suspension rate in bounce mode for 5% of the load carried by the strut. These results for unconnected and interconnected system show that unconnected suspension have significantly higher suspension rate since the effective working area in this case is the piston head area as opposed to rod area in the case of interconnected system. Similar trend is observed for 20% load assigned to the strut as shown in Figure 3.20. In this case, however, the suspension rate is considerably larger due

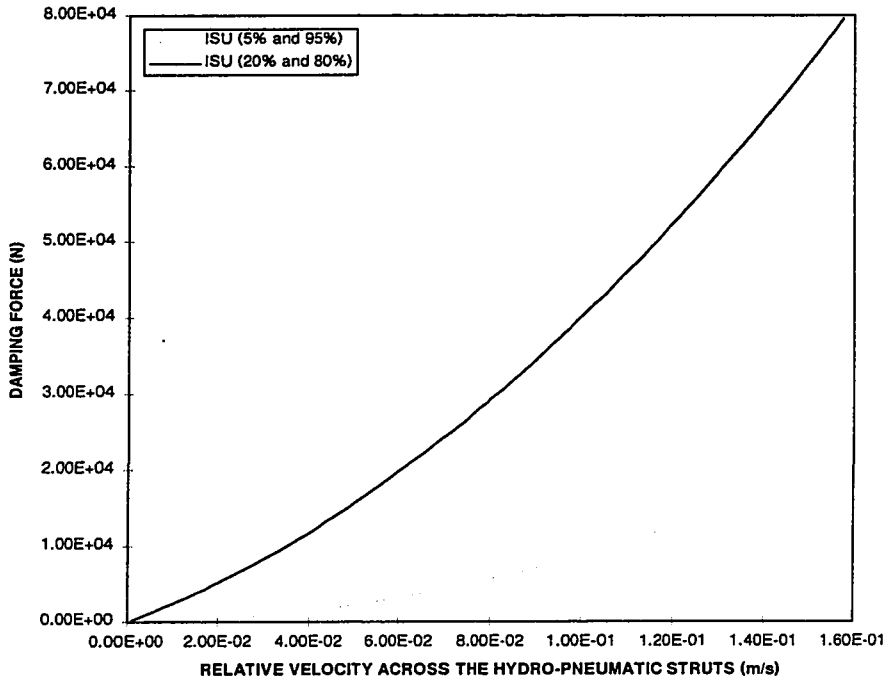

Figure 3.15 Damping force developed by single interconnected strut of spring loaded interconnected hydro-pneumatic unit under bounce mode at different load

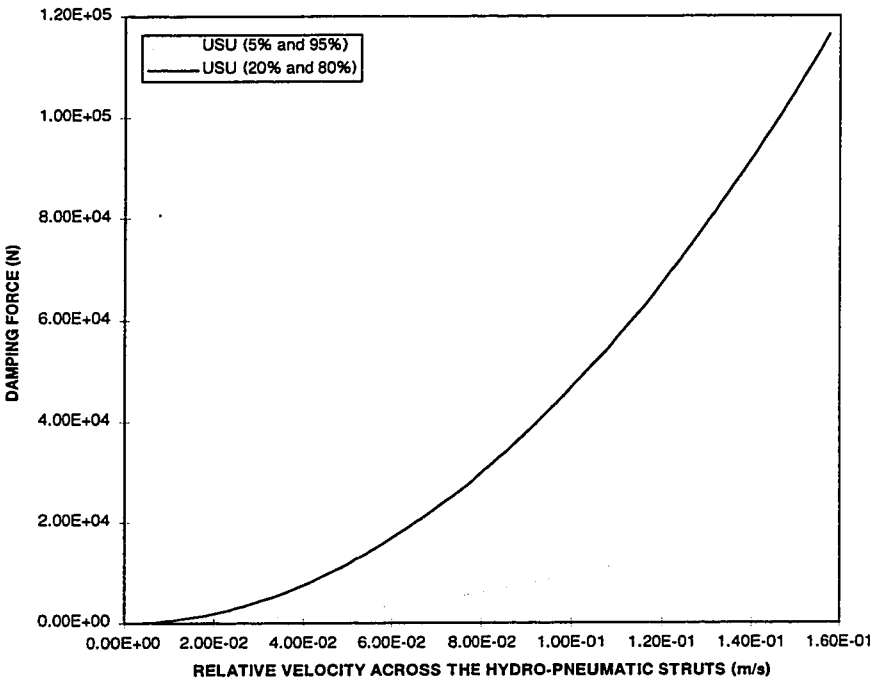

Figure 3.16 Damping force by single independent strut of spring loaded independent hydro-pneumatic unit under bounce mode at different load combination

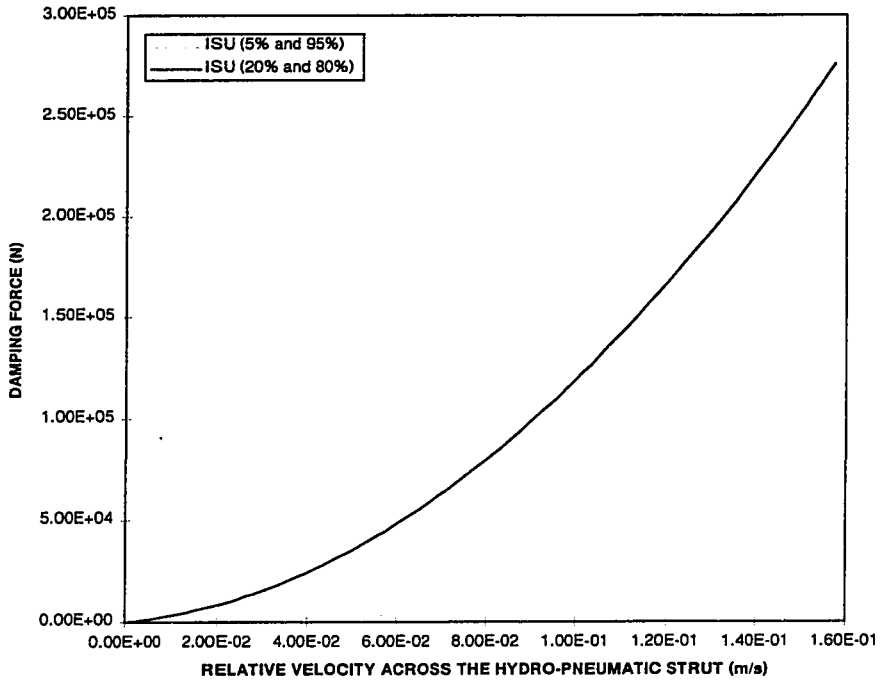

Figure 3.17 Damping force developed by single interconnected strut of spring loaded hydro-pneumatic suspension under roll mode at different load combination

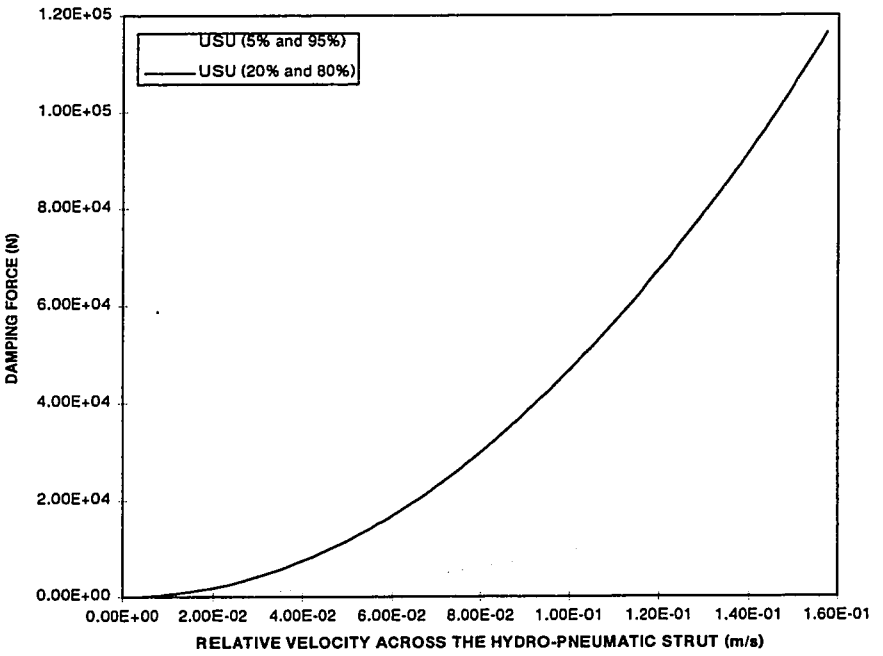

Figure 3.18 Damping force by single independent strut of spring loaded independent hydro-pneumatic unit under roll mode at different load combination

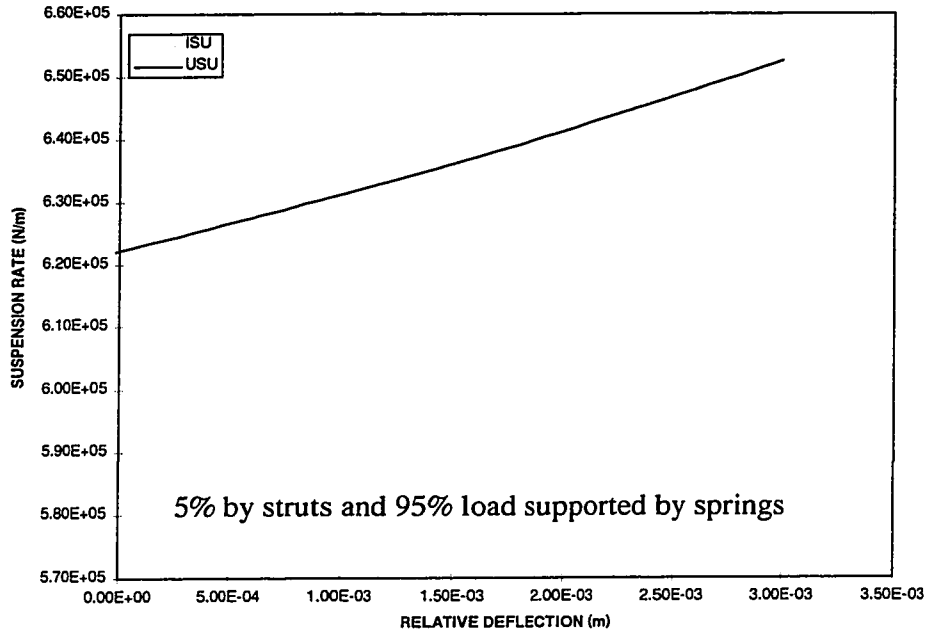

Figure 3.19 Suspension rate of two different suspension systems

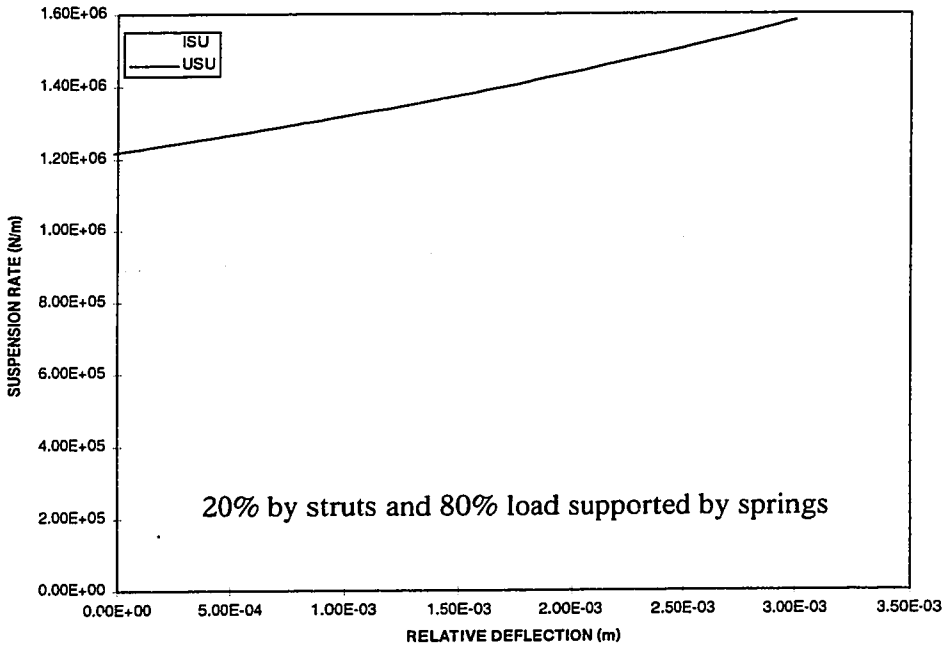

Figure 3.20 Suspension rate of two different suspension systems

to air spring hardening effect. Larger ride rate in suspension is not desirable as it adversely effects the ride quality.

The most interesting aspect of interlink suspension system is the effective roll properties. Figure 3.21 shows effective roll stiffness as a function of sprung mass roll angle for 100% load supported by interconnected and unconnected struts. As expected, the roll stiffness is larger for the interconnected system where as shown the stiffness in both cases decreases slightly for an increase in the roll angle. This results from the fact that in hydro-pneumatic system, the sprung mass moves upwards under a pure roll input effectively reducing the gas spring effect. Similar trend is again observed for 5% load carried by strut as shown in Figures 3.22. In this case with parallel spring, however, effective roll stiffness is significantly larger than that of pure struts. Furthermore, in the case of parallel spring supporting bulk of the load, the drop in the roll stiffness with increasing roll angle is significantly less. For pure strut the roll stiffness was found to reduce by 20% for a roll angle of 0.18 radian, whereas for spring supported system the reduction is less than 1% for the same roll angle.

For the results obtained so far, it is evident that increase in percentage load to strut increases damping force as well as suspension rate in the bounce mode. Its effect on the transient response of the sprung mass is shown in Figure 3.23 under a half sine pure bounce road input.

As the result shows, there is a trade off involved in selecting the percentage load assignment to struts and springs. As it was shown earlier, 5% and 95% load distribution to

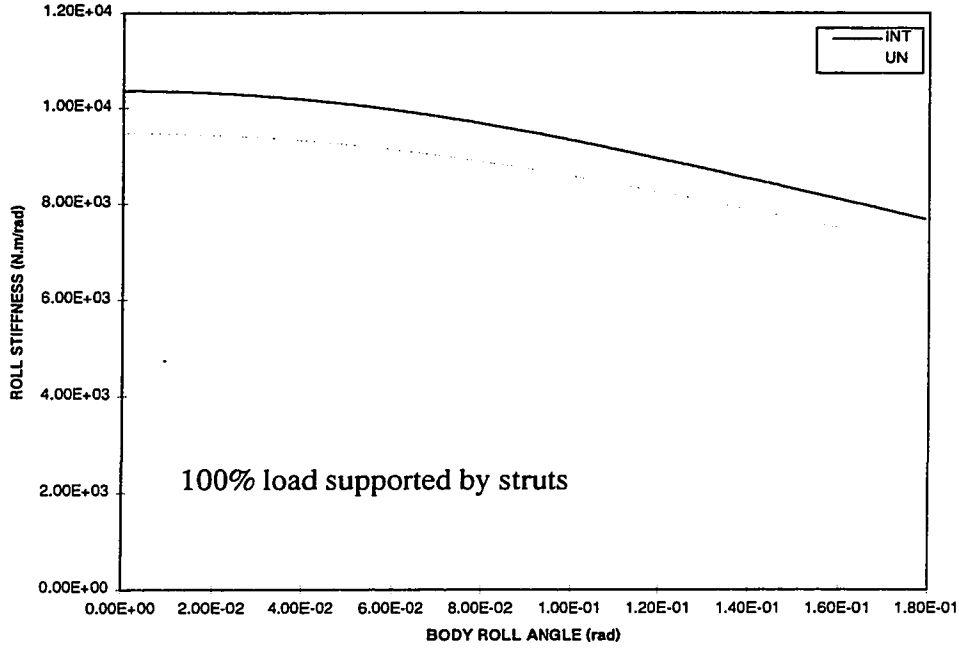

Figure 3.21 Roll stiffness capability of suspensions with hydro-pneumatic struts

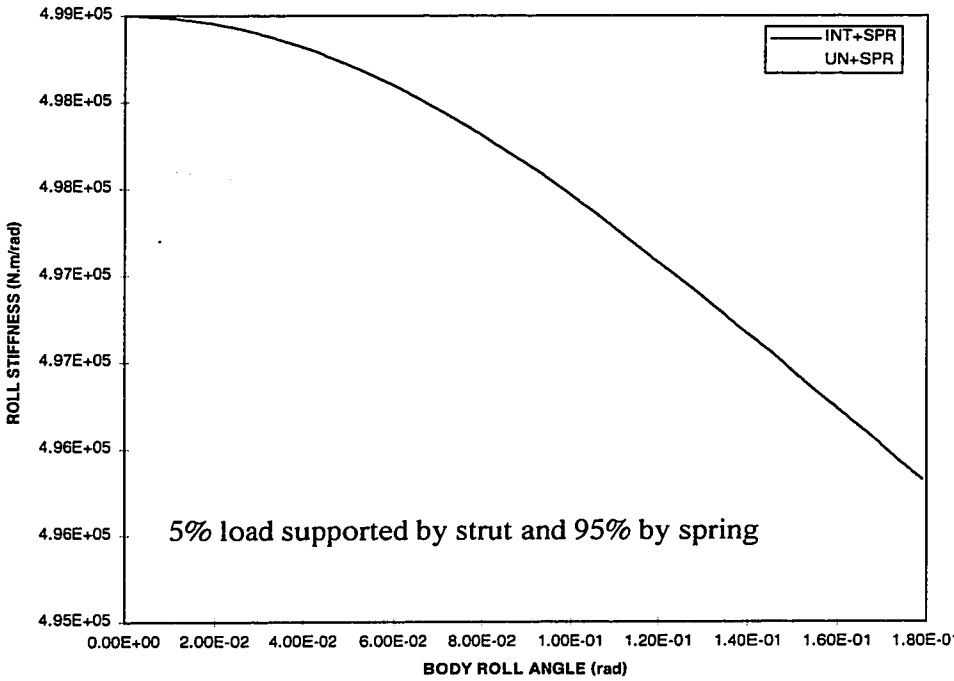

Figure 3.22 Roll stiffness capability of spring loaded hydro-pneumatic suspensions

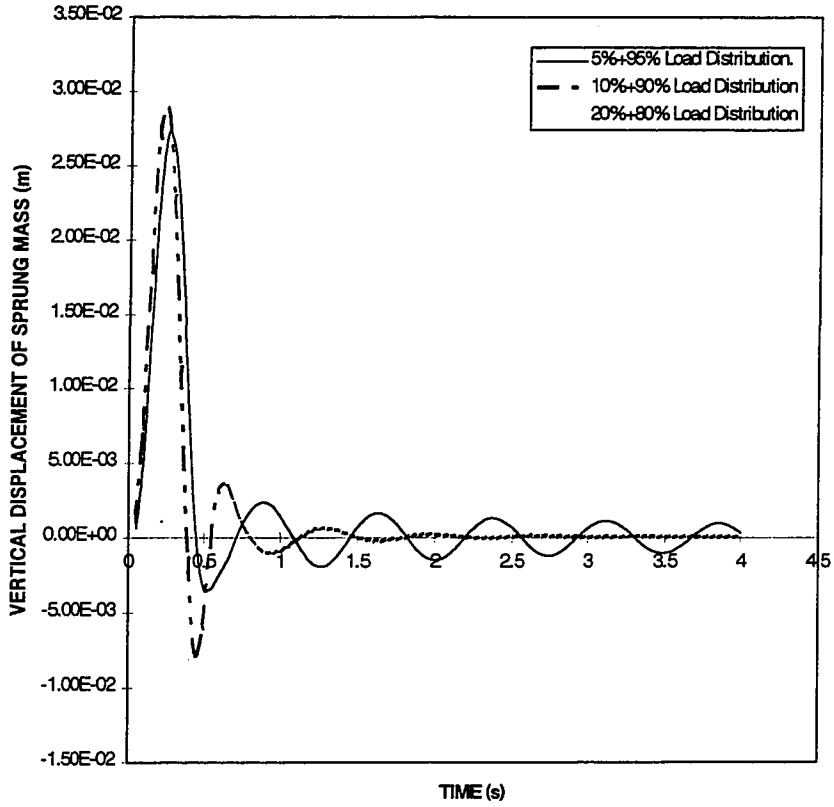

Figure 3.23 Vertical displacement response of sprung mass under different load distribution on struts and mechanical springs in suspension unit. Excitation: 0.02m in-phase half sine road input

strut and spring, respectively lead to peak pressure of (218 Psi) whereas 20% and 80% load distribution lead to pressure of over (408 Psi). Since practical design of interconnected suspension is a key issue in this dissertation, 5% and 95% load to strut and spring, respectively, is selected as the base line system.

On the bases of parameteric study and practical design considerations, three interconnected configurations namely: ISU-1, ISU-2 and ISU-3 are selected for variation in piston and piston rod area, as shown in Table 3.4. In each case mechanical spring stiffness (k) is selected such that 95% of load is supported by the spring and that static deflection of the suspension is around 0.168 m.

For each of the interconnected configuration identical bar is included to obtain enhanced roll stiffness. Table 3.4 further presents two configurations for unconnected system with parallel spring carrying 95% of the load. These configurations with out anti-roll bar is referred to as USU and with anti-roll bar is referred to as USUA. A comparative study of suspension static properties is next presented for the five different configurations presented in Table 3.5.

3.7 PROPERTIES OF SELECTED SUSPENSION CONFIGURATIONS

Suspension properties for the five different configurations presented in Table 3.5 are computed and compared at design ride height. Static properties are obtained in terms of suspension rate, roll stiffness and effective static deflection for identical load carrying capacity. These properties for the five configurations are presented in Table 3.5. The primary differences in the three interconnected configurations are piston and rod size. The

TABLE 3.4

Simulation parameters of different spring loaded hydro-pneumatic suspension units

Parameters	Interconnected with antiroll bar (ISU-1)	Interconnected with antiroll bar (ISU-2)	Interconnected with antiroll bar (ISU-3)	Independent (USU)	Independent with anti-roll bar (USUA)
Static gas Pressure P_o (N/m^2)	2588154.5	2767104.7	3412922.0	2562909.1	2562909.1
Static gas volume V_o (m^3)	5.37195×10^{-5}	5.37195×10^{-5}	4.18237×10^{-5}	4.18237×10^{-5}	4.18237×10^{-5}
Effective piston head area A_2 (m^2)	1.44×10^{-3}	1.34634×10^{-3}	1.07785×10^{-3}	1.07785×10^{-3}	1.07785×10^{-3}
Effective rod side area A_1 (m^2)	4.376×10^{-5}	5.92×10^{-5}	6.322×10^{-5}	-	-
Piston rod area A_r (m^2)	1.39624×10^{-3}	1.28714×10^{-3}	1.02465×10^{-3}	-	-
Dia. of interlinked pipe D (m)	0.0029	0.0029	0.0029	-	-
Length of interlinked pipe L (m)	1.4246922	1.4246922	1.4246922	-	-
Orifice area a (m^2)	0.0016×10^{-3}	0.0016×10^{-3}	0.0016×10^{-3}	0.0016×10^{-3}	0.0016×10^{-3}
Linear spring stiffness k (N/m)	498099.03	498099.03	498099.03	498099.03	498099.03
Roll stiffness of anti-roll bar (KNm/rad)	146.6	146.6	146.6	-	146.6

TABLE 3.5

Static properties of spring loaded hydro-pneumatic suspension units

Suspension Property	Interconnected with antiroll bar (ISU-1)	Interconnected with antiroll bar (ISU-2)	Interconnected with antiroll bar (ISU-3)	Unconnected USU	Unconnected with antiroll bar USUA
Load carrying capacity (N)	138419	138419	138419	138419	138419
Suspension rate (KN/m)	592	583	584	597	597
Roll stiffness (KNm/rad)	732	718	720	520	702
Amplification factor	1.062	1.091	1.12	1.0	3.79
Effective static deflection	0.1689	0.172	0.1867	0.1678	0.1678

resulting ride height suspension rate in all cases are comparable where unconnected systems yield the largest as it is a function of piston head area. The effective roll stiffness for all configurations with anti-roll bar are also comparable. The roll stiffness amplification factor as defined in equation (3.41) for interconnected system are also presented in Table 3.5. As shown, the configuration ISU-3 leads to the largest amplification factor. For unconnected system without antiroll bar the amplification factor is one, whereas, for the one with the antiroll bar is larger as it is defined by equation (3.56). For each of the configurations the resulting static deflection were found to be around the largest value of 0.168 m.

The dynamic properties of the suspension configurations are further evaluated as functions of vertical and roll displacements of the sprung mass with respect to the unsprung mass. Figure 3.24 presents the vertical suspension rates for the five configurations with both unconnected system USU and USUA (with antiroll bar) showing the same rates. As these results illustrate, all suspensions due to gas spring component exhibit progressively hardening properties. For the selected parameters highest rate is provided by the unconnected system whereas, the lowest rate is obtained due to interconnected ISU-2. ISU-1 provides an intermediate rate.

Similar plot for effective roll stiffness as a function of relative roll angle between sprung and unsprung mass is shown in Figure 3.25. Roll stiffness of all the interconnected and unconnected system with antiroll bar are comparable and has similar trend. In all cases the roll stiffness tends to decrease with an increase in roll angle. As discussed earlier, this results due to hydro-pneumatic struts where the strut under compression has hardening effect that leads to vertical motion of sprung mass under pure roll inputs.

For isolation of vibration, damping properties of the suspension plays the most important role. The vertical and roll damping properties are therefore evaluated for the five configurations. Since antiroll bar has no influence on the damping properties the results for USU and USUA are identical as shown in Figures 3.26 and 3.27. The damping forces are primarily produced due to flow through a fixed orifice and through interconnected pipes. The damping force of a single strut in bounce mode (Figure 3.26) is computed under identical vertical velocities of the right and left wheels, while damping force in roll mode

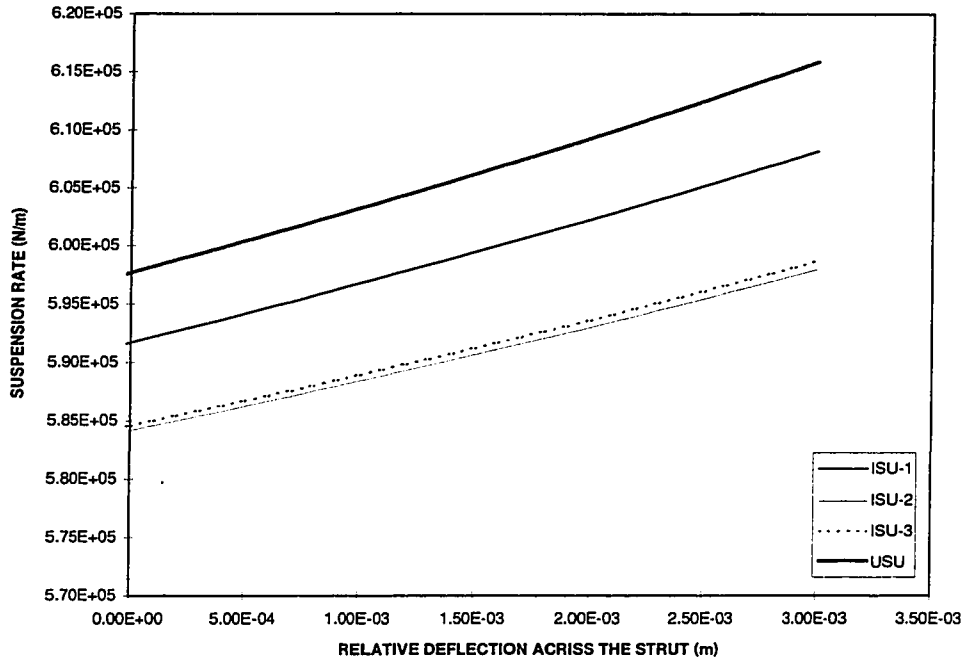

Figure 3.24 Suspension rate of various suspension units

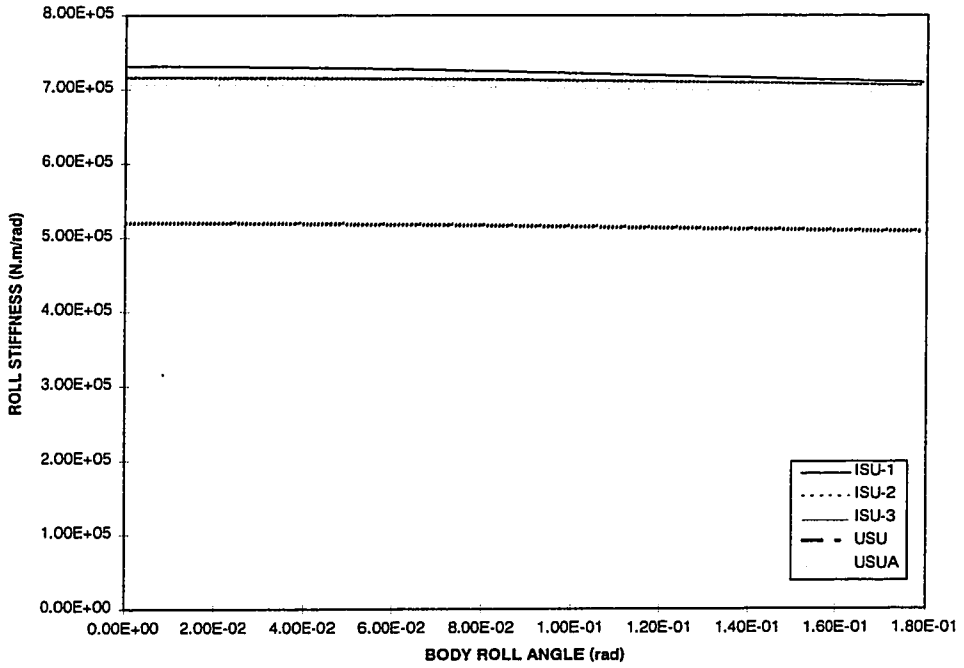

Figure 3.25 Roll stiffness of various suspensions

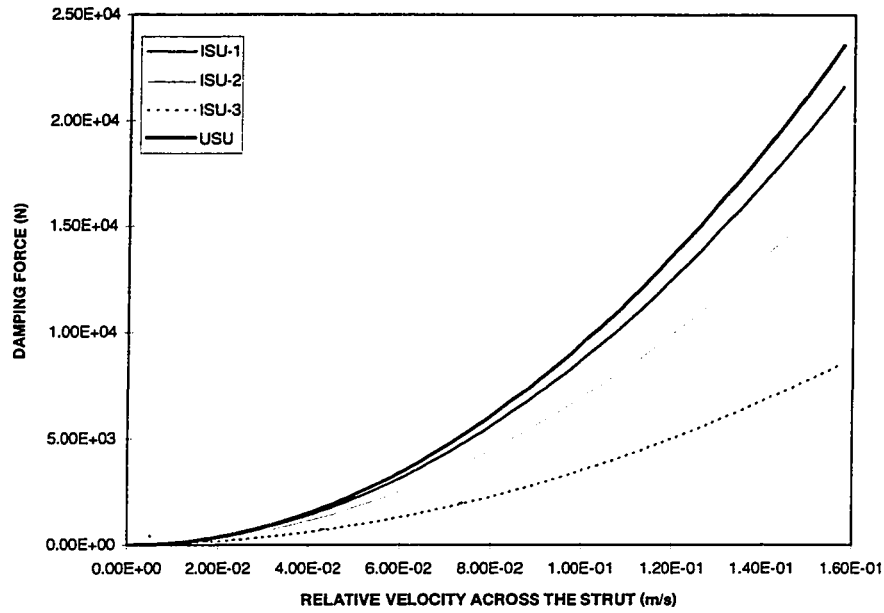

Figure 3.26 Damping force developed by one strut under bounce mode

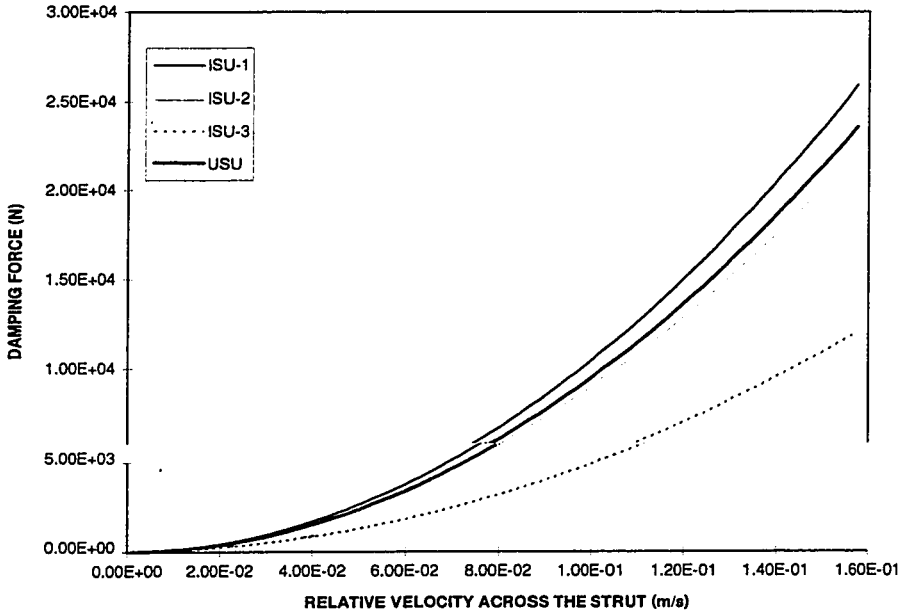

y%Á

Figure 3.27 Damping force developed by one strut under roll mode

(Figure 3.27) is computed by subjecting the right and left wheels to out of phase vertical velocities. These results clearly indicate that even for identical orifice area, the resulting damping properties are quite different due to different piston area ratio. Among the interconnected systems ISU-1 produces the largest damping force both in bounce and roll, while ISU-3 produces the lowest. In bounce mode unconnected system produces the highest damping force as all flow is through the orifice. However, for roll mode interconnected system can be configured to produce larger damping force than that of unconnected system as shown in Figure 3.27.

3.8 SUMMARY

Analytical expression of four different suspension properties namely: load carrying capacity, suspension rate, damping properties in bounce and roll mode and roll stiffness are derived to describe the static and dynamic properties of interconnected and unconnected suspension units. Parametric study has been carried out to investigate the influence of mechanical spring on size and parameters of hydro-pneumatic struts. On the basis of parametric study five different suspension configurations are developed namely: spring loaded interconnected hydro-pneumatic suspension ISU-1, ISU-2 and ISU-3 with anti-roll bar, Spring loaded unconnected hydro-pneumatic suspension USU and unconnected with anti-roll bar USUA are finally developed. In chapter 4, these different suspension configurations are used to investigate the dynamic response of the vehicle.

CHAPTER-4

DYNAMIC RESPONSES OF THE SPRING LOADED INTERCONNECTED HYDRO-PNEUMATIC SUSPENSION WITH FIXED ORIFICE DAMPING

4.1 INTRODUCTION

Ride quality and directional performance of road vehicles are strongly dependent on the vehicle suspension characteristics. In order to assess the ride quality and directional response of the vehicle in terms of sprung mass and unsprung mass responses, different types of input are introduced through tire-terrain interface and by steering input. Ride quality can be assessed in terms of acceleration perceived by the driver and passenger through suspension unit during road disturbances. Vehicle control performances are assessed in terms of the ability of suspension unit to counteract the roll moment during directional maneuvers and during lane changing. In this chapter, 4-DOF roll plane vehicle model developed in chapter 2 is investigated for transient ride and roll responses. A comparative study is carried out for the vehicle equipped with different suspension configurations proposed in chapter 3. The types of excitations arising from the tire-terrain interaction and steering inputs used in this investigation are discussed in brief. Vibration transmissibility characteristics of different suspensions with fixed orifice are investigated by using harmonic excitations arising from the tire-terrain interactions. The roll performance characteristics of the suspension systems are evaluated in terms of the transient and steady state roll responses of sprung and unsprung masses during constant

radius turning and lane change maneuvers. Simulation results for the nonlinear systems are obtained of the proposed models in time-domain by using forth order Runge-Kutta method [57, 58].

4.2 EXCITATIONS TO THE ROLL PLANE MODEL

Input data are selected to be representative of typical excitations arising from steering maneuvers and tire-terrain interface. The excitations arising from the tire-road contact can be expressed by in-phase and out-of-phase sinusoidal harmonic excitations in the frequency range of 0.015 Hz to 12 Hz, in order to assess the vertical, roll and lateral vibration transmission response of the suspension systems. The excitations arising from the steering input can be expressed as steady state and transient lateral acceleration experienced by the sprung and unsprung masses.

4.2.1 LATERAL ACCELERATION EXCITATIONS

The sprung and unsprung masses of a vehicle experience roll motion and centrifugal acceleration during a directional maneuver. Although the roll motion of the sprung mass yields a small roll moment due to its lateral displacement, the centrifugal acceleration cause the primary overturning moment on the vehicle [50, 59]. Figures 4.1 and 4.2 demonstrate the type of steady state lateral acceleration experienced during constant radii maneuvers and transient lateral acceleration experienced by vehicle during continuous lane changing maneuvers. The handling quality of the vehicle is primarily related to the

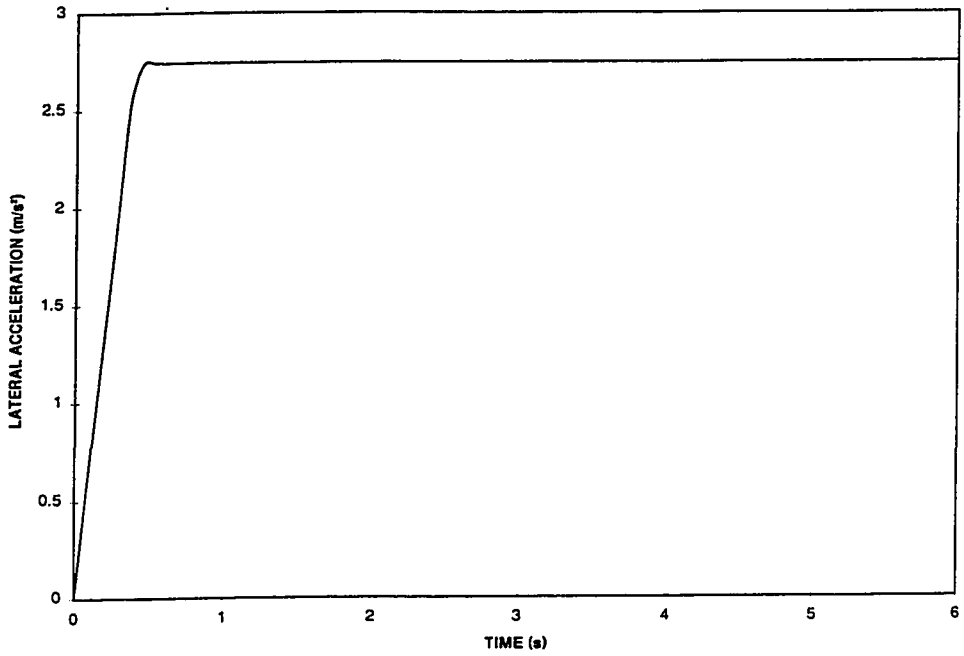

Figure 4.1 Step lateral acceleration experienced by vehicle during steady state turning

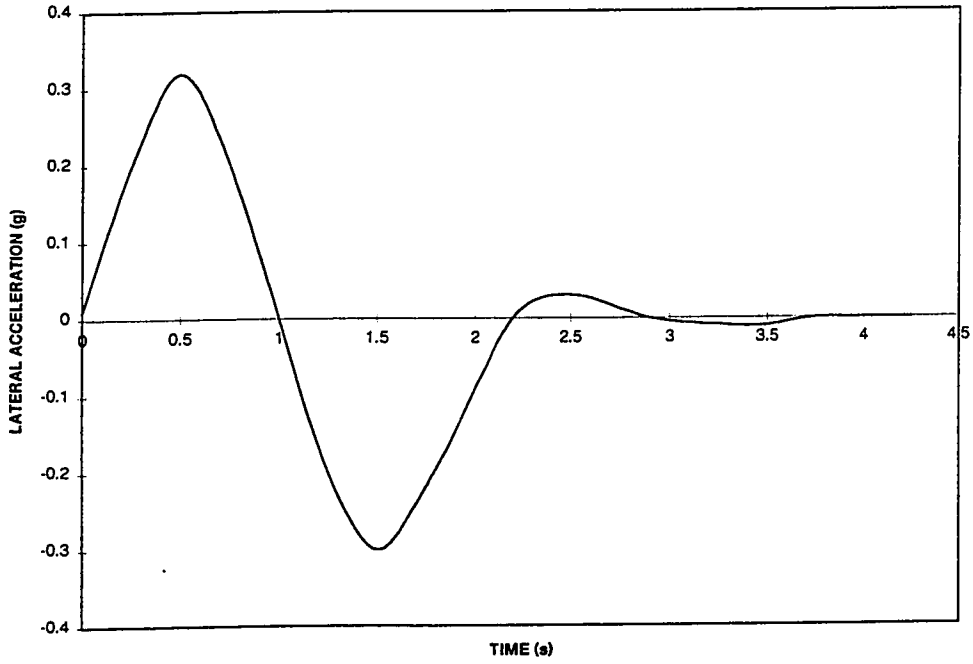

Figure 4.2 Transient lateral acceleration of bus during a continuous lane change maneuver

vehicle's ability to counteract the roll / overturning moment caused by the lateral displacement or centrifugal acceleration. Various studies on the directional handling of heavy vehicles have concluded that rollover threshold, which is the maximum value of lateral acceleration that a vehicle can withstand during a steady turn, lies in the range of 0.3 g to 0.5 g [52].

Field tests were conducted on a highway bus to identify the nature of realistic lateral acceleration excitations. Although, the maximum lateral acceleration of 0.5 g was measured on the skid-pad, the maximum level of lateral acceleration measured during a continuous lane change maneuver at maximum permissible speed was obtained as 0.3 g. The transient lateral acceleration measured on a highway bus during a continuous lane change maneuver at 110 km/h, shown in Figure 4.2 is used in this investigation. The maximum level of lateral acceleration excitation experienced by the sprung and unsprung masses can thus be limited to 0.3 g. Figure 4.2 further reveals that lateral acceleration during a continuous lane change maneuver can be approximated by a sinusoidal input with a frequency of approximately 0.3 Hz. The magnitude and frequency of lateral acceleration excitation, however, decrease when the maneuvers are performed at reduced speeds. The lateral acceleration excitation, shown in Figure 4.2, is thus taken as realistic input under severe maneuvers.

4.2.2 Excitations Due to Tire-Terrain Interactions

The ride quality of a vehicle is measured in terms of response magnitude in the frequency domain. Human body is most sensitive to vertical vibration over a range of 4-8 Hz, and to

horizontal vibration up to 2 Hz [50]. Various studies have been performed to analyze for ride vibration characteristics of buses. Results reveal the following [60]:

(I) The passengers perceived appreciable level of low frequency vertical vibration due to tire-terrain interaction.

(II) The level of longitudinal vibration is considerably smaller than that of vertical vibration.

(III) Passengers perceived significant level of lateral vibration due to out-of-phase excitation under left and right wheel and also a second source of excitation due to centrifugal acceleration developed during turning action.

The lateral vibration at the passenger's location is frequently experienced due to out-of-phase road input and the high seated location of the passengers. Thus the analysis of ride comfort requires nature and description of the road profile and magnitude of lateral acceleration. System vibration developed due to random road input are expressed in terms of displacement as well as acceleration power spectral densities. Alternatively, ride quality can be effectively assessed using deterministic inputs, in terms of the vibration transmissibility over a frequency range of 0.015 to 12.0 Hz. Relative transient response characteristics of different suspensions may be evaluated using a bump excitation characterized by a half sine pulse as well as a step input shown in Figures 4.3 and 4.4, respectively. Two types of road excitations are used to assess the relative vibration transmissibility characteristics of the bus suspension models: (I) in-phase excitation,

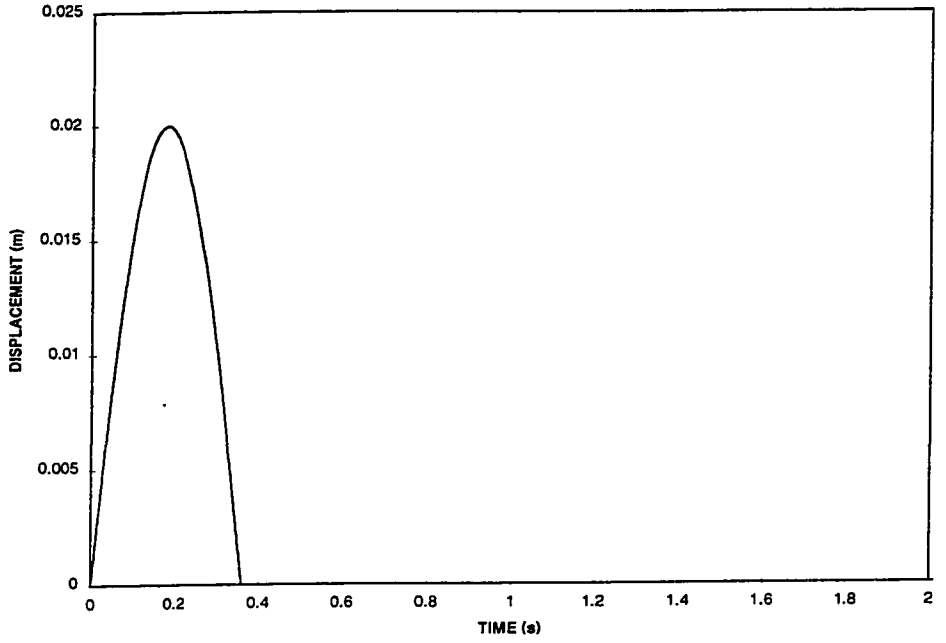

Figure 4.3 Half-sine displacement occurring at tire-terrain interface

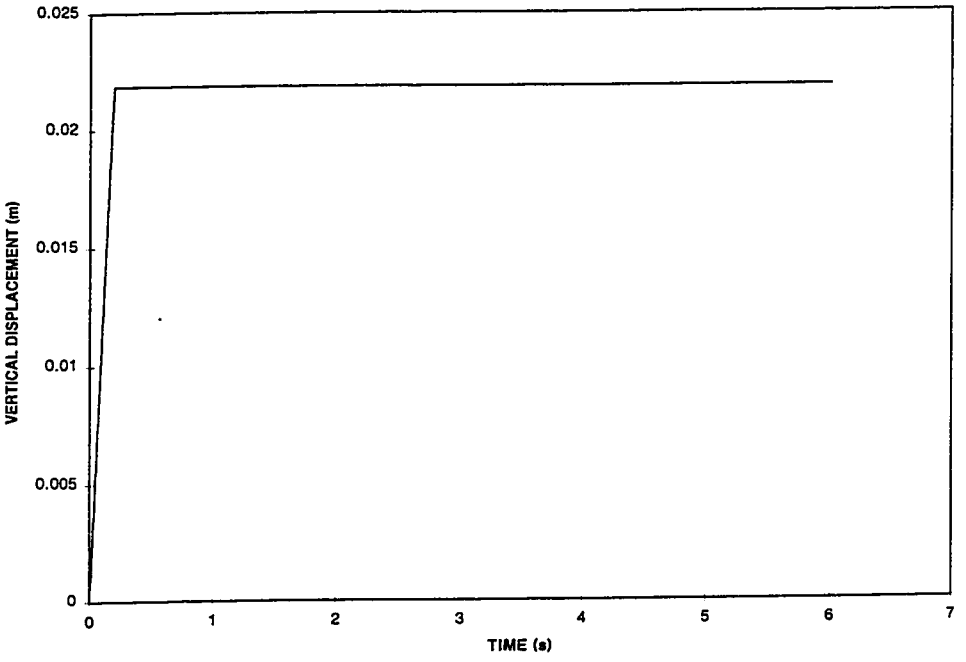

Figure 4.4 Step road input occurring at tire-terrain interface

right and left tires experiencing identical amplitude of vertical sinusoidal excitations; and (II) out-of phase excitation, left and right tires experiencing identical level of vertical excitation 180 degree out-of-phase with respect to each other. The vehicle response to the in-phase excitation will express only the level of vertical vibration transmitted through the suspension unit, while the response to the out-of-phase excitation will provide vertical, roll, and lateral vibration transmission characteristics of the suspension systems.

4.3 VEHICLE RESPONSE TO LATERAL ACCELERATION EXCITATIONS

The equations of motion of 4-DOF roll plane vehicle model with different suspension units have been described in Chapter 2. The handling characteristics of vehicle models are evaluated by introducing lateral acceleration excitations encountered during steady turn and lane change maneuvers. Lateral acceleration experienced by vehicle during constant radii maneuvers and continuous lane changing maneuvers have been presented in Figures 4.1 and 4.2, respectively.

4.3.1 Response to a Constant Lateral Acceleration

Roll response of sprung mass of the vehicle equipped with five different suspension configurations subject to steady state lateral acceleration during a constant radii maneuver are presented in Figures 4.5 and 4.6. These results represent transient roll velocity and acceleration response to step input can be ranked according to their level of damping force developed under roll mode. As can be observed, vehicle with interconnected suspension ISU-3 shows highest peak velocity among all suspensions considered. This is

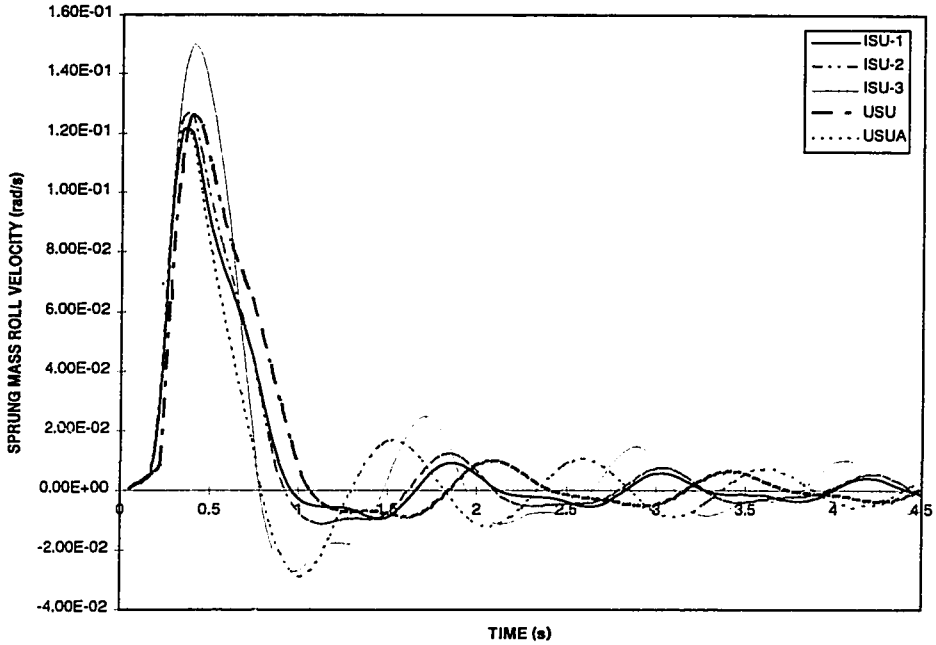

Figure 4.5 Roll velocity response of sprung mass equipped with different suspension units subject to a step lateral acceleration during steady state maneuvers

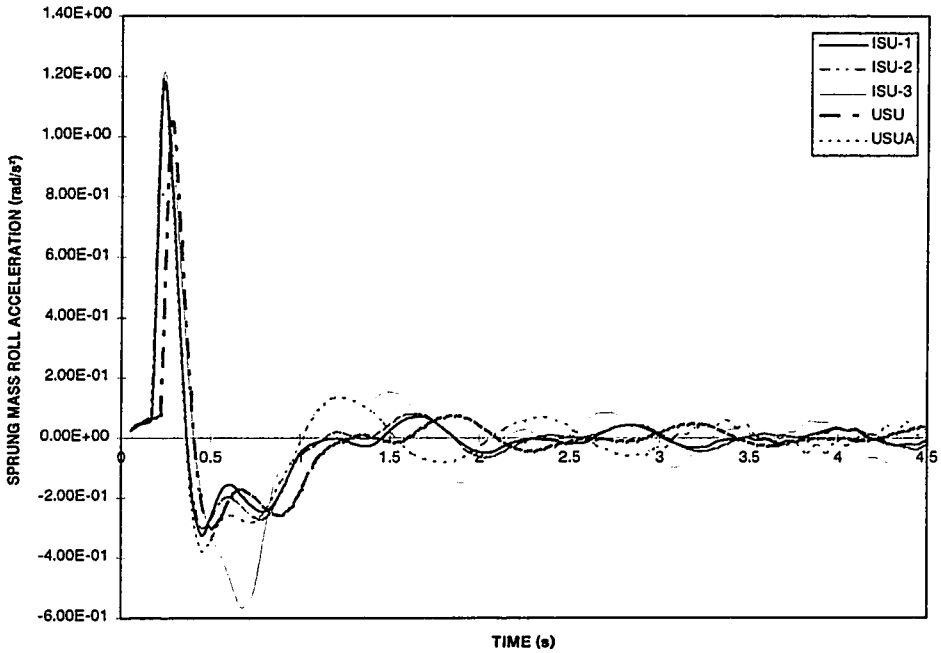

Figure 4.6 Roll acceleration response of sprung mass of vehicle equipped with different suspension units subject to a step lateral acceleration during steady turning manuevers

due to low damping force developed by strut under roll mode as described in previous chapter. The peak is the lowest and the rate of decay is the fastest when vehicle is equipped with ISU-1 suspension. This is due to the high damping force developed by this suspension in roll mode.

4.3.2 Response to a Transient Lateral Acceleration

Roll angle response of sprung mass with different vehicle suspensions, subjected to transient lateral acceleration during a lane change maneuver is presented in Figure 4.7. The corresponding roll velocity of the sprung mass is shown in Figure 4.8. Figures 4.7 and 4.8 clearly show that interconnected suspension in roll plane have better capability to control the body roll angle and roll velocity as compared to unconnected vehicle suspension. This is mainly due to the presence of interconnection between the hydraulic struts, which provides extra damping resulting from laminar fluid flow through the interlink pipes. Unconnected suspension with anti-roll bar exhibits effective anti-roll capability due to presence of anti-roll stiffeners. Similar response can also be obtained by interconnected system such as ISU-2. Peak amplitude roll angle of interconnected suspension units and unconnected suspension with anti-roll bar are observed over the range of 0.03 to 0.034 radians, while peak amplitude of sprung mass of unconnected system without anti-roll bar is observed around 0.042 radian. Roll velocity response of sprung mass with interconnected suspensions and independent suspension with anti-roll bar are observed around 0.15 radian per second. Peak amplitude of roll velocity of sprung mass with unconnected suspension is computed around 0.18 radian/sec.

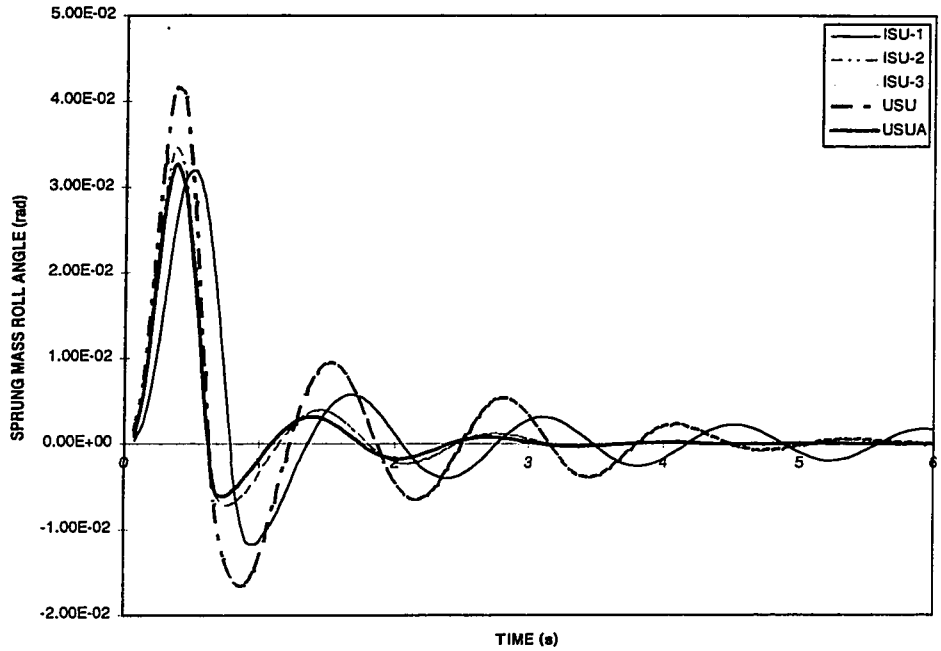

Figure 4.7 Roll angle response of sprung mass equipped with different suspension configurations subject to transient lateral acceleration

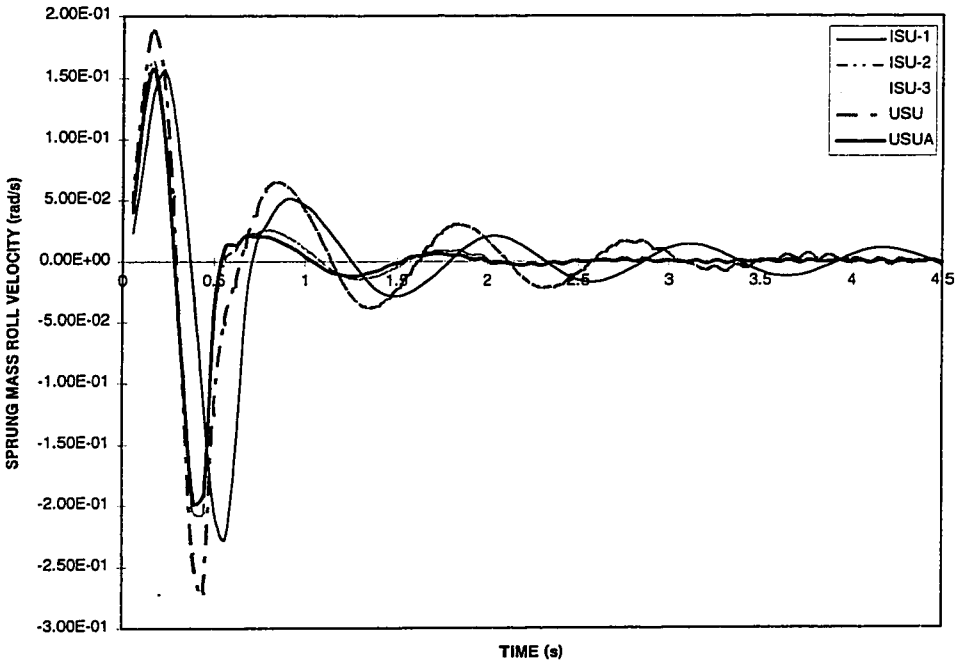

Figure 4.8 Roll velocity response of sprung mass equipped with different suspension configurations subject to transient lateral acceleration

4.4 VEHICLE RESPONSE TO ROAD EXCITATIONS

Dynamic ride characteristics of the vehicle employing various suspension configurations are analyzed in terms of transient vertical and roll response of the sprung mass, when subjected to excitations at the tire-terrain interface. The vertical shock attenuation characteristics are evaluated for in-phase half-sine excitation, while the roll attenuation characteristics are evaluated for an out-of -phase half-sine bump excitation. A step road input is further used at the right tire-terrain interface to evaluate the bounce and roll response characteristics of the interconnected and unconnected hydro-pneumatic suspension units.

For each of the five suspension configurations, transient response is obtained when subjected to a half-sine in-phase excitation of 0.02 m. Sprung mass vertical displacement, velocity and acceleration responses are shown in Figures 4.9, 4.10 and 4.11, respectively. As the results show, interconnected ISU-1 configuration along with unconnected USUA leads to similar and lowest response magnitude. In all cases ISU-3 provides the highest response. This is attributed to the fact that ISU-3 configuration yields highest damping. Vertical displacement response of the unsprung mass for the same input is shown in Figure 4.12 for the five different suspension configurations. In this case the trend shows that unconnected system leads to highest peak with fastest decay, whereas interconnected system ISU-3 leads to lowest peak.

For each of the five suspension configurations, the transient responses are next

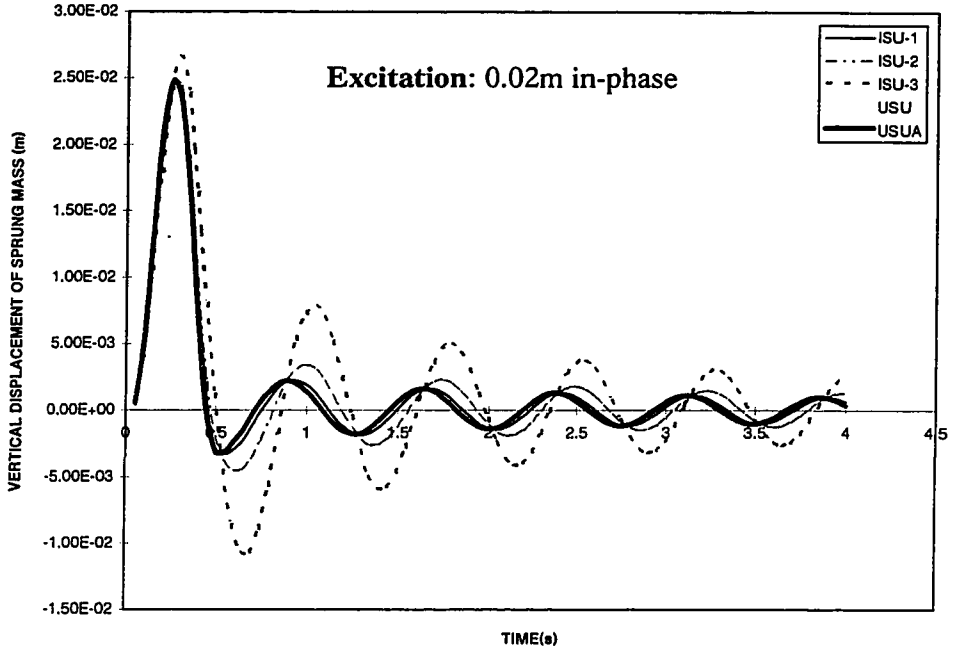

Figure 4.9 Sprung mass displacement response with different suspension units by using in-phase half-sine vertical road input

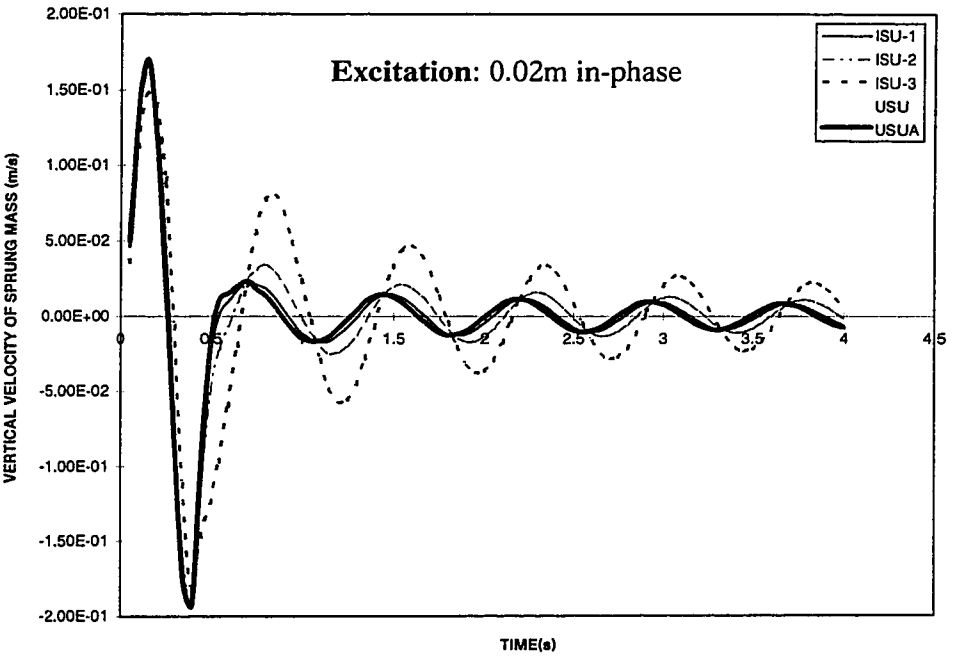

Figure 4.10 Sprung mass velocity response with different suspension units by using in-phase half-sine vertical road input

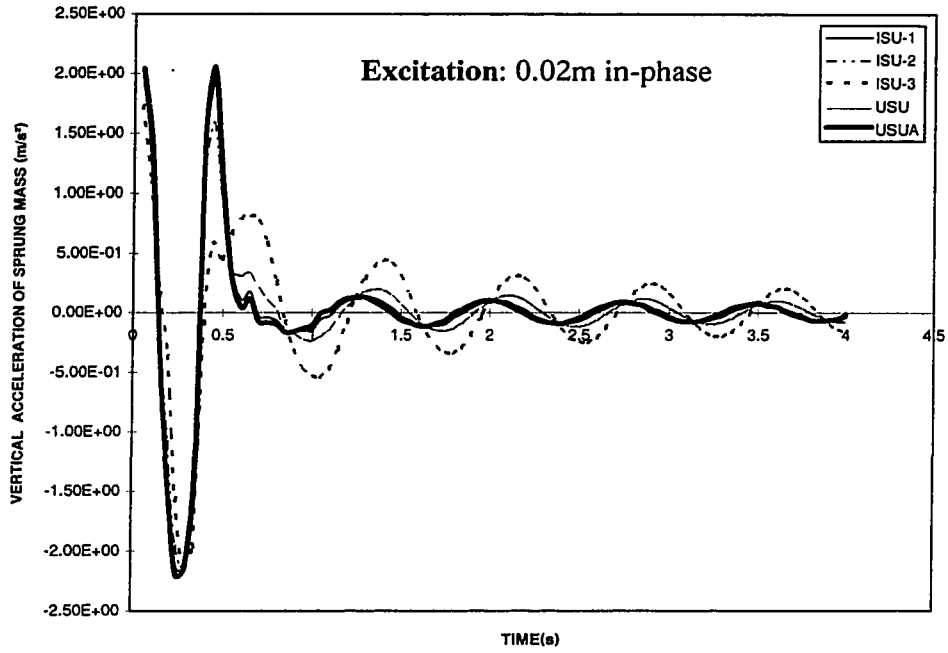

Figure 4.11 Sprung mass acceleration response with different suspension units by using in-phase half-sine vertical road input

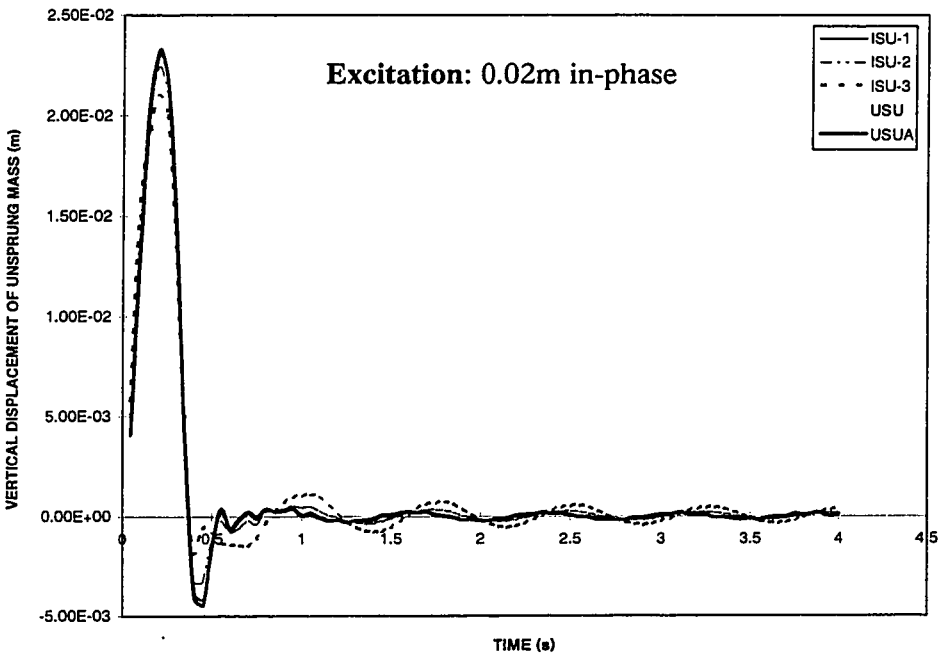

Figure 4.12 unsprung mass displacement response with different suspension units by using in-phase half-sine vertical road input

obtained for out-of-phase half-sine excitation of 0.02 m. The resulting transient roll response of the sprung mass are shown in Figure 4.13. Figure 4.14 presents the corresponding sprung mass roll velocities. The figures clearly reveal that peak roll displacement response of the vehicle is due to ISU-3 as it has high suspension damping in the roll mode. For the same reason, the decay of response is also rapid. The vehicle with ISU-1 yields the lowest values of peak roll displacement and velocity due to its low roll mode damping characteristics. However, as expected, the decay in this case is slower. These results further demonstrate insignificant influence of anti-roll bar since body roll angle is small under the given input. The roll response in term of ride can be compared with the roll response results in terms of handling under transient lateral acceleration input presented in Figure 4.7. The comparison reveals that among interconnected systems, ISU-1 provides the best ride and worst handling response. It can then be concluded that high damping is desirable for handling, while low damping is preferable for ride quality. This conflicting requirement, however, can not be satisfied by a suspension with fixed orifice damping.

The performance of the five suspension configurations is next examined under step input. Sprung mass response in terms of displacement and velocity are indicators of shock attenuation performance of the suspension units. The simulation results for sprung mass displacement and velocity are shown in Figures 4.15 and 4.16. Similar to previous results, configuration ISU-3 due to high damping, leads to highest peak under shock with fastest decay of the response. As shown, the response of all other configuration under shock was found to be similar. The response of the unsprung mass under the same input

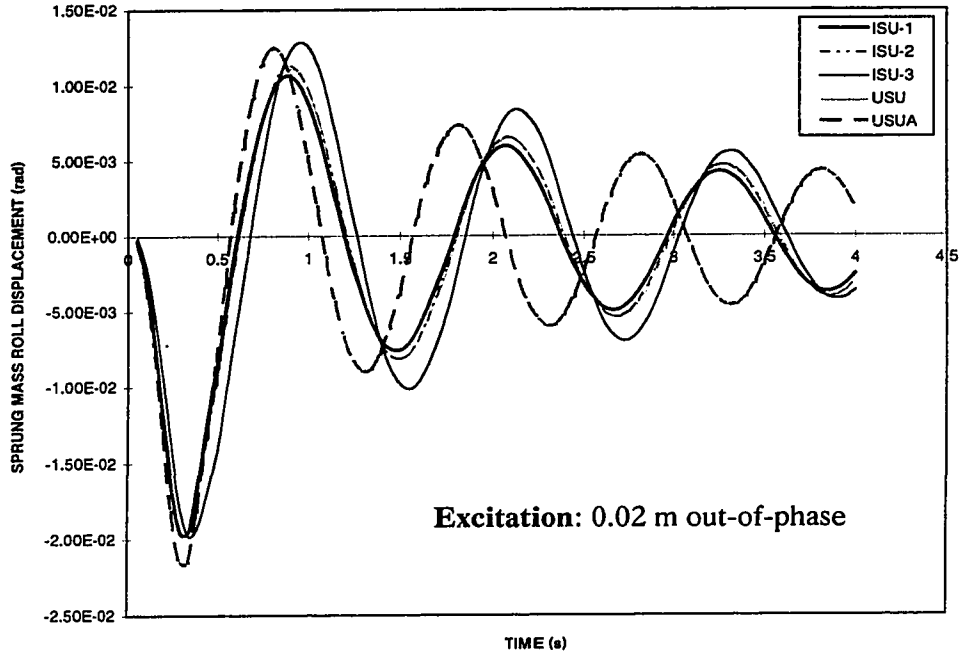

Figure 4.13 Roll displacement response of sprung mass with different suspension units by using out-of-phase half-sine road input

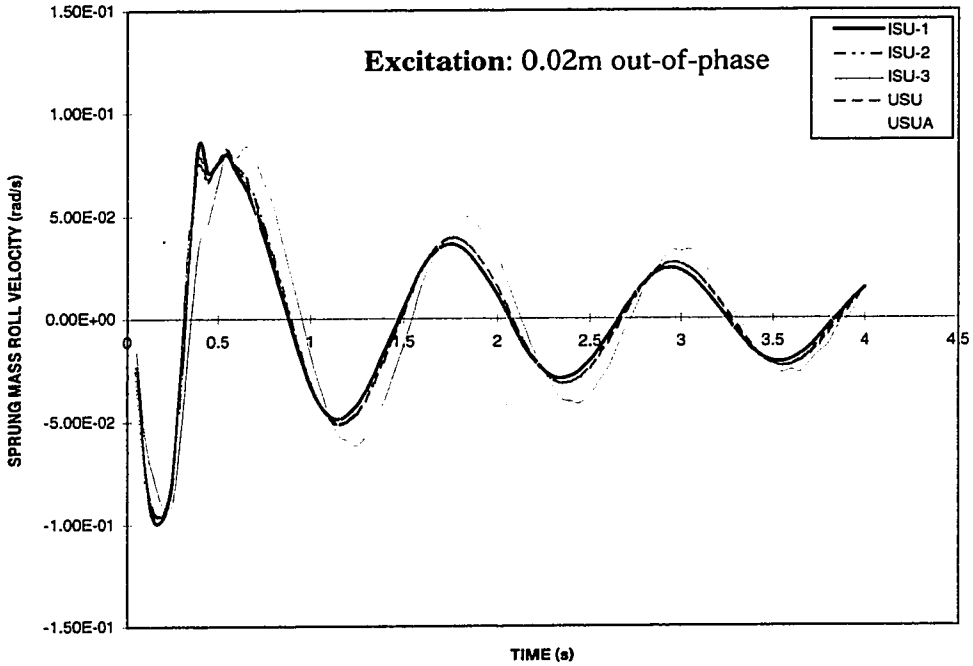

Figure 4.14 Roll velocity response of sprung mass with different suspension units by using out-of-phase half-sine road input

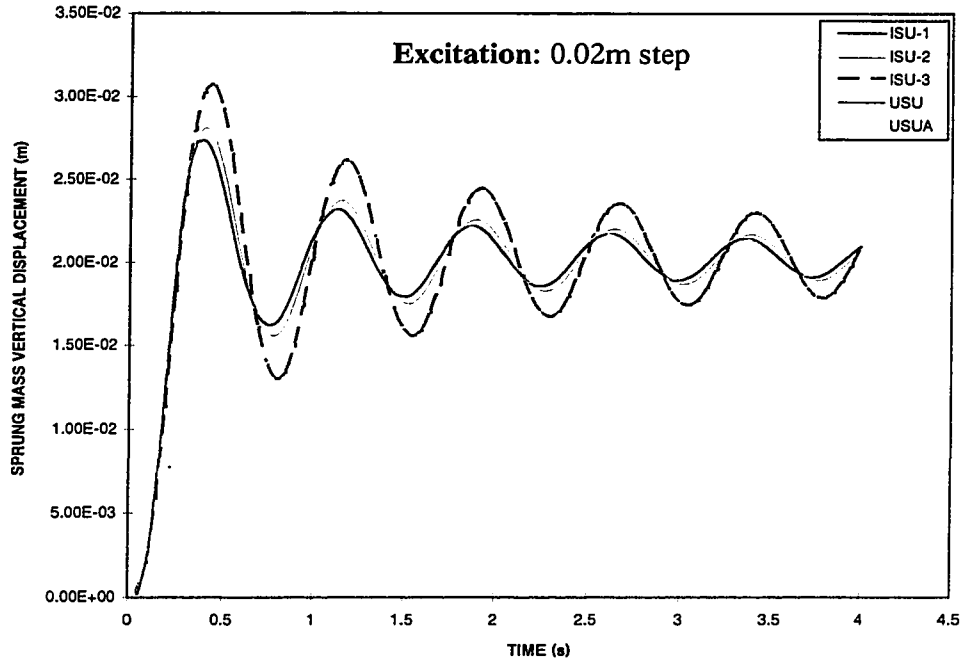

Figure 4.15 Vertical displacement response of sprung mass with different suspension units under step road input

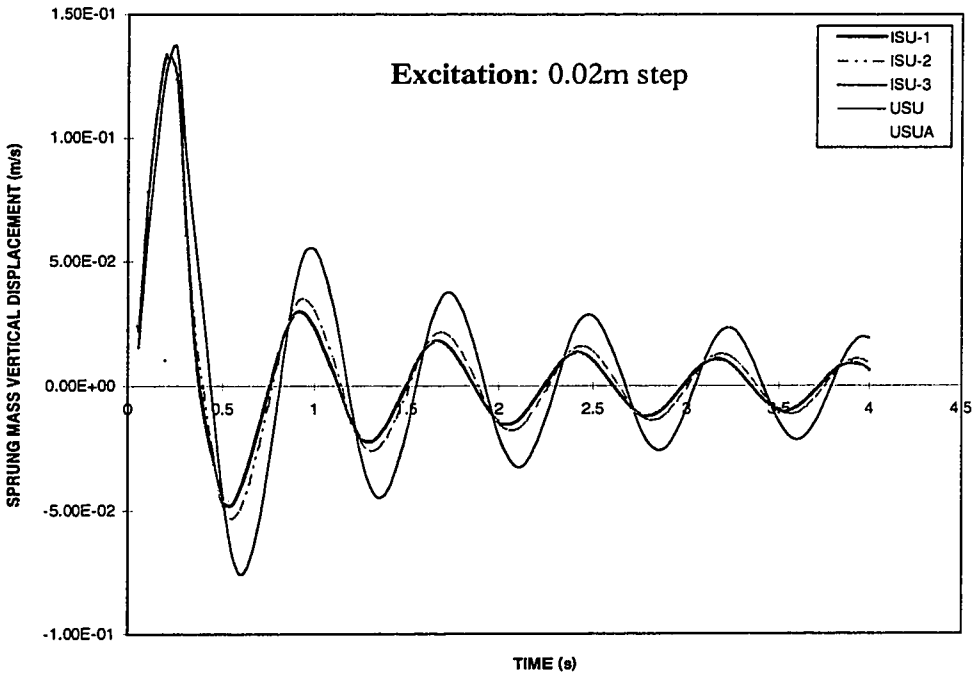

Figure 4.16 Vertical velocity response of sprung mass with different suspension units under step road input

are shown in Figure 4.17 and 4.18. Although unsprung mass displacement is similar for all configurations, the unsprung mass velocity for ISU-3 is again the largest.

4.5 FREQUENCY RESPONSE CHARACTERISTICS

The differential equations of motion of the various spring loaded hydro-pneumatic suspension models are solved in the frequency-domain for harmonic road and lateral acceleration excitations. The ride performance characteristics of various suspension units are evaluated in terms of vertical, and lateral accelerations transmitted to the sprung mass, and the handling performance is evaluated in terms of vertical and roll displacements of the sprung and unsprung masses. The relative vertical and roll displacement transmissibility of sprung mass and unsprung masses are evaluated under 0.01m in-phase and out-of-phase harmonic excitations at the right and left-tires and the sprung mass is expected to perceive 0.4g lateral acceleration excitation. The vibration isolation characteristics of various suspensions are evaluated by computing the ratio of the steady state response amplitude to the equivalent excitation amplitude in time domain within a desired frequency range. Vibration isolation characteristics are expressed by the following transmissibility ratios:

$$\text{Vertical displacement transmissibility of sprung mass} = \left|\frac{X_s}{X_{ie}}\right|$$

$$\text{Vertical displacement transmissibility of unsprung mass} = \left|\frac{X_u}{X_{ie}}\right|$$

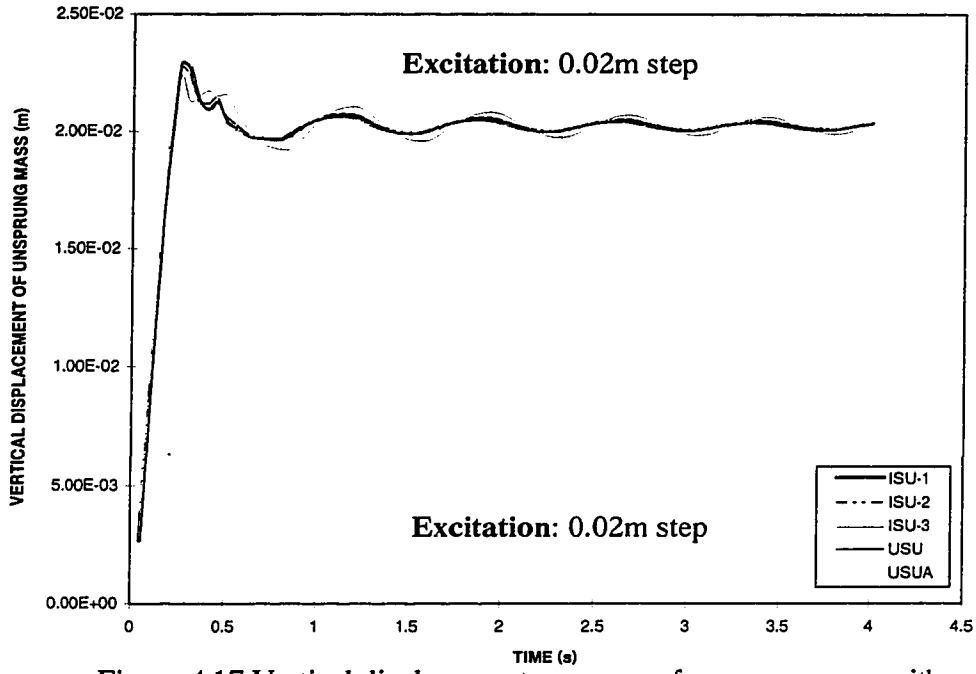

Figure 4.17 Vertical displacement response of unsprung mass with different suspension units by using step road input

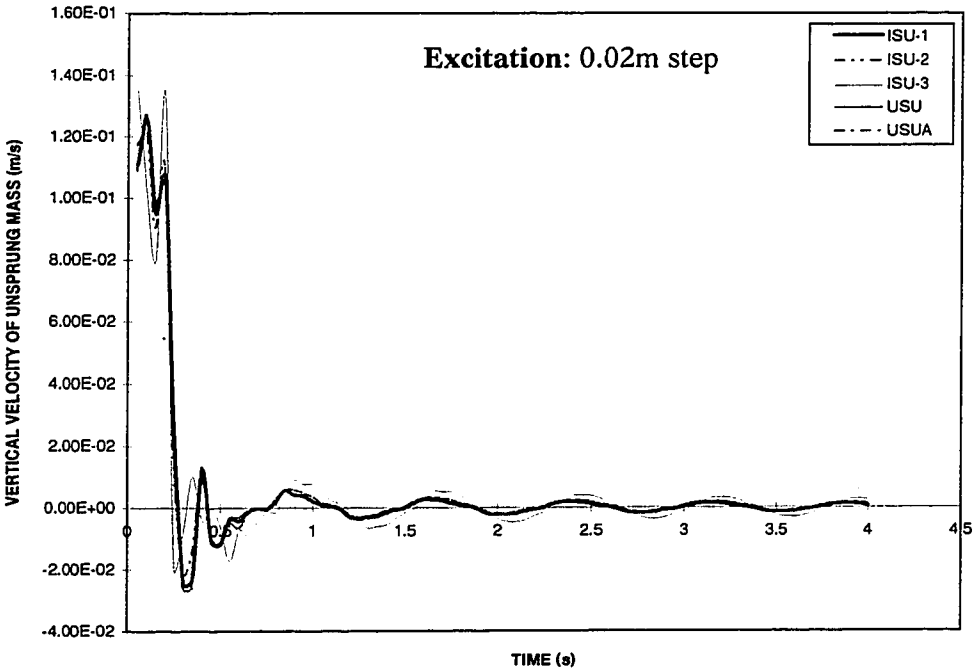

Figure 4.18 Vertical velocity response of unsprung mass with different suspension units under step rod input

Roll angle transmissibility of sprung mass = $\left|\frac{\phi_s}{\phi_{ie}}\right|$

Roll angle transmissibility of unsprung mass = $\left|\frac{\phi_u}{\phi_{ie}}\right|$

where X_s, X_u are the steady state displacement responses of sprung mass and unsprung masses, respectively; X_{ie} is the amplitude of sinusoidal vibration; ϕ_s,ϕ_u are the steady state roll responses of sprung mass and unsprung masses, respectively; and ϕ_{ie} is equivalent amplitude of roll angle due to out-of-phase input.

In the evaluation of frequency response, the influence of orifice area on the transmissibility characteristic of interlink suspension system ISU-1 is first examined. Figures 4.19 and 4.20 present the sprung and unsprung mass displacement transmissibility responses for orifice area in the range of 0.0016x 10^{-3} to 0.0042x $10^{-3}m^2$. These results demonstrate the influence of orifice size on the peak transmissibility and natural frequencies of the sprung and unsprung masses. The baseline model with orifice size 0.0016x $10^{-3}m^2$ leads to acceptable sprung mass transmissibility peak of less than 2.0. This however, leads to a shift in the response of unsprung mass to 3.55 Hz. The transmissibility performance of the selected five suspension configurations is next carried out for the baseline orifice size.

Vertical transmissibility response of sprung mass of the vehicle fitted with various spring loaded hydro-pneumatic suspensions in terms of displacement, velocity and

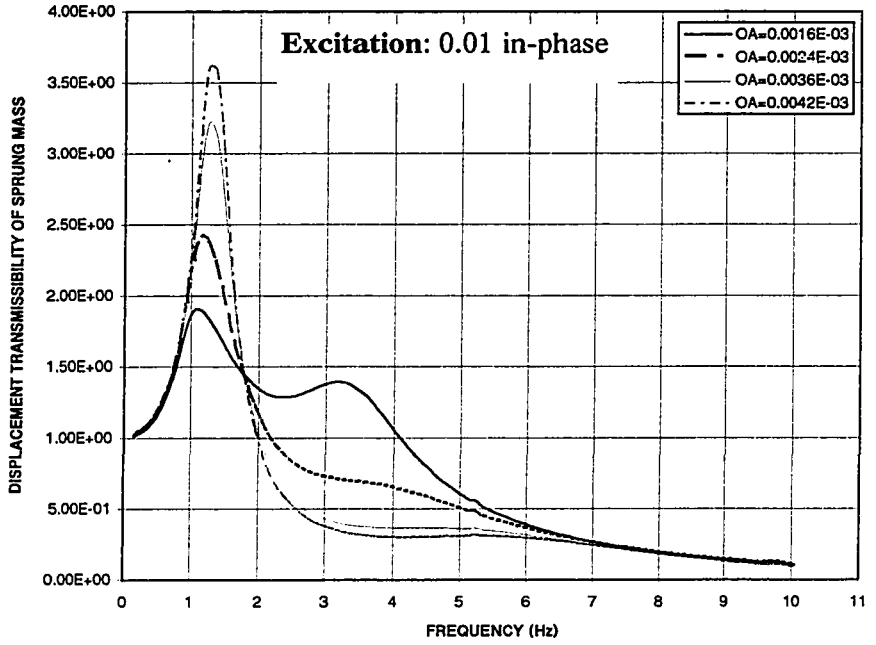

Figure 4.19 Influence of orifice area on the vertical displacement transmissibility response of sprung mass with ISU-1 under in-phase sine road input

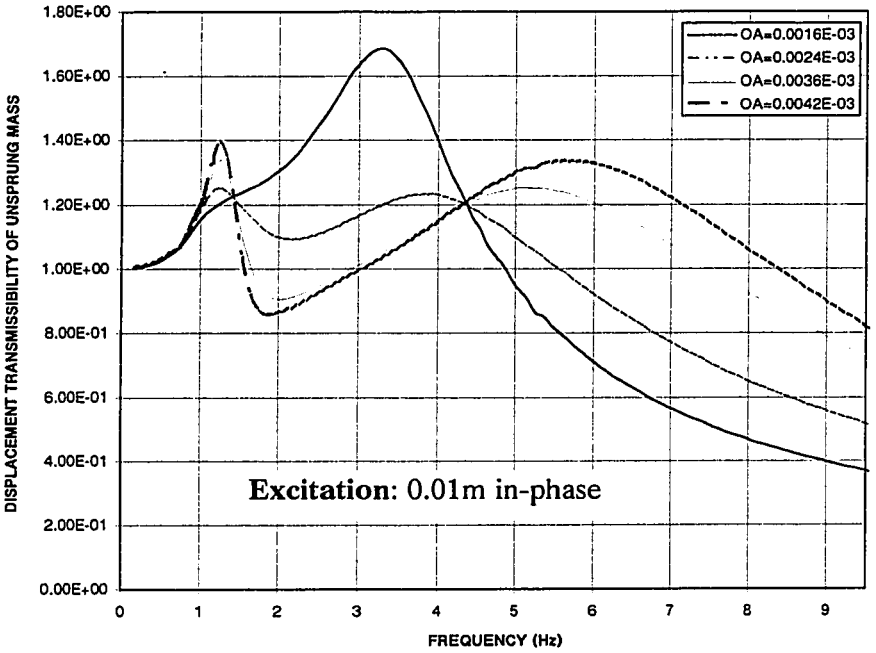

Figure 4.20 Influence of orifice area on the vertical displacement of unsprung mass transmissibility response with ISU-1 under in-phase sine road input

acceleration transmissibility under in-phase sinusoidal excitation are shown in Figures 4.21, 4.22 and 4.23, respectively. In the absence of roll excitation, the response obtained by unconnected system with and without antiroll bar (USUA and USU) are identical in all cases. Among the interconnected systems, ISU-3, due to its low effective damping yields highest sprung mass peak transmissibility with lowest response for higher frequencies. These results also show that interconnected system ISU-1 and ISU-2 can provide suspension performance in comparison to unconnected system over the frequency range. All the suspension units exhibit almost same sprung mass resonant frequency around 1.05 Hz, while transmissibility response of sprung mass of various suspensions as shown depends upon the design configuration of struts and its components. The corresponding unsprung mass displacement transmissibility is presented in Figure 4.24. The resonant frequencies of unsprung masses of suspension units ISU-1 and USU/USUA are observed to be same and around 3.5 Hz, however, the resonant frequencies of unsprung mass of interconnected suspension ISU-3 is observed as 4.6 Hz due to low damping developed by strut. A summary of bounce natural frequencies for the five configurations are presented in Table 4.1. Among all the suspension configurations considered, the best sprung mass response over the frequency range can be obtained by that of ISU-2 which gives a transmissibility of 1.45 with good response over high frequencies. In general ride quality of a vehicle is related to the vibration transmissibility of sprung mass in the frequency range of 4-8 Hz [4], where sprung mass resonance peak around 1.0 Hz should also be reasonable. High damping is desired to reduce the amplitude of vibration around the bounce natural frequency of the vehicle. The vibration

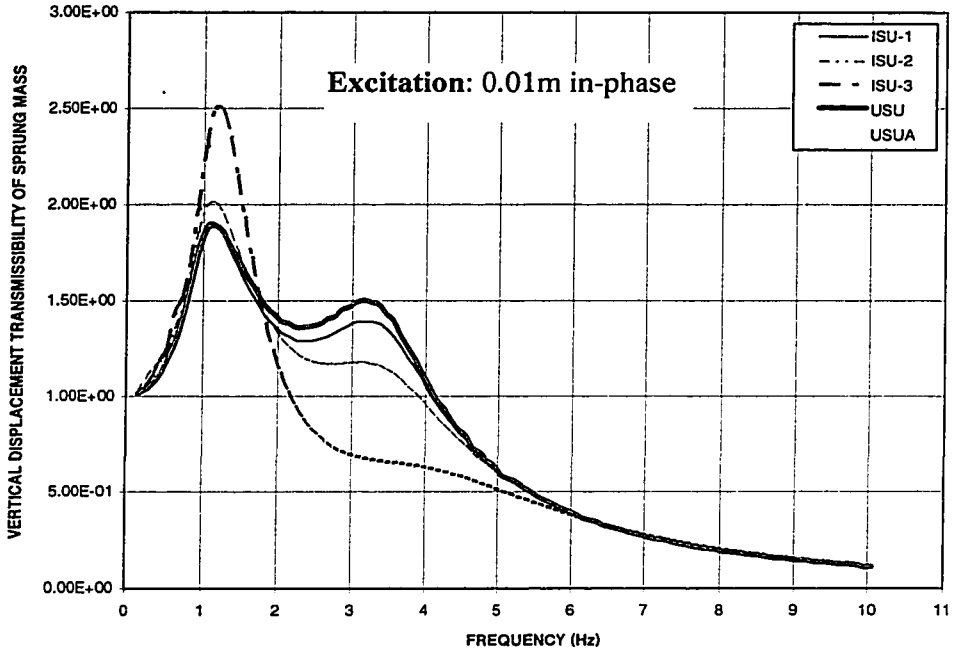

Figure 4.21 Displacement transmissibility characteristics of sprung mass of vehicle with different suspension unit subject to in-phase sine road input

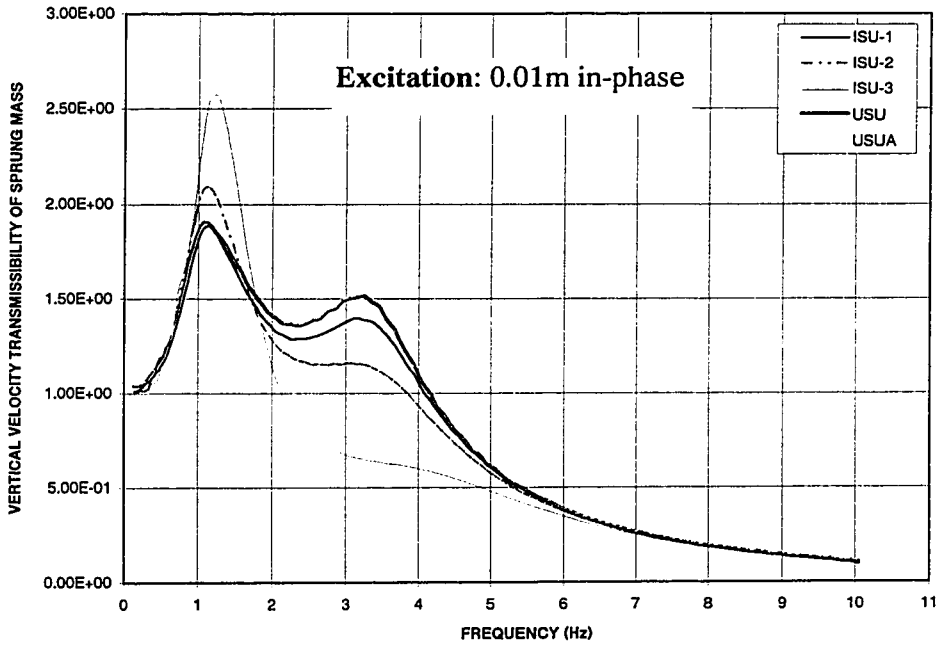

Figure 4.22 Velocity transmissibility characteristics of sprung mass with different suspension units subject to in-phase sine road input

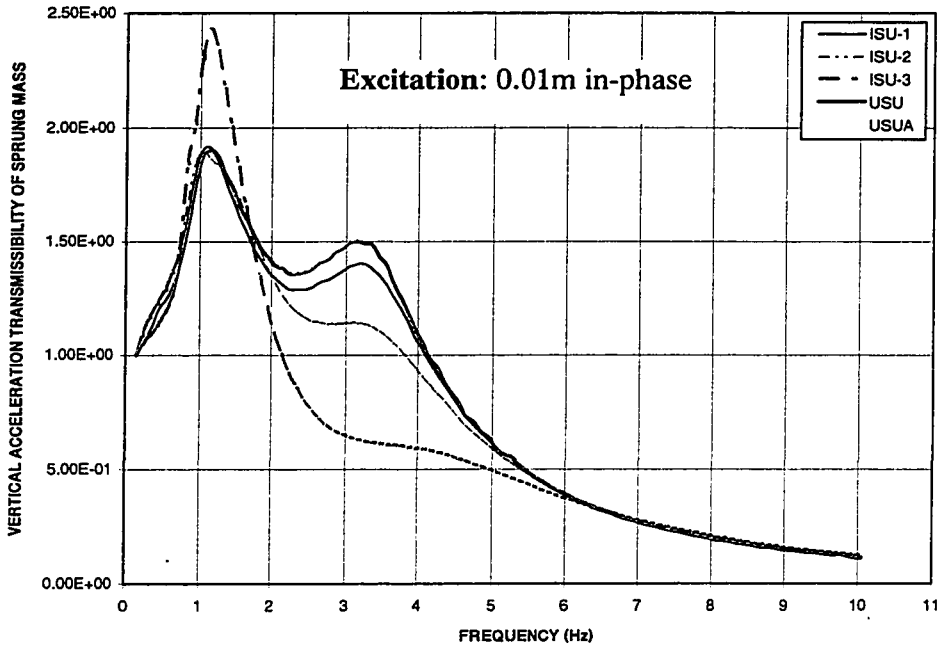

Figure 4.23 Acceleration transmissibility characteristics of sprung mass with different suspension units subject to in-phase sine road input

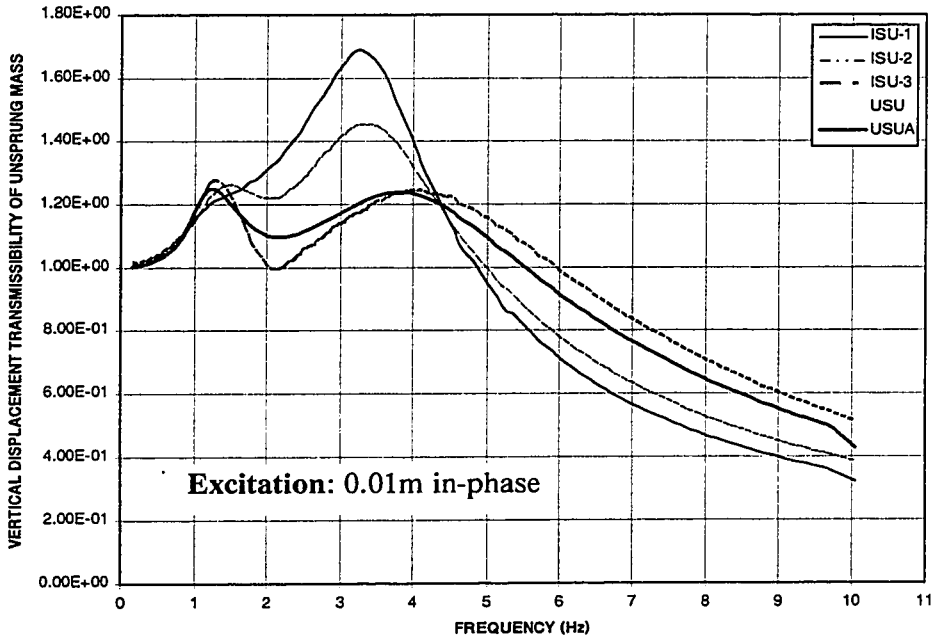

Figure 4.24 Displacement transmissibility characteristics of unsprung mass with different suspension units subject to in-phase sine road input

Table 4.1

Bounce resonant frequencies of sprung and unsprung masses with different suspension units under 0.01m in-phase sinusoidal road input

Masses	Interlinked ISU-1	Interlinked ISU-2	Interlinked ISU-3	Independent USU	Independent USUA
Sprung	1.05 Hz	1.15 Hz	1.25 Hz	1.05 Hz	1.05 Hz
Unsprung	3.35 Hz	3.35 Hz	4.55 Hz	3.25 Hz	3.25 Hz

isolation performance of heavily damped passive suspension, however, deteriorated considerably in the higher frequency range. The low damped suspension is desirable when the excitation frequency is beyond the natural frequency. This conflicting requirement demands a design compromise when fixed orifice is used. Based on the overall performance it can be concluded that configuration ISU-2 provides the best performance over the entire frequency range.

The roll angle transmissibility responses of the sprung and unsprung masses of different suspension units exhibit resonant peaks corresponding to roll resonant frequencies. The roll resonant frequencies of vehicle employing various suspensions, under 0.01m out-of-phase harmonic excitation, are listed in Table 4.2. As shown, the

highest roll resonance frequency (0.85 to 0.95 Hz) is provided by ISU-1 and USUA due to high effective roll stiffness in the interlink and anti-roll bar, respectively.

Table 4.2

Roll resonant frequencies of sprung and unsprung masses with different suspension units under 0.01 out-of-phase sinusoidal excitation

Masses	Interlinked ISU-1	Interlinked ISU-2	Interlinked ISU-3	Independent USU	Independent USUA
Sprung	0.85 Hz	0.65 Hz	0.75 Hz	0.65 Hz	0.95 Hz
Unsprung	6.75 Hz	4.35 Hz	5.35 Hz	4.35 Hz	4.35 Hz

These results further show a shift in the resonance frequency for change in configurations. As it was shown earlier, change in configuration leads to variation in the effective stiffness rate and damping properties. The shift is more pronounced at higher frequencies where velocity is large. This can be mainly attributed to hardening effect of the air springs in the struts.

The roll transmissibility for sprung and unsprung masses under 0.01m out-of-phase harmonic excitation is shown in Figures 4.25 and 4.26, respectively. Comparison of these results for the five configurations clearly reveals that ISU-1 leads to highest peak

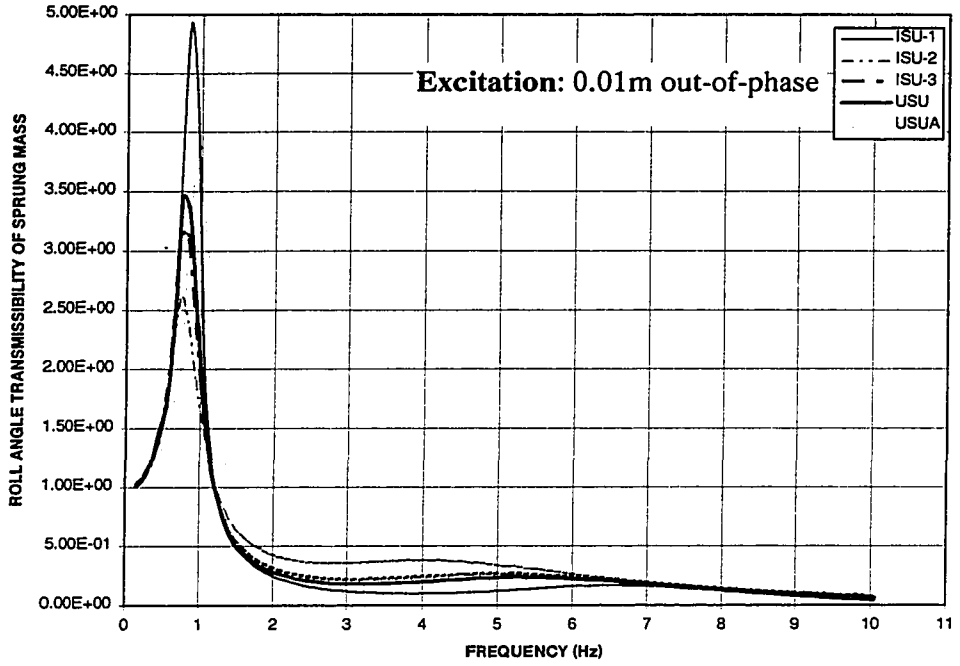

Figure 4.25 Roll angle transmissibility response of sprung mass equipped with different suspension units subject to out of phase sinusodial road input

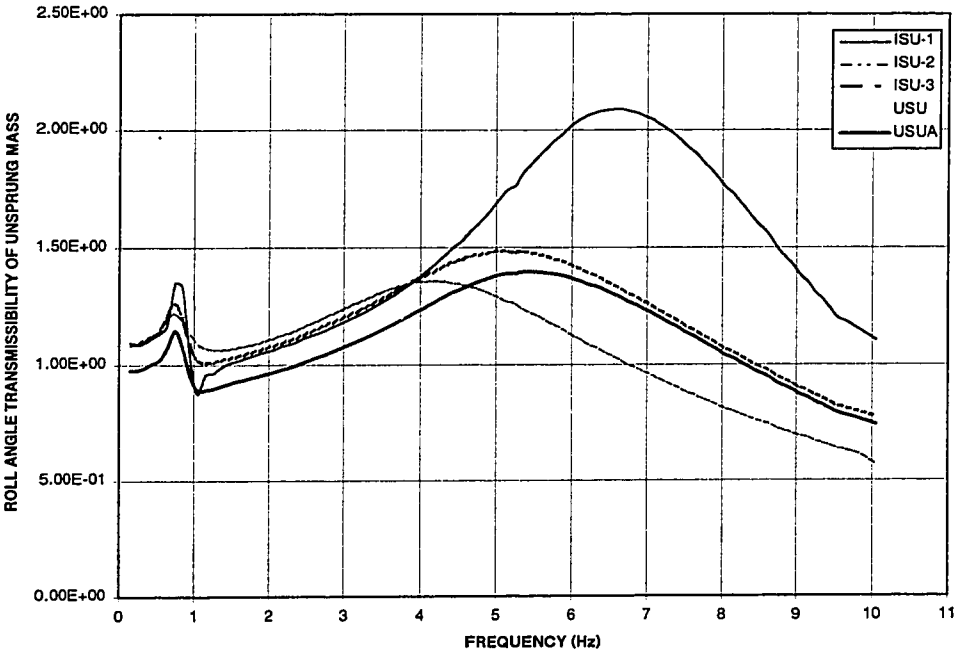

Figure 4.26 Roll angle transmissibility characteristics of unsprung mass with different suspension units subject to out-of-phase sine road input

for both sprung and unsprung mass transmissibility. The most acceptable performance of sprung mass roll transmissibility over the entire frequency range is provided by ISU-2. The unsprung mass transmissibility for this configuration although is not the best, it is comparable to other configurations.

The results obtained in this chapter for ride and handling under transient input demonstrated the conflicting requirements for suspension damping. The conflict is again evident for superior performance at resonance and high frequencies. These conflicting damping requirement for the suspension can not be satisfied by a fixed orifice suspension. In the next chapter, selected suspension configurations are examined for their performance when tunable variable dampers are employed.

4.6 SUMMARY

In this chapter, 4-DOF roll plane vehicle model with fixed orifice restriction as developed in chapter 2 is investigated for ride and roll performance characteristics. A comparative study is carried out for vehicle equipped with different suspension configurations. Two types of excitation due to tire-terrain interaction and steering inputs are used to carry out the performance of different suspension units. Further, vibration transmissibility characteristics of different suspension are investigated by using harmonic in-phase and out-of-phase sinusoidal road inputs. In chapter 5, variable damped spring loaded interconnected suspension model in roll plane is analytically developed to obtain the improved vibration isolation performance at high frequency range.

CHAPTER 5

DETERMINISTIC ANALYSIS OF THE INTERCONNECTED SUSPENSION WITH TUNABLE SEQUENTIAL DAMPING

5.1 INTRODUCTION

Passive springs and dampers are widely used in conventional vehicle suspensions, in order to isolate the vibration. Although these conventional systems are simple, inexpensive and reliable, they support the vehicle load and protect the passengers from the external disturbances, their performance potential is surely limited. The main limitation of such types of suspension is that they provide fixed damping characteristics. High damping is desired to control the amplitude of vibration response when frequency of excitation is around the natural frequency of the system. On the other hand, low value of damping is desirable when excitation frequencies are far above the natural frequency [61]. In order to overcome the inherent performance limitation of fixed orifice vibration isolation systems, it is desirable to develop an adaptive and variable isolation system which could provide limiting damping force at higher relative velocities. Active vehicle suspensions, with parameters that change with variations in excitation and response characteristics, provide improved vibration isolation performance. Recent advances in optimization techniques in automatic control have lead to the study of numerous active vibration isolators and vehicle suspension systems [62, 63]. However, the requirement of

an external energy source and control systems with number of sensors restrict the implementation of active vehicle suspension in ordinary vehicles [64, 65].

Alternatively, in this chapter, passive pressure limiting control scheme is proposed to achieve the variable sequential damping in interlinked hydro-pneumatic vehicle suspension system. The pressure limiting valve may be opened during the compression or extension strokes under certain conditions to allow fluid flow through the valve opening and thus reducing the damping force. The pressure relief valves are easily tuned through selection of preset pressure, which in turn can provide desirable damping characteristics. The tuning methodology, as preset pressure, is based on the pressure differential developed at resonance, which is discussed in this chapter. Computer simulation technique is used to investigate ride performance characteristic of interconnected suspension by using different tuning factor and is then compared with fixed orifice interconnected suspension ISU-1, as frequency domain results in chapter 4 reveal that ISU-1 has the better performance as compared to the other interconnected suspensions.

5.2 ANALYTICAL MODELING OF A PASSIVE SEQUENTIAL INTERCONNECTED HYDRO-PNEUMATIC DAMPER

Concept of Tunable pressure Limited Hydraulic Damper

Variable damping can be achieved through pressure relief valves, while command signals are generated from pressure differentials, $P_{23\ell}$ and P_{23r}, across the left and right orifices of the suspension unit. Pressure differential equations (2.66) and (2.67) reveal that the

pressure differential $P_{23\ell}$ and P_{23r}, and hence the damping forces, depend upon the square of relative velocity across the hydraulic struts. For a constant amplitude of excitation, and at high excitation frequencies, the effect of damping force will be high and thus system shows poor vibration isolation performance. The vibration isolation performance of the system can be improved by limiting the magnitude of damping forces at high excitation frequencies by implementing the pressure limiting valve with a tunable preset limiting value $(P_{23})o$. Assuming the effects of the relief valve dynamics to be negligible, an ideal control scheme of the tunable pressure limited interconnected hydraulic damper can be expressed as:

$$F_{d\ell}= \begin{matrix} P_{23l}A_{2l} - P_{23l}A_{1l} + P_{2rll}A_{1l}; |p_{23i}| < (p_{23})_o \\ P_{23Vl}A_{2l} - P_{23Vl}A_{1l} + P_{2Vrll}A_{1l}; \text{otherwise} \end{matrix} \text{ or}$$

$$F_{dr}= \begin{matrix} P_{23r}A_{2r} - P_{23r}A_{1r} + P_{2llr}A_{1r}; |p_{23r}| < (p_{23})_o \\ P_{23Vr}A_{2r} - P_{23Vr}A_{1r} + P_{2Vllr}A_{1r}; \text{otherwise} \end{matrix} \qquad (5.1)$$

where,

F_{dl}, F_{dr} = damping force developed by left and right side of tunable pressure limited damper (N)

P_{23l}, P_{23r} = pressure differential across the fixed orifice (Pa)

Tunable damping force equation can be expressed in terms of relative velocity by substituting the values of $P_{23\ell}$, P_{23r}, $P_{2rl\ell}$, $P_{2\ell lr}$ from Equations (2.66), (2.65), (2.71), and (2.72) respectively; as derived in chapter 2, while $P_{23v\ell}$ and P_{23vr} in these equations be expressed as:

$$P_{23v\ell} = \frac{\varrho}{2}\left(\frac{A_{1r}\dot{Z}_r - A_{2\ell}\dot{Z}_\ell}{C_d a_{v\ell}}\right)^2 \text{sgn}(A_{1r}\dot{Z}_r - A_{2\ell}\dot{Z}_\ell) \tag{5.2}$$

$$P_{23vr} = \frac{\varrho}{2}\left(\frac{A_{1\ell}\dot{Z}_\ell - A_{2r}\dot{Z}_r}{C_d a_{vr}}\right)^2 \text{sgn}(A_{1\ell}\dot{Z}_\ell - A_{2r}\dot{Z}_r) \tag{5.3}$$

$P_{23v\ell}$, P_{23vr} = pressure differential across the left and right valve opening (Pa)

a_{vl}, a_{vr} = left and right Valve opening area (m^2)

A tunable pressure limiting relief valve is introduced between the strut and accumulator of each suspension unit in order to achieve variable damping. The roll plane model of a vehicle with hydro-pneumatic suspension incorporating pressure limiting valve is presented in Figure 5.1. As shown in the schematic diagram, Figure 5.2, fluid flows through the fixed orifices between chambers II_ℓ and III_ℓ, and II_r and III_r when the magnitude of the pressure differential P_{23i} is less than the preset limiting pressure $(P_{23i})_o$ of the relief valves. In this case the relief valves remain closed and then damping force will be generated due to the fluid flow through the fixed orifice alone. When magnitude of the pressure differential P_{23i} exceeds the preset pressure value $(P_{23i})_o$, the relief valve opens. Due to relief valve opening, fluid will also flow through this opening and thus damping force is reduced. It can be seen that variable damping characteristics can be achieved in an entirely passive manner by using above mentioned control scheme. Such dampers are referred to as sequential damper that are tunable through the selection of preset pressure.

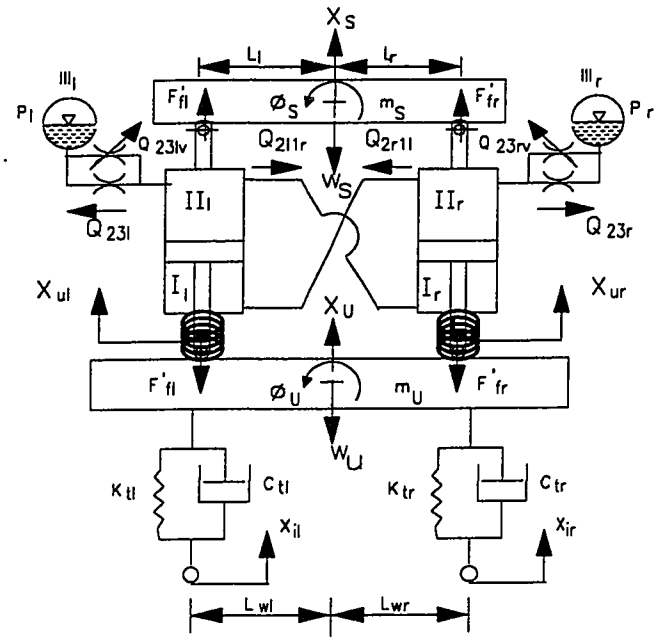

Figure 5.1 Roll plane model of spring loaded interconnected hydro-pneumatic suspension with variable damping

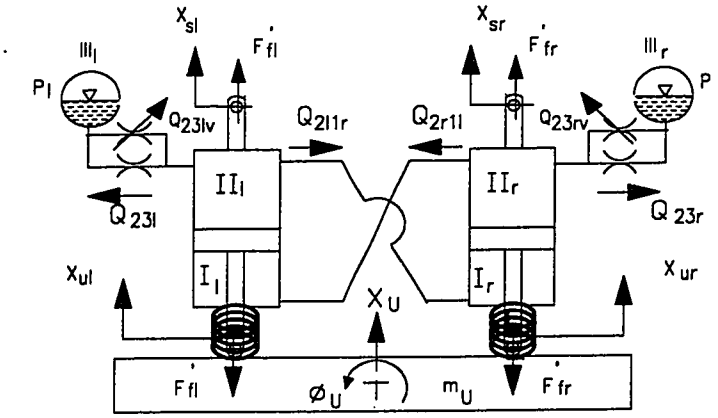

Figure 5.2 Schematic of roll plane model of spring loaded interconnected hydro-pneumatic suspension with passive variable valve opening

5.3 DAMPING PROPERTIES OF SPRING LOADED INTERCONNECTED SUSPENSION WITH TUNABLE PRESSURE LIMITED DAMPER

In order to evaluate the damping characteristics of the proposed interconnected hydraulic damper, a damping parameter β is defined; as the ratio of the damping force F_d to the linear critical damping force of a single degree of freedom vibration isolation system as follows[24]:

$$\beta = \frac{F_d}{2\sqrt{mk|\dot{Z}|}} \tag{5.4}$$

For a linear passive vibration isolation system the damping parameter is simply the damping ratio of the system. However, for non-linear dampers, the damping parameter is no longer a constant.

Tunable Pressure Limited Interconnected Hydraulic Damper

The damping parameters of an ideal tunable pressure limited hydraulic damper can be expressed in terms of two effective damping coefficients as follows:

When $(P_{23i} < (P_{23i})_O$, $(i=\ell,r)$ then

$$\beta = \frac{C_1\dot{Z}^2}{2\sqrt{mk|\dot{Z}|}} \tag{5.5}$$

and, otherwise

$$\beta = \frac{C_2\dot{Z}^2}{2\sqrt{mk|\dot{Z}|}} \tag{5.6}$$

where $C_l = \rho A_2^3 / 2C_d^2 a_1^2$ is the damping coefficient corresponding to the fixed orifice area a_1 and $C_2 = \rho A_2^3 / 2C_d^2 a_{v\ell}^2$ is the damping coefficient corresponding to the effective orifice area $a_{v\ell}$ when pressure relief valve is opened.

These equations 5.5 and 5.6 reveal that the damping parameter of tunable pressure limited interconnected hydraulic damper is proportional to the magnitude of the relative velocity, when pressure differential across the orifice is less than the preset limiting pressure, as in case of a fixed orifice damper. When pressure differential exceeds the preset pressure $(P_{23i})_o$, pressure relief valves open, and the corresponding damping parameter is decreased due to higher magnitude of the valve opening area.

5.4 TUNING METHOD OF VARIABLE DAMPING

In view of vibration isolation performance, it is desirable to achieve a high value of damping parameter around the resonant frequency such that the resonant peak can be appropriately controlled [66]. On the other hand, it is also desirable to produce a low value of damping parameter at high excitation frequencies to isolate the mass effectively. The modified interconnected hydraulic damper with tunable damping characteristics can meet the above requirements for effective isolation of mass from base excitations. Preset limiting pressure $(P_{23i})_0$ can be estimated from linear system response. For a two degree of freedom vibration isolator system as shown in Figure 5.3, the maximum value of equivalent damping parameter is determined at resonant frequency, it is the ratio of linear damping coefficient to the critical damping coefficient. The equivalent damping

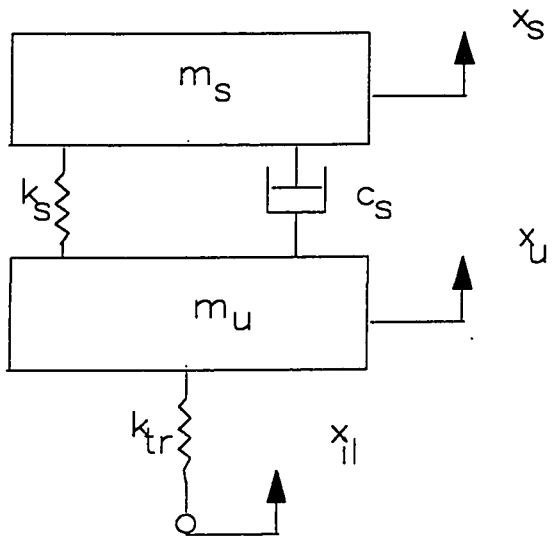

Figure 5.3 2-DOF dynamical system

parameter at resonance can be related to the relative velocity response in the following manner:

$$\beta_{eq|\omega=\omega_n} = \frac{\left|\dot{x}_i\right|}{2\left|\dot{z}\right|\sqrt{1-2\zeta}} \tag{5.7}$$

where, $\dot{x}_i$ is the input velocity, $\dot{Z}$ is the relative velocity across the damper, and

$$\zeta = \frac{k_1}{k_2} \tag{5.8}$$

where k_1, k_2 are the spring stiffness

In order to realize an appropriate control of the resonant peak, the minimum value of limiting pressure corresponding to the natural frequency is thus obtained from equation (5.6) and (5.7), as [26]:

$$(P_{23i})_{o|\omega=\omega_n} = \frac{kx_i}{\alpha\sqrt{1-2\zeta}} \tag{5.9}$$

$(P_{23i})_{o|\omega=\omega_n}$ = limiting pressure value at resonance (Pa)

X_i = amplitude of base excitation (m)

k = spring stiffness of interconnected system (N/m)

α = damping force coefficient (m^2), given by:

$$\alpha = A_2 + \lambda A_1 \tag{5.10}$$

$$\lambda = \frac{P_{23r}}{P_{23r}} \tag{5.11}$$

In order to achieve the effective vibration isolation a tuning factor can be introduced such that the limiting pressure corresponds to a appropriate pressure after the resonance:

$$(P_{23i})_o = \gamma \frac{kx_i}{\alpha\sqrt{1-2\zeta}} \tag{5.12}$$

where, γ= tuning factor of pressure limiting interconnected hydraulic damper. The equations of hydraulic damper of vehicle suspension are solved using a 2-DOF system model, often referred as a quarter vehicle model [67], subjected to harmonic excitation at its base. Figure 5.4 and Figure 5.5 present the pressure differential and damping force characteristics as a function of frequency, respectively. These results for fixed orifice and sequential damping demonstrate that in case of fixed orifice pressure differential and damping force increase parabolically with the increase in frequency and in case of sequential damper, pressure differential is not allowed to beyond the preset pressure $(P_{23i})_O$. The P_{23i} is then held around $(P_{23i})_0$, as frequency increases. As shown in Figures 5.4 and 5.5 the tuning factor γ can be selected appropriately to determine relative velocity beyond which the pressure differential should be limited to enhance high frequency response.

Similar to the above results the damping parameter characteristics of the interconnected hydraulic damper as a function of the relative velocity across the hydraulic

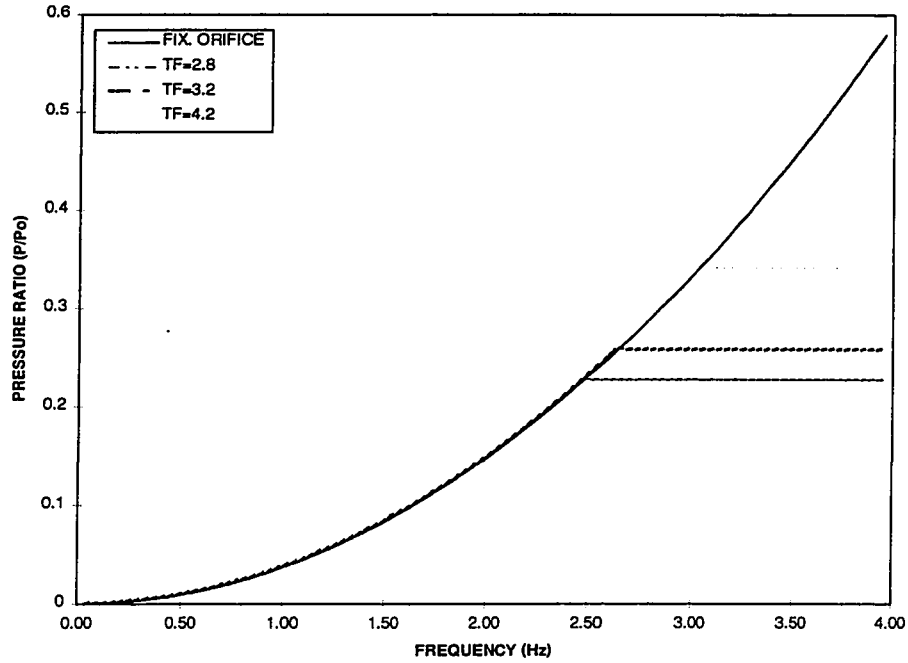

Figure 5.4 Pressure differential characteristics of spring loaded interconnected hydro pneumatic struts with fixed and passive variable orifice mechanism

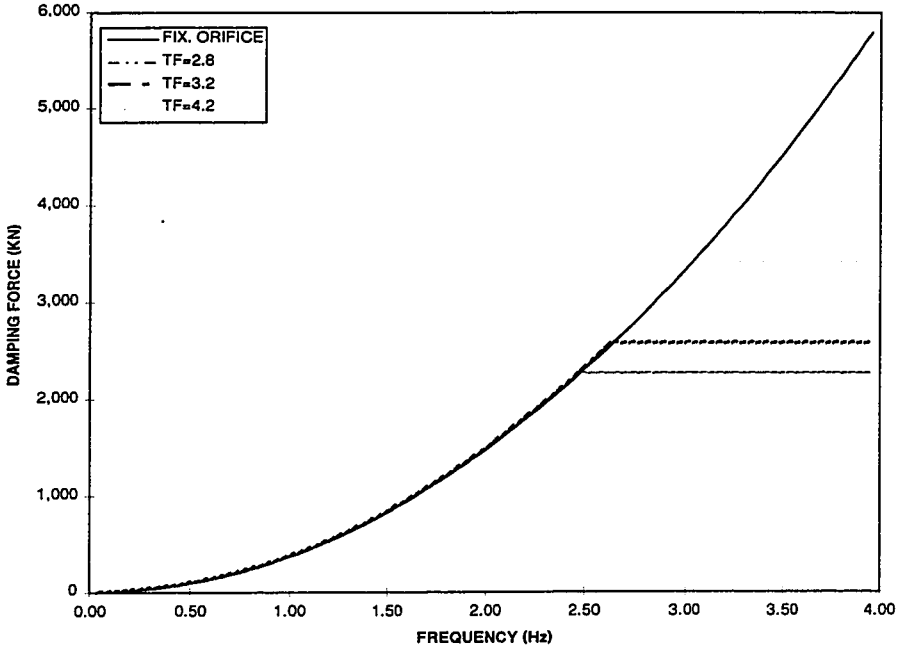

Figure 5.5 Damping force characteristics of spring loaded interconnected hydro-pneumatic struts equipped with fixed and passive variable damping mechanism

strut is shown in Figure 5.6. These results show damping parameter in case of tunable pressure limited dampers at different tuning factors.

5.5 DYNAMIC RESPONSE OF THE SPRING LOADED INTERCONNECTED SUSPENSION SYSTEM WITH SEQUENTIAL DAMPING

Dynamic response of fixed orifice spring loaded interconnected hydro-pneumatic suspension under steady state conditions is computed with variable spring loaded interconnected hydro-pneumatic suspension, in order to demonstrate the effectiveness of the sequential damping on the ride performance. In-phase sinusoidal road excitation with vertical amplitude of 0.01 m at a frequency near 3 Hz is given to investigate the performance of the two different roll plane models. Figure 5.7 shows the steady state acceleration response of sprung mass for suspension ISU-1 and tuning factor of 3.2. It clearly demonstrates that acceleration response of sprung mass with sequential damping have discontinuities which are mainly attributed to the sudden change of the damping force during valve opening. However, these discontinuities are negligible and furthermore, fast opening of valve does not exist in practice. Thus, jerk free and smooth acceleration response of sprung mass can be expected with sequential damping.

For the simulation shown at 3 Hz for 0.01 m excitation amplitude and tuning factor 3.2, the valve remains open for most of the cycle. Fixed orifice is used for short period in each cycle where response for both systems are same. Figure 5.8 illustrates the change of valve opening area during transient as well as steady state condition as a function of time.

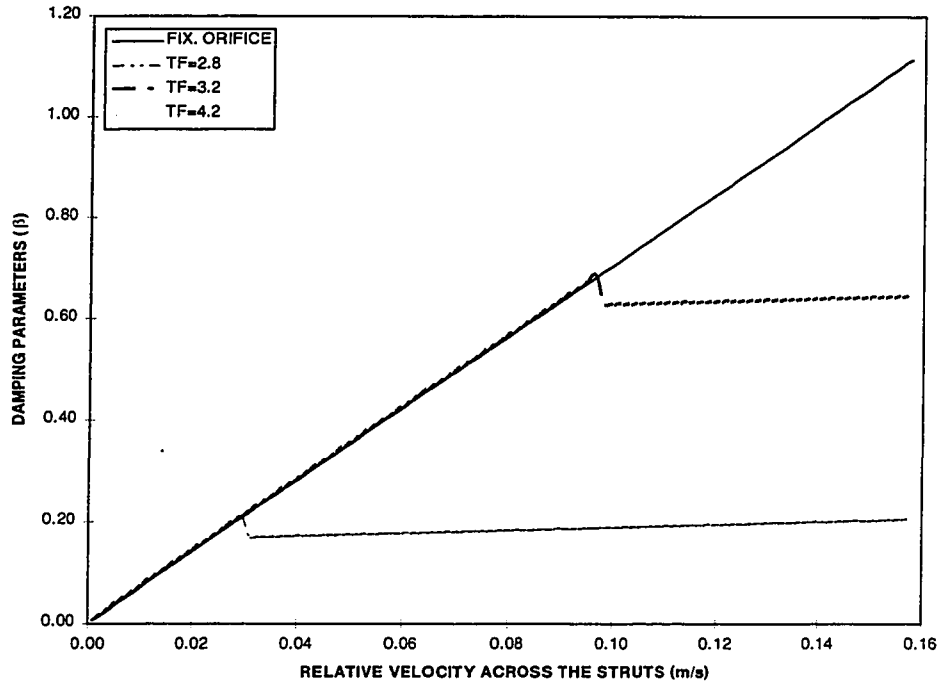

Figure 5.6 Damping characteristics of spring loaded interconnected hydro-pneumatic struts equipped with fixed and passive variable damping mechanism

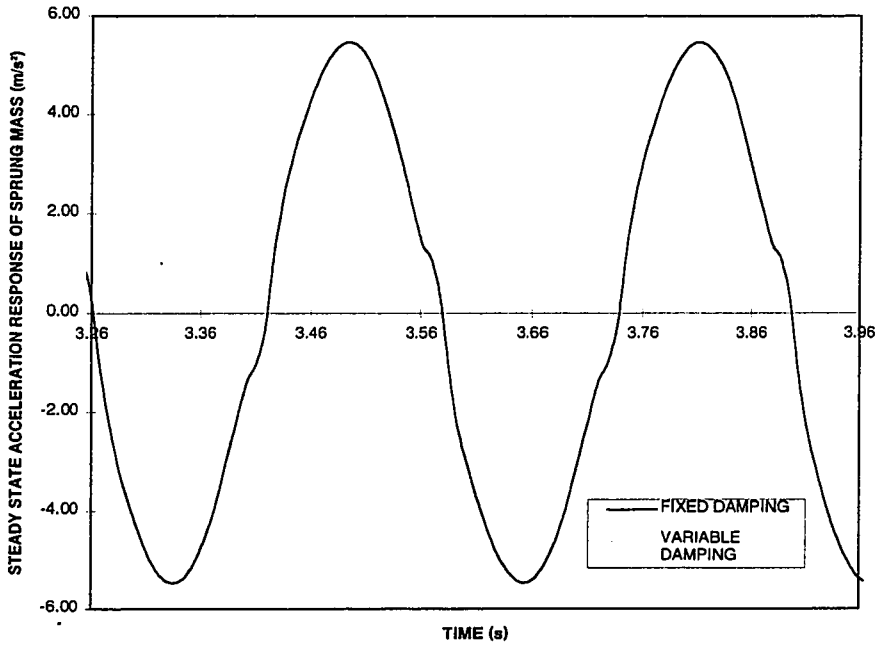

Figure 5.7 Steady state acceleration response of sprung mass with fixed and variable damping mechanism

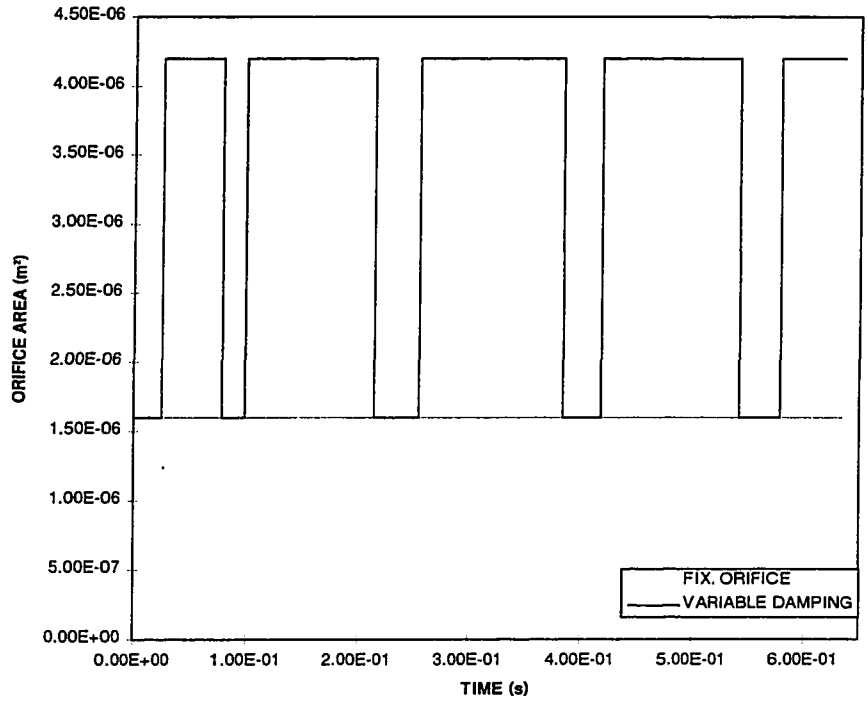

Figure 5.8 Comaprison of orifice area under transient condition with interconnected hydro-pneumatic struts with fixed and variable orifice

5.6 FREQUENCY RESPONSE OF THE INTERCONNECTED SUSPENSION UNIT

Non-linear equation of motion are solved in time domain using Runge-Kutta numerical method at different frequencies to obtain steady state response. Interlink suspension configuration ISU-1 is used with fixed and sequential orifice damping in spring loaded interconnected hydro-pneumatic vehicle suspension models; incorporating non- linear stiffness of gas springs. Vibration isolation performance characteristics of fixed orifice damping is compared with variable damping in terms of root mean square transmissibility of sprung mass and unsprung mass in vertical and roll mode. Performance characteristics in vertical and roll mode are evaluated by using in phase and out-of-phase road excitations with amplitude of 0.01 m. Root mean square value is used to overcome difficulty in peak picking from the time simulation. Which was apparent due to discontinuity in damping force. RMS value is adequate for a comparative study of sequential damping system with that of fixed orifice. Vertical displacement, and velocity transmissibility characteristics of sprung mass of vehicle with fixed orifice and variable orifice dampers are represented in Figures 5.9 and 5.10, respectively. Vertical acceleration transmissibility response of sprung mass and unsprung mass is illustrated in Figure 5.11, and Figure 5.12 respectively. As shown in Figure 5.9 constant orifice damper yields two peaks corresponding to the resonant frequency of sprung mass and unsprung masses of the vehicle, respectively. Furthermore, the unsprung mass resonance as shown earlier, is as low as 3.5 Hz due to high system damping. The transmissibility characteristics of vehicle model with variable damping are identical to those vehicle

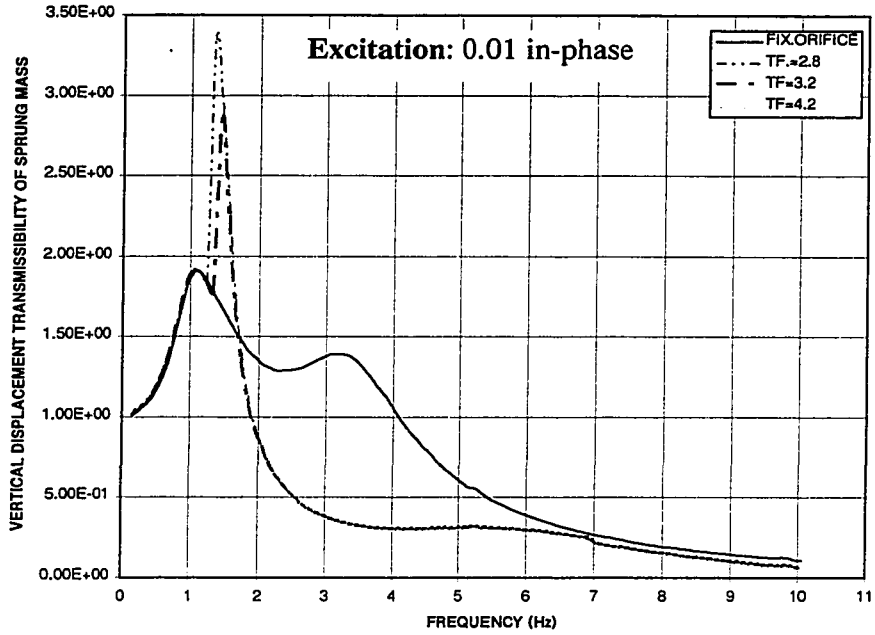

Figure 5.9 RMS vertical displacement transmissibility response of sprung mass subject to in-phase sinusodial road input

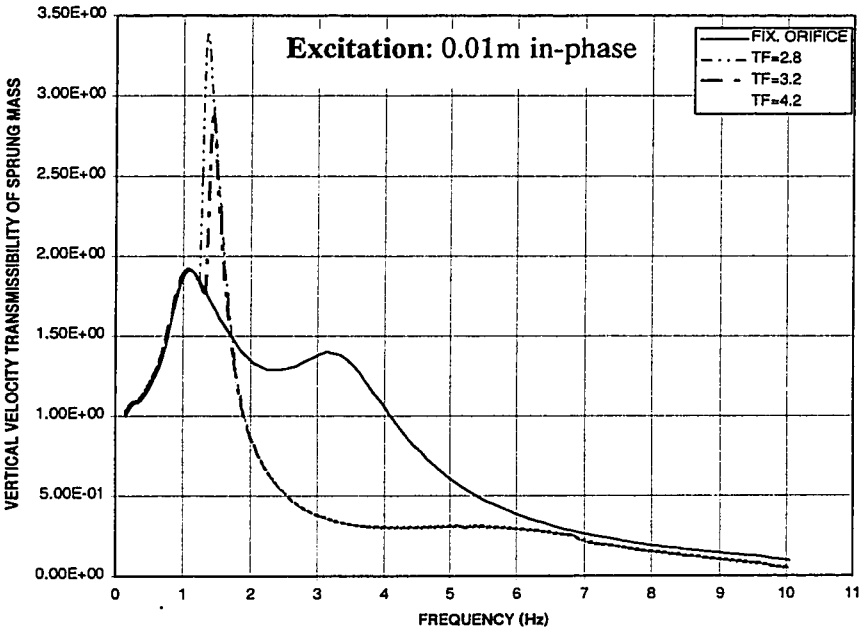

Figure 5.10 RMS vertical velocity transmissibility response of sprung mass subject to in-phase sinusodial excitation

suspension models employing fixed orifice damper at low excitation frequencies of up to 1.2 Hz where the peak differential pressure across the orifice remain less than the preset pressure. The vertical displacement response of sprung mass with sequential damper, however, is considerably reduced at higher excitation frequencies as pressure remains greater than preset pressure for most of the cycle and the valve remains open yielding low damping.

As shown in Figures 5.10 and 5.11 the trend is identical for velocity and acceleration transmissibility of the sprung mass. Due to low damping at higher frequencies these results show the damped natural frequency of unsprung mass at 5.5 Hz as compared to 3.5 Hz for fixed orifice system. Despite suspension high frequency performance of sequential system, it is evident that a narrow sharp peak may be introduced, when the valve starts to open. The shape and size of the peak is a function of tuning factor which dictate how close the response is to the natural frequency. If the valve is opened very close to the natural frequency, the sudden drop in damping leads to a sudden peak which however drops rapidly as frequency is increased. these peaks or their severity can be minimized by appropriate tuning of the sequential damping with small loss in high frequency transmissibility.

The displacement transmissibility of unsprung mass shown in Figure 5.12 also demonstrate the potential benefit of sequential damping in the interconnected interlink suspension system. As these results show, for all tuning factor the peak transmissibility of unsprung mass can be reduced from 1.7 to 1.3 with suspension performance in the

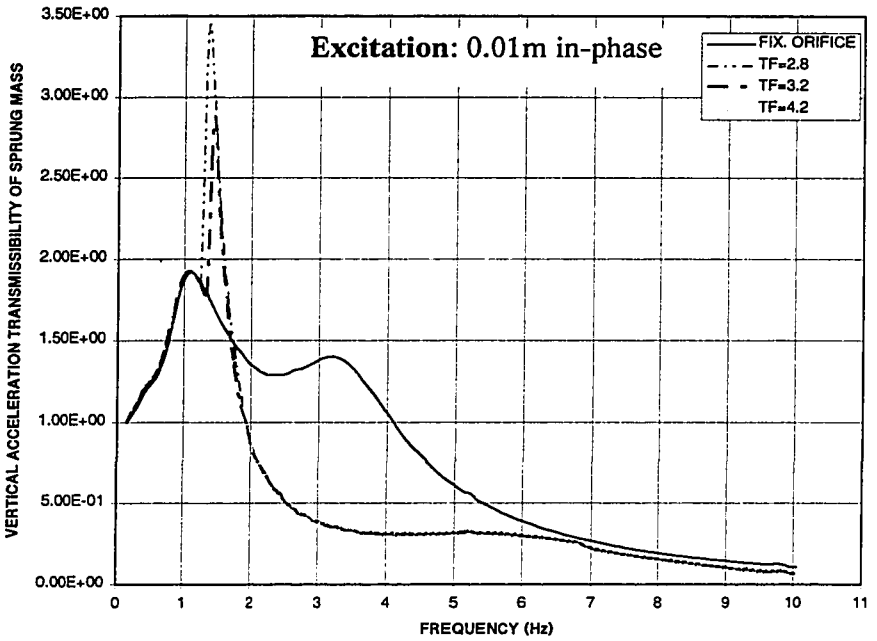

Figure 5.11 RMS vertical acceleration transmissibility of sprung mass subject to in-phase sinusodial excitation

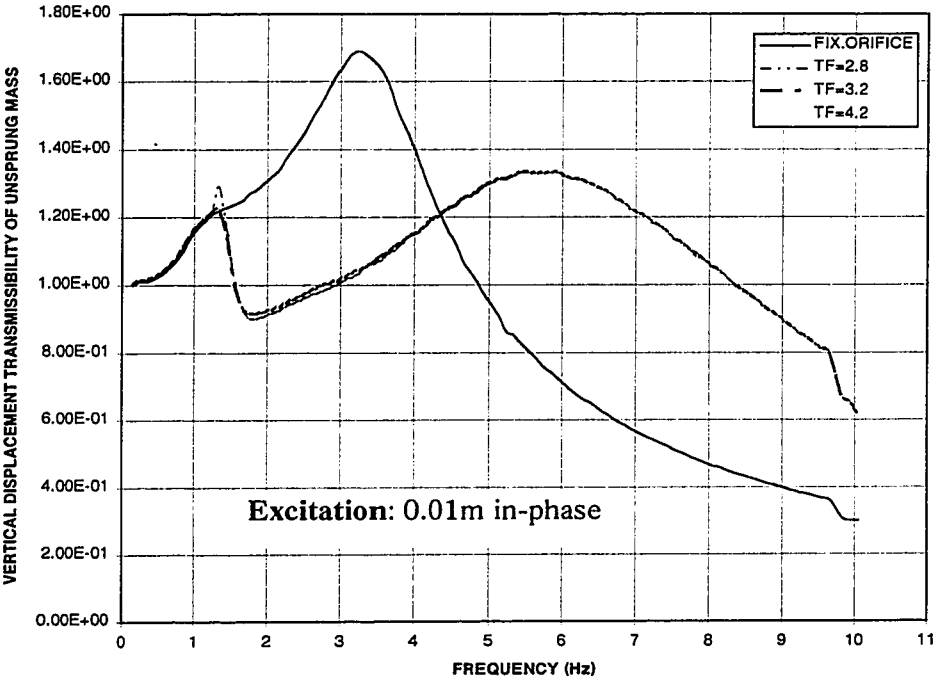

Figure 5.12 RMS vertical displacement transmissibility response of unsprung mass subject to in-phase sinusodial excitation

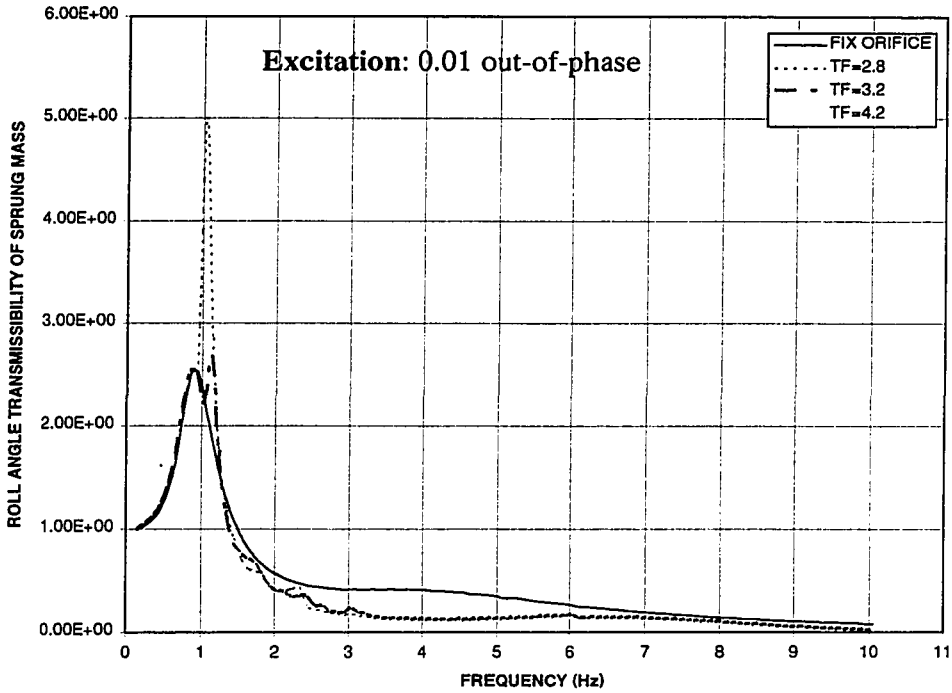

Figure 5.13 RMS roll angle transmissibility response of sprung mass subject to out to phase road excitation

frequency range of 1.5 to 4.5 Hz. From these results it is again evident that unsprung response for sequential damping is around 5.5 Hz as oppose to 3.5 Hz for fixed orifice damping.

Roll transmissibility response of sprung mass and unsprung masses of spring loaded interconnected hydro-pneumatic suspensions with fixed and sequential damping are evaluated by introducing 0.01 m out-of-phase sinusoidal road input. Figure 5.13 illustrates the rms roll angle transmissibility response of sprung mass with fixed and variable orifice restriction. As shown, the roll angle transmissibility responses of sprung mass have the same trend as that of vertical response under in-phase excitation. Again the roll angle transmissibility of sprung mass with variable damper is identical to that with fixed orifice damper until the valve starts to open. For higher excitation frequencies, pressure differential across the orifice restriction exceeds the preset pressure $(P_{23i})_o$ and leads to improved performance due to low damping. The improvement in high frequency roll response, however, is not as significant as that to vertical response. The results shown in Figure 5.13 clearly demonstrate that the sudden peak in the response at the frequency where valve starts to open, can easily be controlled by appropriate selection of tuning factor. It is possible to determine an optimal frequency in comparison to the natural frequency for a given system such that maximum benefit of sequential system can be realized with minimum or no loss near resonance.

5.7 SUMMARY

Non-linear roll plane model of spring loaded interconnected hydro-pneumatic suspension with variable damping is developed. Tuning method of variable sequential damper is described in a passive manner without including valve mechanism. Damping properties of interconnected suspension with tunable pressure limiting valve are derived in terms of damping parameter. The validity of proposed interconnected suspension with variable orifice restriction is verified by comparing the dynamic responses with fixed orifice interconnected hydro-pneumatic suspension model. Performance of the proposed models are compared by using sinusoidal in-phase and out-of-phase road excitations. The comparison revealed that vibration isolation is effectively achieved by using tunable variable sequential hydro-pneumatic damper.

CHAPTER 6

CONCLUSIONS AND RECOMMENDATIONS FOR FUTURE WORK

6.1 GENERAL

The main objective of vehicle suspension is to achieve ride comfort at driver and passenger location, directional control, and roll-stability during lane change and turning maneuvers. All these conflicting requirements are difficult to achieve together, and as a result, suspension designers have to establish a compromise between these conflicting factors. Ride quality is primary design criteria for the highway auto-bus, while achievement of directional control, and handling are considered secondary. As a result, heavy vehicle suspensions are designed to yield high ride comfort and consequently, they yield poor control on handling as well as on roll-stability. In this dissertation, a concept of spring loaded hydro-pneumatic suspension interconnected in roll plane is investigated to achieve an improved compromise between the ride and roll-stability performance characteristics of a heavy vehicle.

6.2 MAJOR HIGHLIGHTS OF THIS INVESTIGATION

The major highlights of this investigation are summarized as follows:

(1) In this investigation, a concept of fluid coupling in hydro-pneumatic suspension, is discussed. Interconnection is developed between two sides of hydro-pneumatic struts in an 4-DOF roll plane model of vehicle with beam in order to evaluate its ride and roll dynamics performance. Mainly three suspension models, namely, spring loaded interconnected hydro-pneumatic, unconnected

hydro-pneumatic with and without anti-roll bar are analytically modeled in roll plane. In all cases parallel mechanical spring is introduced to carry bulk of the load such that practical strut parameters can be realized. The generalized suspension forces are derived by assuming incompressible fluid in hydraulic struts, turbulent fluid flow through the orifice restrictions, laminar fluid flow through interconnected pipes, and polytropic process of gas in accumulators.

(2) The static and dynamic suspension properties of spring loaded interconnected hydro-pneumatic suspension, spring loaded unconnected hydro-pneumatic suspension with anti-roll bar are derived analytically. The suspension properties are expressed in terms of suspension rate, roll stiffness, and damping property both in bounce and roll mode. The influence of mechanical springs, their stiffnesses and interconnections on the overall dynamic property is evaluated and examined.

(3) A set of spring loaded hydro-pneumatic suspension configurations based on strut parameters, namely, interconnected suspensions (ISU-1, ISU-2, ISU-3), unconnected suspension (USU), and unconnected hydro-pneumatic suspension with anti-roll bar (USUA) are selected and evaluated for suspension rate, damping, and roll stiffness properties.

(4) Ride performance characteristics of baseline hydro-pneumatic suspensions (ISU-1, ISU-2, ISU-3, USU, USUA) are investigated for deterministic road excitations, in terms of in-phase and out-of-phase inputs, using fourth order Runge-kutta approach. The roll performance characteristics of on-road vehicle

is evaluated by using out-of-phase road excitation, and measured data of lateral acceleration experienced during a lane change maneuver. Transmissibility characteristics of different suspensions are investigated using harmonic excitations arising from in-phase and out-of-phase tire-terrain interactions.

(5) A pressure limiting control scheme is proposed to achieve the variable sequential damping for spring loaded interconnected hydro-pneumatic vehicle suspension systems in order to obtain an improved vibration isolation performance. The pressure limiting valve may be opened during the compression or expansion strokes when pressure differential across the fixed orifice exceeds the preset pressure. Variable damping is investigated for bounce and roll transmissibility performance under deterministic road excitations.

6.3 CONCLUSIONS

Based on the results of the investigations carried out in this thesis, the following conclusions are drawn:

- Previous studies had shown that interconnected hydro-pneumatic suspensions provided improved ride comfort, very good anti-roll performance and vehicle handling performance. However, the sizes of the struts were unreasonably large for implementation. Further, the pressures were also unreasonably high resulting in seal damage.

  The main objective of this thesis was to study the feasibility of designing interconnected hydro-pneumatic suspensions to be within practically implementable sizes by incorporating parallel mechanical springs to carry bulk

of the vehicle load. The results of the study showed that this is possible if some amount of ride comfort and anti-roll performance are compromised. The parametric study showed that 95% load carried by mechanical springs and 5% load carried by the interconnected hydro-pneumatic suspension is an optimum load distribution that will achieve reasonable strut sizes along with acceptable ride comfort and handling. Since load taken by the struts is reduced, the pressures in struts is also considerably reduced, to be in the range of 250-300 Psi, thus overcoming the seal damage problem in struts.

- The reduction in anti-roll performance because of reduced load taken by the interconnected hydro-pneumatic suspension can be improved by incorporating anti-roll bar.
- Fluid flow through interconnected pipe influences both static as well as dynamic properties of the suspension.
- Working area of interconnected suspension is the square of the piston rod area as against that of the unconnected suspension where the working area is the square of the piston head area. Consequently, the suspension rate of the interconnected system is considerably less than that of the unconnected suspension. The results of the study on interconnected hydro-pneumatic suspension with parallel mechanical springs show that the advantages of the interconnected set up can be retained by compensating the loss of suspension rate through mechanical springs.

- In general high ride comfort can be achieved from interconnected unit as compared to unconnected suspension system.
- Fluid flow through the Interconnected pipe introduces damping which impedes the roll motion. A fixed orifice in the interconnection provides damping to oppose the roll motion, however, it cannot simultaneously satisfy both ride comfort requirements and good handling performance. Providing a passive sequential damper gives high damping near the natural frequency of the sprung mass, low damping in the frequency range between the resonance of sprung mass and unsprung mass, and low damping around the natural frequency of unsprung mass. The sequential damper also provides improved transmissibility both in bounce and roll modes with a slight loss in performance near resonance. The main conclusion in this thesis is that the advantages of an interconnected hydro-pneumatic suspension can be retained and the disadvantages of excessive size and pressures can be eliminated with beneficial effects by incorporating parallel mechanical springs.

6.4 RECOMMENDATIONS FOR FUTURE WORK

The thesis presents the results of the study on spring loaded interconnected hydro-pneumatic suspension with fixed and variable orifice restriction. In view of the excellent potentials demonstrated in the study, it is recommended to undertake the following future work to further explore the performance potentials of the proposed suspension.

(1) A prototype of the proposed spring loaded interconnected suspension with fixed and variable damping can be developed and the corresponding performance

characteristics can be evaluated experimentally. Inlet and outlet flow losses of interconnected pipes can be investigated.

(2) Ride, handling, and roll-stability performance studies can be performed for the proposed model by introducing the pure random and roll random road inputs.

(3) Dynamic properties of passive variable sequential damper in interconnected suspension can be investigated.

(4) Optimization studies can be carried out in order to arrive at an optimal design of spring loaded interconnected hydro-pneumatic to achieve best compromise between vibration isolation performance and handling performance by a single design.

(5) A three-dimensional model can be developed which incorporates fluid flow interconnection in roll, and pitch plane in order to evaluate the ride, anti-roll, and anti-pitch performance of the on-road vehicle suspension.

REFERENCES

1. Liu, P., "Analysis Of An Interconnected Vehicle Suspension," Advanced Automotive Technologies, DSC-Vol. 52, 1993, pp. 279-284.
2. Mohanty, A. K, " Fluid Mechanics", Prentice-Hall, New York, 1986.
3. Pevsner, J. M. , " Equalizing Types of Suspension", Automobile Engineer, January, 1957.
4. Newton, K., " The Motor Vehicle", ISBN 0408010827, London; Boston: Butterworths, 1989.
5. Bastow, B., "Car Suspension and Handling", Pentech Press Limited, London, 1987.
6. Moulton, A. E., " Hydrolastic Springing", Automobile Engineer, September, 1962.
7. Moulton, A. E. and Best, A., " Rubber Springs and Interconnected Suspension Systems", Engineering Design Show Conference, Paper No. 15a, 1970.
8. Moulton, A. E. and Turner, P. W., " Rubber Springs for Vehicle suspension", Proceeding of Automotive Division Institution of Mechanical Engineers, 1956-7, No. 1.
9. Moulton, A. E., and Best, A., " Hydragas Suspension", SAE Paper No. 790374, 1980.
10. Felez, J., and Vera, C., " Bond Graph Assisted Models for Hydro-pneumatic Suspensions in Crane Vehicles," Vehicle System Dynamics, Vol. 16, 1987, pp. 313-332.

11. Tanahashi, H., Shindo, K., and Onuma, T., " Toyota Electronic Modulated Air Suspension for the 1986 SOARER", SAE paper 870541, 1987.

12. Sutton, H. B., " The Potential for Active Suspension Systems", Institute of Mechanical Engineers., Automobile Engineering April/May 1979 (U. K.), pp. 21-24.

13. Cotterell M., " Theoretical Analysis of an Active Suspension Fitted to a London Transport Bus", Institute of Physics, Stress Analysis Group, Annual Conference: Stress, Vibration and Noise Analysis in Vehicle, University of Aston, Birmingham, England, 1975, pp. 253-281.

14. Dominy J., and Bulman D. N., " An Active Suspension for a Formula One Grand Prix Racing Car", Journal of Dynamics Systems, Measurement, and Control, Trans. ASME, Vol. 107, March 1985, pp. 73-78.

15. Aspinall, D. T., and Oliver R. J., " Vehicle Riding Comfort! the Correlation Between Subjective Assessments of Vehicle Ride and Physical Measurements of Vehicle Motion", Motor Industry Research Association Report 1964/10.

16. Demerdash, S. M. EI., and Crolla, D. A., " Hydro-pneumatic Slow Active Suspension With Preview Control", Vehicle Systems Dynamics, Vol. 25, 1996, pp. 369-385.

17. Corolla, D.A., and Horton, D.N.L., " Theoretical Analysis of a Semi-Active Suspension Fitted to an Off-road Vehicle", Vehicle System Dynamics", Vol. 15, 1986, pp. 351-372.

18. Cotterell, M., "Theoretical Analysis of an Active Suspension Fitted to a London Transport Bus". Proceeding of Institution of Mechanical Engineers, Vol. 102, 1982, pp. 23-31.

19. Pitcher, R. H., " Technology Showcase Active Ride Control System", Journal of Terra Mechanics, Vol. 22, No. 4, 1986, pp. 237-243.

20. Corolla, D. A., and Horton, D. N. L., " Active Suspension Control for an Off-Road Vehicle", Proceeding of Institution of Mechanical Engineers, Vol. 201 No. D1, 1987, pp. 3-4.

21. Sireteanu, T., " The Effect of Sequential Damping on Ride Comfort Improvement", Vehicle Noise and Vibration, Institute of Mechanical Engineering Conference Publications 1984-85, pp. 77-82.

22. Van Vliet, M., " Computer Aided Analysis and Design of Off-road Motorcycle Suspensions", Ph.D. Thesis, Mechanical Engineering Department of Concordia University, 1983.

23. Asami, T., H., and Taniguchi, S., " Study on an Oil Damper With Variable Damping Mechanism", Bulletin of JSME, Vol. 28, No. 246, 1985, pp. 2978-2985.

24. Hundal, M. S., "Impact Absorber With Two-Stage Variable Area Orifice Hydraulic Damper", Journal of Sound and Vibration, Vol. 502(2), 1977, pp. 195-202.

25. Rakheja, S., and Sankar, S., " Response of a Sequential Damper to Shock Inputs", Shock and Vibration Bulletin Vol. 57(3), 1987, pp. 9-16.

26. Rakheja, S., Su. H., and Sankar, S., " Analysis of Passive Sequential Hydraulic Damper for Vehicle Suspension", Vehicle System Dynamics, Vol. 19, 1990, pp. 289-312.

27. Su. H, Rakheja, S., and Sankar, S., " Response of a Non-Linear Vehicle Suspension With Tunable Shock Absorber to Random Road Excitations", ASME Diagnostics, V. D. and Special Topics, The 12th ASME Vibration and Noise Conference, Vol. 19, 1990, pp. 289-312.

28. Barak, Pinhas," Design and Evaluation of Adjustable Automobile Suspension", SAE Paper 890089, 1989.

29. Lijima, Y., " The Development of a High-Performance Suspension of the New Nissan 300ZX", SAE Paper 841189, 1984.

30. Aoyama, Yutaka., Kawabata, Kazunobu., et. al., " Development of the Full Active Suspension By Nissan", SAE Paper 901747, 1990.

31. Yokoya, Y., et. al., " Toyota Electronic Modulated Suspension (TEMS) System for the 1993 Soarer", SAE Paper 840341, 1984.

32. Karnopp, D., and Heess, G., " Electronically Controllable Vehicle Suspensions", Vehicle System Dynamics, Vol. 20, 1991, pp. 207-217.

33. Poyser, J., " Development of a Computer Controlled Suspension System", International Journal of Vehicle Design, Vol. 8, No. 1, 1987, pp. 74-86.

34. Sharp, R. S., and Hassan, S. A., " On the Performance of Active Automobile Suspension Systems of Limited Bandwidth", Vehicle System Dynamics, Vol. 16, 1987, pp. 213-225.

35. Solits, M. W., "1987 Thunderbird Turbo Coupe Programmed Ride Control (PRC) Suspension", SAE Paper 870540, 1987.

36. Williams, R. A., and Best, A., " Refined Low Frequency Active Suspension", Institute of Mech. Eng., 1993, C466/028, pp. 285-293.

37. Williams, R. A., Best, A., and Best, Anthony, "Control of A Low Frequency Active Suspension", Control System, March, 1994, Conference Publication No. 388, pp. 338-343.

38. Rosam, N., and Darling, J., "Development and Simulation of a Noval Roll Control System for Interconnected Hydragas Suspension", Vehicle System Dynamics, Vol. 27, 1997, pp. 1-18.

39. D., Beard, D. C., Karnopp, et. al., "Hydraulically Actuated Suspension System for Motor Vehicles", Daimler-Benz AG German Patent DE 4231641A, 1992.

40. D., Scott, " Active Roll Reduction", Automotive Engineer, August/ September Issue, 1992.

41. Duchnowski, L. J., and Hann, S. A., " Modeling and Analysis of an Automobile Semi-Active Suspension", Advanced Automobile Technologies, DSC Vol. 13, ASME, 1989, pp. 321-334.

42. Rakheja, S., and Sankar, S., " Vibration and Shock Isolation Performance of a Semi-Active "on-off" Damper", ASME Journal Of Vibration, Acoustics, Stress and Reliability in Design Vol. 107, 1985, pp. 384-403.

43. Margolis, D. L., " The Response of Active and Semi-Active Suspensions to Realistic Feedback Signals", Vehicle System Dynamics, Vol. 11(5-6), Dec., 1982, pp. 267-282.

44. Margolis, D. L., and Goshtasbpour, M., " The Chatter of Semi-Active on-off Suspensions and Its Cure", Vehicle System Dynamics, Vol. 13, 1984, pp. 129-144.

45. Margolis, D. L., " Semi-Active Suspensions for Military Ground Vehicles Under Off-road Conditions", the 52nd Symposium on Shock and Vibration, New Orleans, Oct., 1981, pp. 27-29.

46. " Measurment and Presentation of Truck Ride Vibration", SAE Paper J1490, 1987.

47. Healey, A. J., "Digital Processing of Measure Vibration Data for Automobile Evaluation", The Design Engineering Technical Conference, Chicago, Illinois, Sept. 26-28, 1997, pp. 45-53.

48. Stikeleather, L. F., " Review of Ride Vibration Standards and Tolerances Criteria", Trans. SAE Paper No. 760413, 1976.

49. Barak, Pinhas," Magic Number in Design of Suspension for Passengers Cars", SAE Paper 911921, 1991.

50. Gillespie, T. D., " Fundamentals of Vehicle Dynamics", SAE Publishing, 1992.

51. Aurell, J., and Edlund, S., " Dynamics of Commercial Vehicles", Automotive Technology International 91, Sterling Publishing Group PLC, pp. 49-57.

52. Stannard, Whitten, Trezenga, " Assessment of Advanced Bus Suspension Technology", UTDC Inc, Transport Canada, TR 449-625-001, March 1987.

53. Liu, P. J., Rakheja, S., and Ahmed, A. K. W., " Properties of an Interconnected Hydro-pneumatic Suspension System", CSME-17-No.94, EIC Accession No. 2397, Vol. 19, No. 4, 1994, pp. 383-395.

54. Rosam, N., and Darling, J., " Modeling and Testing of the Interconnected Hydragas Suspension", 6th International Congress On Hydraulic Engineering in the Vehicle, Angers, May 1994, France.

55. Su. H., " An Investigation of Vibration Isolation Systems Using Active, Semi-Active and Tunable Passive Mechanism With Application To Vehicle Suspension", Ph. D. Thesis, Department of Mechanical Engineering, Concordia University, 1990.

56. Vehicle Dynamics Terminology-SAE J670e, SAE Handbook, 34.215-34.224, 1988.

57. O'Neil, P., " Advanced Engineering Mathematics", Wadsworth, 1996.

58. D'Souza, F., and Garg, V.," Advanced Dynamics, Modeling and Analysis", Prentice Hall, New York, 1984.

59. Wong, J. Y., " The Theory of Ground Vehicles", John Wiley, New York, 1971.

60. Whitehead, J., " The Handling Characteristics of European Intercity Buses", SAE Paper 912678.

61. Chalasani, R. M., " Ride Potential of Active Suspension Systems Part 1, Simplified Analysis Based on a Quarter Car Model", Symposium. ASME Applied Mechanics, 1986, pp. 187-204.

62. Hedric, J. K., and Kortiim, W., " Active Control in Ground Transportation-A State of the Art Review" , Mechanics of Transportation Systems, ASME AMD-15, 1975, pp. 21-40.

63. Goodall, R. M., and Kortiim, W., " Active Control in Ground Transportation-A Review of the State of the Art and Future Potential" , Vehicle System Dynamics Vol. 12, 1983, pp. 225-227.

64. Karnopp, D. C., " Are Active Suspension Really Necessary?", ASME Paper No. &-WA/DE-12, 1978.

65. Deminy, J., and Bulman, D. N., " An Active Suspension for a Formula One Grand Prix Racing Car", Journal of Dynamics of System, Measurement and Control, Vol. 107, 1984, pp. 73-82.

66. Ballany, P. L., " Mechanical Vibration", Theory of Machine, Khanna Publisher, New Delhi, 1987, pp. 1293-1295.